

GEOPHYSICAL MONOGRAPH SERIES

**AGU**  
ADVANCING EARTH  
AND SPACE SCIENCE

Space Physics and Aeronomy Collection

# Magnetospheres in the Solar System

*Editors*

Romain Maggiolo  
Nicolas André  
Hiroshi Hasegawa  
Daniel T. Welling

*Collection Editors in Chief*

Yongliang Zhang  
Larry J. Paxton

**WILEY**



---

Geophysical Monograph Series

## Geophysical Monograph Series

- 212 **The Early Earth: Accretion and Differentiation** *James Badro and Michael Walter (Eds.)*
- 213 **Global Vegetation Dynamics: Concepts and Applications in the MC1 Model** *Dominique Bachelet and David Turner (Eds.)*
- 214 **Extreme Events: Observations, Modeling and Economics** *Mario Chavez, Michael Ghil, and Jaime Urrutia-Fucugauchi (Eds.)*
- 215 **Auroral Dynamics and Space Weather** *Yongliang Zhang and Larry Paxton (Eds.)*
- 216 **Low-Frequency Waves in Space Plasmas** *Andreas Keiling, Dong-Hun Lee, and Valery Nakariakov (Eds.)*
- 217 **Deep Earth: Physics and Chemistry of the Lower Mantle and Core** *Hidenori Terasaki and Rebecca A. Fischer (Eds.)*
- 218 **Integrated Imaging of the Earth: Theory and Applications** *Max Moorkamp, Peter G. Lelievre, Niklas Linde, and Amir Khan (Eds.)*
- 219 **Plate Boundaries and Natural Hazards** *Joao Duarte and Wouter Schellart (Eds.)*
- 220 **Ionospheric Space Weather: Longitude and Hemispheric Dependences and Lower Atmosphere Forcing** *Timothy Fuller-Rowell, Endawoke Yizengaw, Patricia H. Doherty, and Sunanda Basu (Eds.)*
- 221 **Terrestrial Water Cycle and Climate Change Natural and Human-Induced Impacts** *Qihong Tang and Taikan Oki (Eds.)*
- 222 **Magnetosphere-Ionosphere Coupling in the Solar System** *Charles R. Chappell, Robert W. Schunk, Peter M. Banks, James L. Burch, and Richard M. Thorne (Eds.)*
- 223 **Natural Hazard Uncertainty Assessment: Modeling and Decision Support** *Karin Riley, Peter Webley, and Matthew Thompson (Eds.)*
- 224 **Hydrodynamics of Time-Periodic Groundwater Flow: Diffusion Waves in Porous Media** *Joe S. Depner and Todd C. Rasmussen (Auth.)*
- 225 **Active Global Seismology** *Ibrahim Cemen and Yucel Yilmaz (Eds.)*
- 226 **Climate Extremes** *Simon Wang (Ed.)*
- 227 **Fault Zone Dynamic Processes** *Marion Thomas (Ed.)*
- 228 **Flood Damage Survey and Assessment: New Insights from Research and Practice** *Daniela Molinari, Scira Menoni, and Francesco Ballio (Eds.)*
- 229 **Water-Energy-Food Nexus – Principles and Practices** *P. Abdul Salam, Sangam Shrestha, Vishnu Prasad Pandey, and Anil K Anal (Eds.)*
- 230 **Dawn–Dusk Asymmetries in Planetary Plasma Environments** *Stein Haaland, Andrei Rounov, and Colin Forsyth (Eds.)*
- 231 **Bioenergy and Land Use Change** *Zhangcai Qin, Umakant Mishra, and Astley Hastings (Eds.)*
- 232 **Microstructural Geochronology: Planetary Records Down to Atom Scale** *Desmond Moser, Fernando Corfu, James Darling, Steven Reddy, and Kimberly Tait (Eds.)*
- 233 **Global Flood Hazard: Applications in Modeling, Mapping and Forecasting** *Guy Schumann, Paul D. Bates, Giuseppe T. Aronica, and Heiko Apel (Eds.)*
- 234 **Pre-Earthquake Processes: A Multidisciplinary Approach to Earthquake Prediction Studies** *Dimitar Ouzounov, Sergey Pulinet, Katsumi Hattori, and Patrick Taylor (Eds.)*
- 235 **Electric Currents in Geospace and Beyond** *Andreas Keiling, Octav Marghitu, and Michael Wheatland (Eds.)*
- 236 **Quantifying Uncertainty in Subsurface Systems** *Celine Scheidt, Lewis Li, and Jef Caers (Eds.)*
- 237 **Petroleum Engineering** *Moshood Sanni (Ed.)*
- 238 **Geological Carbon Storage: Subsurface Seals and Caprock Integrity** *Stephanie Vialle, Jonathan Ajo-Franklin, and J. William Carey (Eds.)*
- 239 **Lithospheric Discontinuities** *Huaiyu Yuan and Barbara Romanowicz (Eds.)*
- 240 **Chemostratigraphy Across Major Chronological Eras** *Alcides N. Sial, Claudio Gaucher, Muthuvairavasamy Ramkumar, and Valderez Pinto Ferreira (Eds.)*
- 241 **Mathematical Geoenery: Discovery, Depletion, and Renewal** *Paul Pukite, Dennis Coyne, and Daniel Challou (Eds.)*
- 242 **Ore Deposits: Origin, Exploration, and Exploitation** *Sophie Decree and Laurence Robb (Eds.)*
- 243 **Kuroshio Current: Physical, Biogeochemical and Ecosystem Dynamics** *Takeyoshi Nagai, Hiroaki Saito, Koji Suzuki, and Motomitsu Takahashi (Eds.)*
- 244 **Geomagnetically Induced Currents from the Sun to the Power Grid** *Jennifer L. Gannon, Andrei Swidinsky, and Zhonghua Xu (Eds.)*
- 245 **Shale: Subsurface Science and Engineering** *Thomas Dewers, Jason Heath, and Marcelo Sánchez (Eds.)*
- 246 **Submarine Landslides: Subaqueous Mass Transport Deposits From Outcrops to Seismic Profiles** *Kei Ogata, Andrea Festa, and Gian Andrea Pini (Eds.)*
- 247 **Iceland: Tectonics, Volcanics, and Glacial Features** *Tamie J. Jovanelly*
- 248 **Dayside Magnetosphere Interactions** *Qiugang Zong, Philippe Escoubet, David Sibeck, Guan Le, and Hui Zhang (Eds.)*
- 249 **Carbon in Earth's Interior** *Craig E. Manning, Jung-Fu Lin, and Wendy L. Mao (Eds.)*
- 250 **Nitrogen Overload: Environmental Degradation, Ramifications, and Economic Costs** *Brian G. Katz*
- 251 **Biogeochemical Cycles: Ecological Drivers and Environmental Impact** *Katerina Dontsova, Zsuzsanna Balogh-Brunstad, and Gaël Le Roux (Eds.)*
- 252 **Seismoelectric Exploration: Theory, Experiments, and Applications** *Niels Grobбе, André Revil, Zhenya Zhu, and Evert Slob (Eds.)*
- 253 **El Niño Southern Oscillation in a Changing Climate** *Michael J. McPhaden, Agus Santoso, and Wenju Cai (Eds.)*
- 254 **Dynamic Magma Evolution** *Francesco Vetere (Ed.)*
- 255 **Large Igneous Provinces: A Driver of Global Environmental and Biotic Changes** *Richard. E. Ernst, Alexander J. Dickson, and Andrey Bekker (Eds.)*
- 256 **Coastal Ecosystems in Transition: A Comparative Analysis of the Northern Adriatic and Chesapeake Bay** *Thomas C. Malone, Alenka Malej, and Jadran Faganeli (Eds.)*
- 257 **Hydrogeology, Chemical Weathering, and Soil Formation** *Allen Hunt, Markus Egli, and Boris Faybishenko (Eds.)*
- 258 **Solar Physics and Solar Wind** *Nour E. Raouafi and Angelos Vourlidas (Eds.)*
- 259 **Magnetospheres in the Solar System** *Romain Maggiolo, Nicolas André, Hiroshi Hasegawa, and Daniel T. Welling (Eds.)*
- 260 **Ionosphere Dynamics and Applications** *Chaosong Huang and Gang Lu (Eds.)*
- 261 **Upper Atmosphere Dynamics and Energetics** *Wenbin Wang and Yongliang Zhang (Eds.)*

Space Physics and Aeronomy Collection Volume 2  
Geophysical Monograph 259

---

# Magnetospheres in the Solar System

Romain Maggiolo  
Nicolas André  
Hiroshi Hasegawa  
Daniel T. Welling  
*Editors*

Yongliang Zhang  
Larry J. Paxton  
*Collection Editors in Chief*

This Work is a co-publication of the American Geophysical Union and John Wiley and Sons, Inc.

This edition first published 2021  
© 2021 American Geophysical Union

All rights reserved. No part of this publication may be reproduced, stored in a retrieval system, or transmitted, in any form or by any means, electronic, mechanical, photocopying, recording or otherwise, except as permitted by law. Advice on how to obtain permission to reuse material from this title is available at <http://www.wiley.com/go/permissions>.

The right of Romain Maggiolo, Nicolas André, Hiroshi Hasegawa, and Daniel T. Welling to be identified as the editor of this work has been asserted in accordance with law.

### **Published under the aegis of the AGU Publications Committee**

---

Brooks Hanson, Executive Vice President, Science  
Carol Frost, Chair, Publications Committee  
For details about the American Geophysical Union visit us at [www.agu.org](http://www.agu.org)

#### *Registered Office*

John Wiley & Sons, Inc., 111 River Street, Hoboken, NJ 07030, USA

#### *Editorial Office*

111 River Street, Hoboken, NJ 07030, USA

For details of our global editorial offices, customer services, and more information about Wiley products visit us at [www.wiley.com](http://www.wiley.com).

Wiley also publishes its books in a variety of electronic formats and by print-on-demand. Some content that appears in standard print versions of this book may not be available in other formats.

#### *Limit of Liability/Disclaimer of Warranty*

While the publisher and authors have used their best efforts in preparing this work, they make no representations or warranties with respect to the accuracy or completeness of the contents of this work and specifically disclaim all warranties, including without limitation any implied warranties of merchantability or fitness for a particular purpose. No warranty may be created or extended by sales representatives, written sales materials or promotional statements for this work. The fact that an organization, website, or product is referred to in this work as a citation and/or potential source of further information does not mean that the publisher and authors endorse the information or services the organization, website, or product may provide or recommendations it may make. This work is sold with the understanding that the publisher is not engaged in rendering professional services. The advice and strategies contained herein may not be suitable for your situation. You should consult with a specialist where appropriate. Further, readers should be aware that websites listed in this work may have changed or disappeared between when this work was written and when it is read. Neither the publisher nor authors shall be liable for any loss of profit or any other commercial damages, including but not limited to special, incidental, consequential, or other damages.

#### *Library of Congress Cataloging-in-Publication Data*

Names: Maggiolo, Romain, editor. | André, Nicolas, 1977– editor. |  
Hasegawa, Hiroshi, 1974– editor. | Welling, Daniel T., editor.  
Title: Magnetospheres in the solar system / Romain Maggiolo, Nicolas  
André, Hiroshi Hasegawa, Daniel T. Welling, editors.  
Description: Hoboken, NJ : Wiley-American Geophysical Union, [2021] |  
Includes bibliographical references and index.  
Identifiers: LCCN 2020045732 | ISBN 9781119507529 (cloth) | ISBN 9781119829980 (adobe pdf) | ISBN  
9781119815648 (epub)  
Subjects: LCSH: Magnetosphere. | Planets–Magnetospheres.  
Classification: LCC QC809.M35 M32 2021 | DDC 538/.766–dc23  
LC record available at <https://lcn.loc.gov/2020045732>

Cover Design: Wiley

Cover Image: © Marc Ward/Shutterstock

Set in 10/12pt Times New Roman by SPi Global, Pondicherry, India

# CONTENTS

---

List of Contributors .....	ix
Preface .....	xvi
<b>Part I: The Earth Magnetosphere</b> .....	1
<b>1 A Brief History of the Magnetosphere</b> .....	3
<i>David J. Southwood</i>	
<b>2 Large-Scale Structure and Dynamics of the Magnetosphere</b> .....	15
<i>David G. Sibeck and Kyle R. Murphy</i>	
<b>3 The Equations of the Magnetosphere</b> .....	37
<i>Herbert Gunell</i>	
<b>Part II: Fundamental Processes</b> .....	47
<b>4 Magnetic Reconnection in the Near-Earth Magnetotail</b> .....	49
<i>Tsugunobu Nagai</i>	
<b>5 Turbulence and Complexity of Magnetospheric Plasmas</b> .....	67
<i>Marius Echim, Tom Chang, Peter Kovacs, Anna Wawrzaszek, Emiliya Yordanova, Yasuhito Narita, Zoltan Vörös, Roberto Bruno, Wieslaw Macek, Kalevi Mursula, and Giuseppe Consolini</i>	
<b>6 Wave-Particle Interactions in the Earth's Magnetosphere</b> .....	93
<i>Richard M. Thorne, Jacob Bortnik, Wen Li, and Qianli Ma</i>	
<b>7 Cross-Scale Energy Transport in Space Plasmas: Applications to the Magnetopause Boundary</b> .....	109
<i>Katariina Nykyri, Xuanye Ma, and Jay Johnson</i>	
<b>Part III: Solar Wind-Magnetosphere Coupling</b> .....	123
<b>8 Solar Wind Interaction with Earth's Bow Shock</b> .....	125
<i>Georges. K. Parks, Ensang Lee, Zhongwei W. Yang, Naiguo Lin, Suiyan Y. Fu, and Ying Liu</i>	
<b>9 The Magnetosheath</b> .....	137
<i>Yasuhito Narita, Ferdinand Plaschke, and Zoltán Vörös</i>	
<b>10 Dayside Magnetopause Processes</b> .....	153
<i>Stephen A. Fuselier</i>	
<b>11 The Polar Cusps of the Earth's Magnetosphere</b> .....	163
<i>Benoit Lavraud and Karlheinz J. Trattner</i>	
<b>12 The Earth's Low-Latitude Boundary Layer</b> .....	177
<i>Takuma K. M. Nakamura</i>	

<b>Part IV: Magnetosphere–Ionosphere Coupling</b> .....	193
<b>13 Field-Aligned Currents in the Magnetosphere–Ionosphere</b> .....	195
<i>Hermann Lühr and Guram Kervalishvili</i>	
<b>14 Ionospheric Ion Acceleration and Transport</b> .....	207
<i>Andrew W. Yau, Takumi Abe, Mats André, Andrew D. Howarth, and William K. Peterson</i>	
<b>15 Cold Ionospheric Ions in the Magnetosphere</b> .....	219
<i>Mats André, Sergio Toledo-Redondo, and Andrew W. Yau</i>	
<b>16 Magnetosphere–Ionosphere Coupling of Precipitating Electrons and Ionospheric Conductance</b> .....	229
<i>George V. Khazanov, David G. Sibeck, and Mike Chu</i>	
<b>Part V: The Dynamic Magnetosphere</b> .....	243
<b>17 Magnetotail Processes</b> .....	245
<i>Joachim Birn, Andrei Runov, and Yuri Khotyaintsev</i>	
<b>18 The Active Magnetosphere: Substorms and Storms</b> .....	277
<i>Yukitoshi Nishimura and Larry R. Lyons</i>	
<b>19 The Northward IMF Magnetosphere</b> .....	293
<i>Robert C. Fear</i>	
<b>20 A Brief Review of the Ring Current and Outstanding Problems</b> .....	311
<i>Raluca Ilie, Muhammad Fraz Bashir, and Elena A. Kronberg</i>	
<b>21 Source, Loss, and Transport of Energetic Particles Deep Inside Earth’s Magnetosphere (L &lt;4)</b> .....	323
<i>Xinlin Li, Richard S. Selesnick, Hong Zhao, Daniel N. Baker, J. Bernard Blake, and Michael A. Temerin</i>	
<b>22 The Plasmasphere: Its Interactions and Dynamics</b> .....	335
<i>Fabien Darrouzet, Dennis L. Gallagher, and Johan De Keyser</i>	
<b>23 Impact of Ionospheric Ions on Magnetospheric Dynamics</b> .....	353
<i>Elina A. Kronberg, Elena E. Grigorenko, Raluca Ilie, Lynn Kistler, and Dan Welling</i>	
<b>Part VI: Planetary Magnetic Fields</b> .....	365
<b>24 Planetary Magnetic Fields</b> .....	367
<i>Karl-Heinz Glassmeier and Daniel Heyner</i>	
<b>Part VII: Induced Magnetospheres</b> .....	391
<b>25 Induced Magnetospheres: Mars</b> .....	393
<i>Jasper S. Halekas, Janet G. Luhmann, Eduard Dubinin, and Yingjuan Ma</i>	
<b>26 Induced Magnetospheres: Titan</b> .....	407
<i>César Bertucci</i>	
<b>27 Birth of a Magnetosphere</b> .....	427
<i>Hans Nilsson, Etienne Behar, James L. Burch, Christopher M. Carr, Anders I. Eriksson, Karl-Heinz Glassmeier, Pierre Henri, Marina Galand, Charlotte Goetz, Herbert Gunell, and Tomas Karlsson</i>	
<b>28 Induced Magnetospheres: Atmospheric Escape</b> .....	441
<i>David A. Brain</i>	

<b>Part VIII: Giant Planet Magnetospheres</b> .....	453
<b>29 The Magnetodisk Regions of Jupiter and Saturn</b> .....	455
<i>Nicholas Achilleos, Patick Guio, Flavien Hardy, Chris Paranicas, and Arianna M. Sorba</i>	
<b>30 Fast Rotating Magnetospheres: Jupiter and Saturn Plasma Sources, Loss and Transport</b> .....	471
<i>Abigail M. Rymer</i>	
<b>31 Gas Giant Magnetosphere–Ionosphere–Thermosphere Coupling</b> .....	485
<i>Licia C. Ray and Japheth N. Yates</i>	
<b>32 The Radiation Belts of Jupiter and Saturn</b> .....	499
<i>Elias Roussos and Peter Kollmann</i>	
<b>33 Asymmetrical Magnetospheres: Uranus and Neptune</b> .....	515
<i>Christopher S. Arridge and Carol Paty</i>	
<b>Part IX: Mini-magnetospheres and Moon–Magnetosphere Interactions</b> .....	535
<b>34 A Dungey Cycle in the Life of Mercury’s Magnetosphere</b> .....	537
<i>James A. Slavin, Suzanne M. Imber, and Jim M. Raines</i>	
<b>35 The Magnetosphere of Ganymede</b> .....	557
<i>Xianzhe Jia and Margaret G. Kivelson</i>	
<b>36 Overview of Moon–Magnetosphere Interactions</b> .....	575
<i>Joachim Saur</i>	
<b>Part X: Investigating Magnetospheric Processes</b> .....	595
<b>37 Global Simulations</b> .....	597
<i>Joachim Raeder, Kai Germaschewski, William D. Cramer, and John Lyon</i>	
<b>38 Kinetic Modeling in the Magnetosphere</b> .....	607
<i>Stefano Markidis, Vyacheslav Olshevsky, Gábor Tóth, Yuxi Chen, Ivy Bo Peng, Giovanni Lapenta, and Tamas Gombosi</i>	
<b>39 Data-Based Modeling of the Earth’s Magnetic Field</b> .....	617
<i>Nikolai Tsyganenko, Varvara Andreeva, Marina Kubyshkina, Mikhail Sitnov, and Grant Stephens</i>	
<b>40 Multispacecraft Measurements In The Magnetosphere</b> .....	637
<i>Malcolm W. Dunlop, TieYan Wang, XiangCheng Dong, Stein Haarland, QuanQi Shi, HuiShan Fu, Johan De Keyser, Chao Shen, ZhaoJin Rong, Christophe Phillippe Escoubet, ZuYin Pu, and Jonathan Eastwood</i>	
<b>41 Exploring Small Scales with MMS</b> .....	657
<i>James L. Burch and Kyoung-Joo Hwang</i>	
<b>42 Global Energetic Neutral Atom (ENA) Imaging of Magnetospheres</b> .....	673
<i>Pontus C. Brandt</i>	
<b>43 Laboratory Experiments: Putting Space into the Lab</b> .....	699
<i>Mark Koepke</i>	

<b>Part XI: Future Directions</b> .....	715
<b>44 Challenges in Modeling the Outer Magnetosphere</b> .....	717
<i>Gábor Tóth, Yuxi Chen, Zhenguang Huang, and Bart van der Holst</i>	
<b>45 Does a Magnetosphere Protect the Ionosphere?</b> .....	729
<i>Romain Maggiolo and Herbert Gunell</i>	
<b>46 Some Unsolved Problems of Magnetospheric Physics</b> .....	743
<i>Michael H. Denton</i>	
<b>47 Instigators of Future Change in Magnetospheric Research</b> .....	753
<i>Michael W. Liemohn, Amy M. Keesee, L. Kepko, and Mark B. Moldwin</i>	
<b>Index</b> .....	765

## LIST OF CONTRIBUTORS

---

### **Takumi Abe**

Institute of Space and Astronautical Science  
Japan Aerospace Exploration Agency  
Sagamihara, Kanagawa, Japan

### **Nicholas Achilleos**

Department of Physics and Astronomy/  
Centre for Planetary Sciences  
University College London  
London, UK

### **Mats André**

Swedish Institute of Space Physics  
Uppsala, Sweden

### **Varvara Andreeva**

Institute and Department of Physics  
Saint-Petersburg State University  
Saint-Petersburg, Russia

### **Christopher S. Arridge**

Department of Physics  
Lancaster University  
Bailrigg, Lancaster, UK

### **Daniel N. Baker**

Laboratory for Atmospheric and Space Physics  
University of Colorado Boulder  
Boulder, CO, USA

### **Muhammad Fraz Bashir**

Department of Electrical and Computer Engineering  
University of Illinois at Urbana-Champaign  
Urbana, IL, USA

### **Etienne Behar**

Swedish Institute of Space Physics  
Kiruna, Sweden;  
*and*  
Department of Computer Science, Electrical and Space  
Engineering  
Luleå University of Technology  
Kiruna, Sweden

### **César Bertucci**

Instituto de Astronomía y Física del Espacio  
Universidad de Buenos Aires / CONICET  
Buenos Aires, Argentina

### **Joachim Birn**

Space Science Institute  
Boulder, CO, USA;  
*and*  
Los Alamos National Laboratory  
Los Alamos, NM, USA

### **J. Bernard Blake**

Space Sciences Department  
The Aerospace Corporation  
Los Angeles, CA, USA

### **Jacob Bortnik**

Department of Atmospheric and Oceanic Sciences  
University of California  
Los Angeles, CA, USA

### **David A. Brain**

Laboratory for Atmospheric and Space Physics  
University of Colorado Boulder  
Boulder, CO, USA

### **Pontus C. Brandt**

Johns Hopkins University Applied Physics Laboratory  
Laurel, MD, USA

### **Roberto Bruno**

The National Institute for Astrophysics (INAF)  
Rome, Italy

### **James L. Burch**

Southwest Research Institute  
San Antonio, TX, USA

### **Christopher M. Carr**

Department of Physics  
Imperial College London  
London, UK

### **Tom Chang**

Massachusetts Institute of Technology  
Cambridge, USA

### **Yuxi Chen**

Center for Space Environment Modeling  
University of Michigan  
Ann Arbor, MI, USA

**Mike Chu**

NOAA, Cooperative Institute for Research in the Atmosphere  
Colorado State University  
Fort Collins, CO, USA

**Giuseppe Consolini**

The National Institute for Astrophysics (INAF)  
Rome, Italy

**William D. Cramer**

Space Science Center  
University of New Hampshire  
Durham, NH, USA

**Fabien Darrouzet**

Royal Belgian Institute for Space Aeronomy  
Brussels, Belgium

**Johan De Keyser**

Royal Belgian Institute for Space Aeronomy  
Brussels, Belgium

**Michael. H. Denton**

Center for Space Plasma Physics  
Space Science Institute  
Boulder, CO, USA;  
*and*

New Mexico Consortium  
Los Alamos, NM, USA

**XiangCheng Dong**

School of Space and Environment  
Beihang University  
Beijing, China

**Eduard Dubinin**

Max-Planck-Institute for Solar System Research  
Katlenburg-Lindau, Germany

**Malcolm W. Dunlop**

School of Space and Environment  
Beihang University  
Beijing, China;  
*and*

Rutherford Appleton Laboratory  
Didcot, Oxfordshire, UK

**Jonathan Eastwood**

Rutherford Appleton Laboratory  
Didcot, Oxfordshire, UK

**Marius Echim**

Royal Belgian Institute for Space Aeronomy  
Brussels, Belgium;  
*and*  
Institute of Space Science  
Magurele, Romania

**Anders I. Eriksson**

Swedish Institute of Space Physics  
Ångström Laboratory  
Uppsala, Sweden

**Christophe Phillippe Escoubet**

European Space Agency/  
European Space Research and Technology Centre  
Noordwijk, The Netherlands

**Robert C. Fear**

School of Physics and Astronomy  
University of Southampton  
Southampton, UK

**HuiShan Fu**

School of Space and Environment  
Beihang University  
Beijing, China

**Suiyan Y. Fu**

Geophysics Department  
Peking University  
Beijing, China

**Stephen A. Fuselier**

Southwest Research Institute  
San Antonio, TX, USA;  
*and*  
University of Texas at San Antonio  
San Antonio, TX, USA

**Marina Galand**

Department of Physics  
Imperial College London  
London, UK

**Dennis L. Gallagher**

NASA Marshall Space Flight Center  
Huntsville, AL, USA

**Kai Germaschewski**

Space Science Center  
University of New Hampshire  
Durham, NH, USA

**Karl-Heinz Glassmeier**

Institut für Geophysik und extraterrestrische Physik  
Technische Universität Braunschweig  
Braunschweig, Germany

**Charlotte Goetz**

Institut für Geophysik und extraterrestrische Physik  
Technische Universität Braunschweig  
Braunschweig, Germany

**Tamas Gombosi**

Center for Space Environment Modeling  
University of Michigan  
Ann Arbor, MI, USA

**Elena E. Grigorenko**

Space Research Institute of  
Russian Academy of Sciences  
Moscow, Russia;  
*and*

Department of Physics of the Earth  
Saint-Petersburg State University  
Saint-Petersburg, Russia

**Patrick Guio**

Department of Physics and Astronomy/  
Centre for Planetary Sciences  
University College London  
London, UK;  
*and*

Department of Physics and Technology  
Arctic University of Norway  
Tromsø, Norway

**Herbert Gunell**

Royal Belgian Institute for Space Aeronomy  
Brussels, Belgium;  
*and*

Department of Physics  
Umeå University  
Umeå, Sweden

**Stein Haarland**

Birkeland Centre for Space Science  
University of Bergen  
Bergen, Norway

**Jasper S. Halekas**

Department of Physics and Astronomy  
University of Iowa  
Iowa City, IA, USA

**Flavien Hardy**

Department of Physics and Astronomy/  
Centre for Planetary Sciences  
University College London  
London, UK

**Pierre Henri**

Laboratoire de Physique et Chimie de l'Environnement et  
de l'Espace  
UMR 7328 CNRS – Université d'Orléans  
Orléans, France

**Daniel Heyner**

Institut für Geophysik und extraterrestrische Physik  
Technische Universität Braunschweig  
Braunschweig, Germany

**Andrew D. Howarth**

Department of Physics and Astronomy  
University of Calgary  
Calgary, AB, Canada

**Zhenguang Huang**

Center for Space Environment Modeling  
University of Michigan  
Ann Arbor, MI, USA

**Kyoung-Joo Hwang**

Southwest Research Institute  
San Antonio, TX, USA

**Raluca Ilie**

Department of Electrical and Computer Engineering  
University of Illinois at Urbana-Champaign  
Urbana, IL, USA

**Suzanne M. Imber**

Department of Climate and Space Sciences and  
Engineering  
University of Michigan  
Ann Arbor, MI, USA;  
*and*

Department of Physics and Astronomy  
University of Leicester  
Leicester, UK

**Xianzhe Jia**

Department of Climate and Space Sciences and  
Engineering  
University of Michigan  
Ann Arbor, MI, USA

**Jay Johnson**

Department of Engineering  
Andrews University  
Berrien Springs, MI, USA

**Tomas Karlsson**

Department of Space and Plasma Physics  
School of Electrical Engineering and  
Computer Science  
KTH Royal Institute of Technology  
Stockholm, Sweden

**Amy M. Keesee**

Department of Physics and Space Science Center  
University of New Hampshire  
Durham, NH, USA

**Larry Kepko**

Space Weather Laboratory  
Heliophysics Science Division  
NASA Goddard Space Flight Center  
Greenbelt, MD, USA

**Guram Kervalishvili**

GFZ – German Research Centre for Geosciences  
Section 2.3, Geomagnetism  
Potsdam, Germany

**George V. Khazanov**

NASA Goddard Space Flight Center  
Greenbelt, MD, USA

**Yuri Khotyaintsev**

Swedish Institute of Space Physics  
Uppsala, Sweden

**Lynn Kistler**

Space Science Center  
University of New Hampshire  
Durham, NH, USA

**Margaret G. Kivelson**

Department of Climate and Space Sciences and  
Engineering  
University of Michigan  
Ann Arbor, MI, USA;  
*and*  
Department of Earth, Planetary, and Space Sciences  
University of California  
Los Angeles, CA, USA

**Mark Koepke**

Department of Physics and Astronomy  
West Virginia University  
Morgantown, WV, USA;  
*and*  
Department of Physics  
University of Strathclyde  
Glasgow, UK

**Peter Kollmann**

Johns Hopkins University Applied Physics Laboratory  
Laurel, MD, USA

**Peter Kovacs**

Mining and Geological Survey of Hungary  
Budapest, Hungary

**Elena A. Kronberg**

Max Planck Institute for Solar System Research  
Göttingen, Germany;  
*and*  
Department of Earth and Environmental Sciences  
(Geophysics)  
Ludwig Maximilian University of Munich  
Munich, Germany

**Marina Kubyshkina**

Institute and Department of Physics  
Saint-Petersburg State University  
Saint-Petersburg, Russia

**Giovanni Lapenta**

Department of Mathematics  
Katholieke Universiteit Leuven  
Leuven, Belgium

**Benoit Lavraud**

Institut de Recherche en Astrophysique et Planétologie  
CNRS, UPS, CNES  
Université de Toulouse  
Toulouse, France;  
*and*  
Laboratoire d'astrophysique de Bordeaux  
CNRS  
Université de Bordeaux  
Pessac, France

**Ensang Lee**

School of Space Research  
Kyung Hee University  
Yongin, South Korea

**Wen Li**

Center for Space Physics  
Boston University  
Boston, MA, USA

**Xinlin Li**

Laboratory for Atmospheric and Space Physics  
University of Colorado Boulder  
Boulder, CO, USA;  
*and*  
Department of Aerospace Engineering Sciences  
University of Colorado Boulder  
Boulder, CO, USA

**Michael W. Liemohn**

Department of Climate and Space Sciences and  
Engineering  
University of Michigan  
Ann Arbor, MI, USA

**Naiguo Lin**

Space Sciences Laboratory  
University of California, Berkeley  
Berkeley, CA, USA

**Ying Liu**

Key Laboratory for Space Weather  
Chinese Academy of Sciences  
Beijing, China

**Janet G. Luhmann**

Space Sciences Laboratory  
University of California  
Berkeley, CA, USA

**Hermann Lühr**

GFZ – German Research Centre for Geosciences  
Section 2.3, Geomagnetism  
Potsdam, Germany

**John Lyon**

Department of Physics and Astronomy  
Dartmouth College  
Hanover, NH, USA

**Larry R. Lyons**

Department of Atmospheric and Oceanic Sciences  
University of California  
Los Angeles, CA, USA

**Qianli Ma**

Department of Atmospheric and Oceanic Sciences  
University of California  
Los Angeles, CA, USA;  
*and*  
Center for Space Physics  
Boston University  
Boston, MA, USA

**Xuanye Ma**

Center for Space and Atmospheric Research and Physical  
Sciences Department  
Embry-Riddle Aeronautical University  
Daytona Beach, FL, USA

**Yingjuan Ma**

Earth, Planetary and Space Sciences  
University of California  
Los Angeles, CA, USA

**Romain Maggiolo**

Royal Belgian Institute for Space Aeronomy  
Brussels, Belgium

**Wieslaw Macek**

Space Research Centre  
Polish Academy of Sciences  
Warsaw, Poland

**Stefano Markidis**

KTH Royal Institute of Technology  
Stockholm, Sweden

**Mark B. Moldwin**

Department of Climate and Space Sciences and  
Engineering  
University of Michigan  
Ann Arbor, MI, USA

**Kyle R. Murphy**

NASA Goddard Space Flight Centre  
Greenbelt, MD, USA;  
*and*  
Department of Astronomy  
University of Maryland  
College Park, MD, USA

**Kalevi Mursula**

Department of Physics  
University of Oulu  
Oulu, Finland

**Takuma K. M. Nakamura**

Space Research Institute  
Austrian Academy of Sciences  
Graz, Austria;  
*and*  
Institute of Physics  
University of Graz  
Graz, Austria

**Yasuhito Narita**

Space Research Institute  
Austrian Academy of Sciences  
Graz, Austria

**Tsugunobu Nagai**

Institute of Space and Astronautical Science  
Japan Aerospace Exploration Agency  
Sagamihara, Japan

**Hans Nilsson**

Swedish Institute of Space Physics  
Kiruna, Sweden

**Yukitoshi Nishimura**

Department of Electrical and Computer Engineering and  
Center for Space Physics  
Boston University  
Boston, MA, USA

**Katariina Nykyri**

Center for Space and Atmospheric Research and Physical  
Sciences Department  
Embry-Riddle Aeronautical University  
Daytona Beach, FL, USA

**Vyacheslav Olshevsky**

KTH Royal Institute of Technology  
Stockholm, Sweden

**Chris Paranicas**

Johns Hopkins University Applied Physics Laboratory  
Laurel, MD, USA

**Georges. K. Parks**

Space Sciences Laboratory  
University of California, Berkeley  
Berkeley, CA, USA

**Carol Paty**

Department of Earth Sciences  
University of Oregon  
Eugene, OR, USA

**Ivy Bo Peng**

Lawrence Livermore National Laboratory  
Livermore, CA, USA

**William K. Peterson**

Laboratory of Atmospheric and Space Physics  
University of Colorado Boulder  
Boulder, CO, USA

**Ferdinand Plaschke**

Space Research Institute  
Austrian Academy of Sciences  
Graz, Austria

**ZuYin Pu**

School of Earth and Space Sciences  
Peking University  
Beijing, China

**Joachim Raeder**

Space Science Center  
University of New Hampshire  
Durham, NH, USA

**Jim M. Raines**

Department of Climate and Space Sciences and  
Engineering  
University of Michigan  
Ann Arbor, MI, USA

**Licia C. Ray**

Department of Physics  
Lancaster University  
Lancaster, UK

**Zhaojin Rong**

Institute of Geology and Geophysics  
Chinese Academy of Sciences  
Beijing, China

**Elias Roussos**

Max Planck Institute for Solar System Research  
Goettingen, Germany

**Andrei Runov**

Department of Earth, Planetary, and Space Sciences  
University of California  
Los Angeles, CA, USA

**Abigail M. Rymer**

Johns Hopkins University Applied Physics Laboratory  
Laurel, MD, USA

**Joachim Saur**

Institut für Geophysik und Meteorologie  
University of Cologne  
Cologne, Germany

**Richard S. Selesnick**

Space Vehicles Directorate  
Air Force Research Laboratory  
Kirtland AFB, NM, USA

**Chao Shen**

Harbin Institute of Technology  
Shenzhen, China

**QuanQi Shi**

Institute of Space Sciences  
Shandong University  
Weihai, China

**David G. Sibeck**

NASA Goddard Space Flight Center  
Greenbelt, MD, USA

**Mikhail Sitnov**

Johns Hopkins University Applied Physics Laboratory  
Laurel, MD, USA

**James A. Slavin**

Department of Climate and Space Sciences and  
Engineering  
University of Michigan  
Ann Arbor, MI, USA

**Arianna M. Sorba**

Department of Physics and Astronomy/  
Centre for Planetary Sciences  
University College London  
London, UK

**David J. Southwood**

Space and Atmospheric Physics  
Imperial College  
London, UK

**Grant Stephens**

Johns Hopkins University Applied Physics Laboratory  
Laurel, MD, USA

**Michael A. Temerin**

Space Sciences Laboratory  
University of California  
Berkeley, CA, USA

**Richard M. Thorne**

Department of Atmospheric and Oceanic Sciences  
University of California  
Los Angeles, CA, USA

**Sergio Toledo-Redondo**

Institut de Recherche en Astrophysique et Planétologie  
CNRS, UPS, CNES  
Université de Toulouse  
Toulouse, France

**Gábor Tóth**

Center for Space Environment Modeling  
University of Michigan  
Ann Arbor, MI, USA

**Karlheinz J. Trattner**

Laboratory for Atmospheric and Space Physics  
University of Colorado Boulder  
Boulder, CO, USA

**Nikolai Tsyganenko**

Institute and Department of Physics  
Saint-Petersburg State University  
Saint-Petersburg, Russia

**Bart van der Holst**

Center for Space Environment Modeling  
University of Michigan  
Ann Arbor, MI, USA

**Zoltán Vörös**

Space Research Institute  
Austrian Academy of Sciences  
Graz, Austria

**TieYan Wang**

Rutherford Appleton Laboratory  
Didcot, Oxfordshire, UK

**Anna Wawrzaszek**

Space Research Centre  
Polish Academy of Sciences  
Warsaw, Poland

**Dan Welling**

Department of Physics  
University of Texas at Arlington  
Arlington, TX, USA

**Zhongwei W. Yang**

Key Laboratory for Space Weather  
Chinese Academy of Sciences  
Beijing, China

**Japheth N. Yates**

European Space Astronomy Centre  
European Space Agency  
Madrid, Spain

**Andrew W. Yau**

Department of Physics and Astronomy  
University of Calgary  
Calgary, AB, Canada

**Emiliya Yordanova**

Swedish Institute of Space Physics  
Uppsala, Sweden

**Hong Zhao**

Laboratory for Atmospheric and Space Physics  
University of Colorado Boulder  
Boulder, CO, USA

## PREFACE

---

Introduced in 1958, the term magnetosphere refers to the magnetic cavity surrounding a celestial body. Invisible to the human eyes, magnetospheres can only be explored through the development of instruments, theories and numerical models. With the advent of the space age we have started exploring them in situ and accumulated an impressive amount of data over the years. Sixty years after the term magnetosphere was been defined, it is challenging to review the existing knowledge on solar system magnetospheres in one single book.

This book provides an overview of the magnetospheres in the solar system, from the small induced magnetospheres that form around unmagnetized bodies to the large magnetospheres of the giant planets. Magnetospheres are highly complex, structured and time-dependent systems constantly interacting with the solar wind and the components of the planetary systems, such as their ionosphere, atmosphere, surface, rings, and moons. Each magnetosphere is unique and contains various intertwining subregions, particle populations, and plasma processes. This explains the scientific interest of magnetospheric physics: magnetospheres are accessible natural laboratories for studying fundamental physical processes of universal application. Moreover, the Earth's magnetosphere is a key component of our near-space environment on which our modern societies are increasingly dependent.

The book is divided in eleven sections that cover the current state of our understanding as well as future directions for scientists. Part I starts with a brief history of magnetospheres and presents the basic principles and equations. Part II addresses the fundamental processes that govern magnetospheric physics. The three following sections are dedicated to the Earth's magnetosphere, the most studied and best known of the solar system magnetospheres. They respectively focus on its coupling with the Earth's ionosphere (part III), its coupling with the solar wind (part IV), and its dynamics (part V). The next sections are oriented toward other solar system bodies. After a discussion about planetary magnetic fields in part VI, we focus on the induced magnetospheres in part VII, on the

magnetospheres of giant planets in part VIII and, in part IX, on "minimagnetospheres", such as those of Mercury and magnetized moons. Part X considers the tools that are used to investigate magnetospheric processes. Finally, part XI discusses the key questions and challenges to be addressed in the coming years, providing some insights on the future developments of magnetospheric research. The chapters contained herein include contributions from experimentalists, theoreticians, and numerical modelers.

We hope that this book will be a resource for both the novice researcher and the experienced scientist. For those less acquainted with current topics in Earth and planetary magnetospheric research, this book will provide the background material required to be knowledgeable on the current state of the art. For experts, it will act as a reference to the most important magnetospheric science breakthroughs and help expand the reader's horizons with its coverage of the diverse near-body regions in space. With this book, we hope that the reader will comprehend most of the features of magnetospheres and find the keys to delve as far as possible into them.

We gratefully acknowledge support and guidance from Rituparna Bose and Daniel Finch of John Wiley & Sons, Inc. through the book proposal process, the external peer review of the chapters, and the book production process. We also thank all the authors for their contribution and all the reviewers for their assistance.

This book is dedicated to the memory of Richard M. Thorne.

**Romain Maggiolo**

*Royal Belgian Institute for Space Aeronomy,  
Belgium*

**Nicolas André**

*Research Institute in Astrophysics  
and Planetology, France*

**Hiroshi Hasegawa**

*Japan Aerospace Exploration Agency, Japan*

**Daniel T. Welling**

*University of Texas at Arlington, USA*

# **Part I**

## **The Earth Magnetosphere**



# 1

## A Brief History of the Magnetosphere

David J. Southwood

### ABSTRACT

The early history of the magnetosphere is taken from the earliest suggestions of a material transport between Sun and Earth by Sabine in the nineteenth century, through the work of both Birkeland and Chapman and coworkers in the early twentieth century to the naming of the magnetosphere, the proposal of the open magnetosphere, and the discoveries of the first decade and a half of the space age.

### 1.1. INTRODUCTION

One could begin a history of the magnetosphere as early as 1600 when Gilbert published his “De Magnete,” which first treated the magnetism of the Earth as having an embedded planetary dipole. Alternatively, one could start with the coining of the term by Thomas Gold in the early space age in 1959. As neither Gilbert nor Gold really understood what turned out to be the most sensitive and basic scientific issues, it is probably a good compromise to start with Edward Sabine in 1852 (Sabine, 1852). In his report to the Royal Society of London, Sabine was the first to glimpse dimly the nature of the electromagnetic coupling between the Sun and Earth that is fundamental to both the formation of the magnetosphere and also its activity.

### 1.2. BRITISH WORK IN THE NINETEENTH CENTURY

Edward Sabine was a both scientist and a soldier, in the latter capacity seeing service in North America in the War of 1812. His interest in geophysics stemmed initially from working in geodesy. He moved from measuring terrestrial gravity to the study of the terrestrial magnetic field, which he realized needed to be surveyed

globally. No doubt after pointing out to his superiors in a maritime nation with a global empire the relevance of understanding the magnetic field for navigational purposes, Colonel Sabine set up magnetic observatories across the globe. His 1852 paper reports results on the variation of the field with time at the widely separated locations of Toronto and Hobarton (now Hobart, Tasmania). Diurnal variations are seen but also there are disturbances detected at both sites widely separated in longitude and latitude. The most important comment he makes for our purpose is to relate his results to those of a German astronomer, Heinrich Schwabe, who had proposed from a long record of solar observations that sunspots exhibited a regular 11 year cycle. Sabine noted that the variation in global magnetic activity appeared to match Schwabe’s sunspot period. He further noted that Schwabe had failed to detect any change in terrestrial climate on the same scale. He then goes on to make the prescient remark “*But it is quite conceivable that affections of the gaseous envelope of the Sun, or causes occasioning those affections, may give rise to sensible magnetical effects at the surface of our planet, without producing sensible thermic effects.*” The word “sensible” here is in the (archaic) sense of “detectable”.

The first observations of what we now know to be a direct correlation between a solar phenomenon and a geomagnetic response came within a few years. In 1859 a global magnetic disturbance occurred, now called the

---

*Space and Atmospheric Physics, Imperial College, London, UK*

---

*Space Physics and Astronomy Collection Volume 2: Magnetospheres in the Solar System, Geophysical Monograph 259, First Edition.*

Edited by Romain Maggiolo, Nicolas André, Hiroshi Hasegawa, and Daniel T. Welling.

© 2021 American Geophysical Union. Published 2021 by John Wiley & Sons, Inc.

DOI: 10.1002/9781119815624.ch1

Carrington storm (Carrington, 1860). There is an irony in this attribution. What Carrington actually reported to the Royal Astronomical Society was the first observation of white light flares on the Sun. In his report he does refer to an almost simultaneous magnetic disturbance followed about 17 hours later by large magnetic disturbances. The observations would have been provided by Balfour Stewart and came from Kew (near London) (Stewart, 1860). In the discussion of the magnetic observations, Carrington was asked whether there was a direct relationship between the magnetic disturbances and the extreme solar event; he replied cautiously "... *While the contemporary occurrence may deserve noting, he would not have it supposed that he even leans towards hastily connecting them. One swallow does not make a summer.*" (Carrington, 1860). Balfour Stewart (1860) reported on the magnetic events and had no such caution. Extended magnetic disturbances were recorded globally between 28 August and 2 September 1859. He pointed out that auroral displays were seen in parts of the British Empire (e.g. in the Caribbean, in India) where they had never been seen before or since. In his report on those disturbances, he described Carrington's observations but after gently criticizing Carrington's caution, he invoked specifically Sabine's earlier result. "*Since General Sabine has proved that a relation subsists between magnetic disturbances and sun spots, it is not impossible to suppose that in this case our luminary was taken in the act.*" Removing the British understatement, this statement directly supports the notion of a Sun–Earth connection.

The quasi-instantaneous signal would have been due to modification of the ionospheric conductivity by incident X-ray and UV radiation, thus enhancing the magnetic signals associated with the daily dynamo motion in the ionosphere. The delayed signal would have been the shock of flare material arriving and disrupting the magnetosphere. It would be years before these explanations became common currency.

Carrington's caution reflected the tenor of the times. In that era, Kelvin and Rayleigh ruled the British scientific roost and neither scientist was inclined to accept that material could move directly through space from Sun to Earth. Despite his referring directly to Sabine's (1852) result and the events of 1859, Kelvin's assessment was made clear in his presidential address to the Royal Society in 1892 (Kelvin, 1892).

Southwood (2015) credits Stewart with keeping alive the idea that there might be a material connection between the Sun and Earth following Carrington's report. As we see later, it was carried forward by his student Arthur Schuster. Schuster also did much to elucidate solar and lunar patterns. Using four magnetic stations, Schuster and Lamb (1889) provided the basic breakdown of the regular magnetic diurnal patterns of disturbance fixed with respect to the Sun and also a lunar component

originally identified by Sabine (1861). However, by the end of the nineteenth century there remained an open question over the largest global disturbances, which show no obvious link with time of day but did vary in intensity over the solar cycle. The codification of the lunar ( $L$ ) and Solar ( $S_q$ ) quiet day current patterns was undertaken by Sydney Chapman (1913) using much more coverage (21 stations) (Matsushita, 1968). The global magnetic pattern for the magnetically disturbed periods or geomagnetic storms was also distinctive. The pattern was called the disturbance system ( $S_D$  or  $DS$ ). Following a large amount of magnetic survey work for the British Royal Observatory, Chapman (1919) published a paper outlining the magnetic disturbance patterns and containing what is the first attempt by a Briton for a theory. However, before we look at what he said and where it led, one should note that there had been much earlier suggestions concerning the source of geomagnetic disturbances and the aurorae they bring in their wake.

### 1.3. SCANDINAVIAN WORK IN THE NINETEENTH CENTURY

The British analysis of magnetic disturbances was statistical. It was assumed that the signals originated in motion of a conducting part of the atmosphere. The synching of signals with lunar or solar phase makes a statistical approach natural. Unsurprisingly, Chapman wanted to look at the disturbed magnetic signals in a similar way. This was not the approach of the Scandinavians who lived under the aurora and saw it night by night.

Kristian Birkeland is one of Norway's greatest scientists. He was born in 1867 in Kristiania, later to become Oslo. From a comfortable background, his exceptional nature showed early on. After university in Kristiania, in 1893, he left to go to Paris to study at the Ecole Polytechnique where his initial interest was in the new science of electromagnetism coming from Maxwell's unifying equations. After travel elsewhere in Europe he returned to Norway to become the youngest professor in the university in Kristiania.

Even for a Norwegian from as far south as present-day Oslo, the aurora is a natural interest. Until the nineteenth century the aurora was often assumed to be an atmospheric effect. Despite the concurrent auroral disturbances in the great magnetic storm of 1859 referred to above, the question of auroral origin and any electromagnetic effect or link to the Sun appears not to have been examined much further in the UK. It was Birkeland who picked up the scientific challenge of explaining the aurora.

Birkeland's life and work are ably discussed in Egeland and Burke's monograph (Egeland and Burke, 2005). When he returned to Norway, Birkeland was thoroughly

grounded in electromagnetism and experimental technique. Moreover, he was well aware of the new discovery of the electron by J. J. Thompson in 1897. He suspected that this new physics may contain an explanation of auroral origin. Never a man to shy from experimental work or observation, he organized a series of expeditions to northern Norway and arranged subsidiary observations elsewhere in Russia and Iceland. Although the first expedition was abandoned through extreme weather, the work established over time a vast body of observations documented in a series of volumes (Birkeland, 1901, 1908, 1913). The height of the aurora was shown to be around 100km. The electromagnetic nature of the aurora itself was firmly established by showing that horizontal currents, the auroral electrojet, flow in the actual displays. Birkeland speculated that the source of the auroral light is due to electrons of extraterrestrial origin impacting the upper atmosphere. He had constructed a model Earth in a vacuum chamber (a *terrella*) and on exposing it to a beam of electrons succeeded in creating a ring of light around the magnetic poles, mimicking the shape of the actual auroral zone. He sent a paper to *Nature* advancing his idea that the aurora represents incident beams of electrons of solar origin. At this point, fate intervened as the paper was sent to Arthur Schuster to referee. Schuster recommended rejection as he pointed out that the beam of negatively charged particles would be quenched by an electric field as the Sun would charge positive and the Earth charge negative. Birkeland recognized that the argument was correct and immediately modified the idea to propose an electrically neutral stream of charged particles from the Sun, i.e. what is now called plasma. Possibly stung by the rejection, Birkeland never resubmitted the modified idea to *Nature* but included it in the formal reports of the expeditions. The report published in 1908 (Birkeland, 1908) included a sketch like that reproduced in Figure 1.1 (from Southwood, 2015). Diagrams such as this, showing downward current entering the upper atmosphere at one longitude, flowing through it horizontally and leaving by an upward return current at a separate longitude, are now commonplace. Birkeland had made the first sketch of the three-dimensional electrical current system of an auroral disturbance. The sketch would be recognized today.

#### 1.4. SCHISM

*Nature* is a British journal and, in the early years of the twentieth century, Britain was possibly the most important scientific nation. It seems likely that had Birkeland's corrected idea been published in the British literature, it might have forestalled what became a major schism in the science community. Part of the problem was philosophical but Southwood and Brekke (2017) suggest that

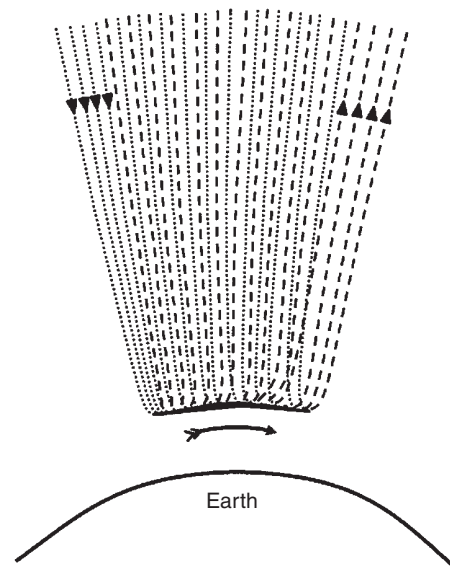


**Figure 1.1** Reproduction from Southwood (2015) of the sketch on p. 105 of Volume 1 of Birkeland's report on the 1902–1903 polar expeditions (Birkeland, 1908). It is not quite clear in Birkeland's text, but the dotted and dashed lines represent the streaming charges of opposite sign in a charge neutral stream from the Sun.

part was personal embarrassment for a man who was fast becoming the dominant British name in the field. As already noted, Chapman (1919) had made a major analysis of magnetic data associated with what had been identified as the disturbed time current system. However, the paper included an appendix that put forward the same idea that Birkeland had originally propounded more than a decade before. Chapman proposed that the disturbances were due to electrons incident on the atmosphere. The error was caught rapidly after publication by Lindemann (1919), who published a critique effectively suggesting, as Birkeland had done already, that there might be a neutral stream of positive and negatively charged particles from the Sun. Southwood (2015) pointed out that, although Chapman was most likely unaware of Birkeland's idea, Schuster (1911) appeared to have grasped the idea. However, after 1919, British references [and even American references (e.g. Parker, 1969)] attribute the neutral stream notion to Lindemann.

The antipathy between the British and Scandinavian schools continued for around 40 years until sophisticated results from space brought it to an end. The discussion by Fukushima (1994) is informative. Chapman felt statistical information was fundamental. He also had a mathematical reason for ignoring the possibility of currents flowing into and out of the upper ionized atmosphere, the ionosphere. It was a uniqueness theorem. The magnetic perturbations recorded on the surface of the Earth could always be attributed to a unique set of currents in the conducting

ionosphere if it was assumed no current flowed in and out of the top of the ionosphere. For any given field pattern these were referred to as the equivalent current system. There had, nonetheless, been work by Vestine and Chapman (1938) that purported to show that the purely horizontal current model of Chapman fitted data better. Fukushima (1969) showed that the model proposed by Vestine and Chapman to represent that of Birkeland was somewhat unreasonable. Changing the assumption to something more rational revealed that there was little to choose between the systems. Fukushima (1971) further showed explicitly that the current system above the ionosphere is shielded from the ground, i.e. undetectable.

### 1.5. CHAPMAN-FERRARO: A CAVITY IN A STREAM OF CHARGED PARTICLES FROM THE SUN

In 1927, V. C. A. Ferraro began postgraduate study with Chapman at Imperial College London. Chapman's earlier work had shown that a geomagnetic storm began with an increase of the magnetic field worldwide. The delay between evidence of anything occurring on the Sun and the arrival emphasized that the solar-terrestrial connection was not through electromagnetic radiation but was transmitted via material (corpuscular) means. Chapman gave Ferraro the magnetic storm problem to study (Ferraro, 1969). He was to examine the effect of a neutral unmagnetized stream of charged particles from the Sun impinging on the terrestrial magnetic field (Chapman and Ferraro, 1930, 1931, 1932, 1933). The theory preceded any notion of magnetohydrodynamics and frozen-in magnetic field; space between the Earth and the Sun was treated as unmagnetized. The stream was shown to enclose the geomagnetic field in a cavity. This was the first identification of a terrestrial magnetic domain that would eventually be named the magnetosphere. The geomagnetic field cavity was bounded by a current sheet now called the magnetopause. The confinement of the terrestrial field within a bubble within the stream well explained the existence of a terrestrial magnetic cavity, whose internal field would increase if increased outflow occurred from the Sun. The mathematical solution used to illustrate the magnetic confinement used a two-dimensional image dipole, as shown in Figure 1.2. 30 years later, Jim Dungey published an analytic two-dimensional solution of the Chapman-Ferraro problem in 1961 (Dungey 1961a). By then, computers had advanced enough that three-dimensional numerical solutions were about to appear (Spreiter and Briggs, 1962).

Unfortunately, as it stood, the Chapman-Ferraro model did not explain much more about magnetic storms than the increase in global field at storm onset. One feature of the model is the points marked Q in Figure 1.2, where the

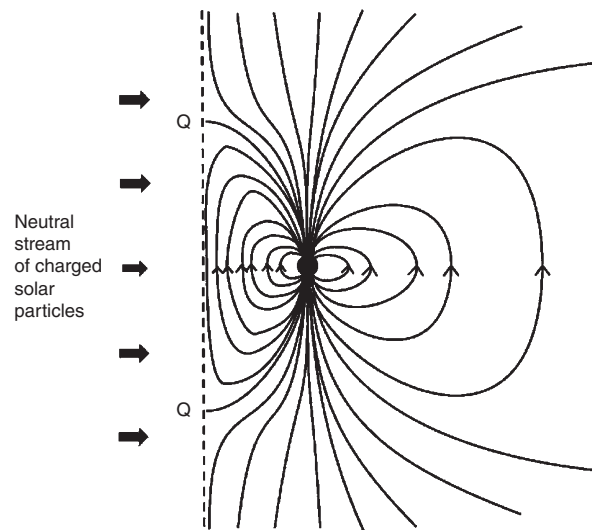


**Figure 1.2** The Chapman-Ferraro cavity. Reproduction of Chapman and Ferraro's sketch of the noon-midnight meridian of the enclosure of the Earth's field by a neutral stream of solar charged particles. The field pattern shown is produced by an image dipole on the left hand side. The letters Q mark magnetic neutral points on the boundary.

field goes to zero. It was recognized that particles might enter the cavity here and guided by the field would impinge on the atmosphere at auroral latitudes. Nevertheless, although the latitude was right, there was no mechanism to explain how the aurora was seen on the nightside.

A second major problem was that after the initial increase in terrestrial field in the main phase of a geomagnetic storm, the field was depressed generally by a much larger amount than the initial enhancement. Daglis et al. (1999) note that the depression of the field in the main phase had been known since the nineteenth century. (Fitzgerald, 1892), Chapman (1919), and, two years earlier, Schmidt (1917) had suggested that the depression was due to solar charged particles encircling the Earth. Chapman and Ferraro's theory did propose that solar particles somehow progressively penetrated to the terrestrial magnetic cavity so that the current built up but understanding would really only arrive once a significant external field was allowed for.

### 1.6. ALFVÉN: THEORY OF STORMS AND THE ADVENT OF MAGNETOHYDRODYNAMICS

In the 1940s, Hannes Alfvén and his research group based in Stockholm became the major proponents of the Scandinavian school.

Alfvén (1939, 1940) proposed a new storm model focused on explaining the access of charged particles to make the ring current and the aurora. It was wrong, partly due to a complete rejection of Chapman's ideas. The

theory assumed that a magnetized incident charged particle stream was able to simply flow onto the Earth field. In other words, there was no allowance for a magnetopause.

Alfvén himself was a great admirer of Birkeland and the model does resemble a development of his ideas. The model also introduced the important idea of there being an electric field within the terrestrial environment due to the solar interaction, effectively placing a voltage imposed from outside on the terrestrial system. The induced electric field meant that there was a potential for the solar material to do work on the terrestrial system. In practice, the absence of inclusion of the effects that cause the magnetopause to form meant that Alfvén's electric field was in the wrong direction. Nevertheless, its introduction was important.

In 1942, Alfvén made an enormous step in a short *Nature* paper (Alfvén, 1942), which introduced the idea of the magnetic field being frozen into a perfectly conducting medium like a plasma. This is seen as the invention of magnetohydrodynamics (MHD). It explained the magnetized nature of any plasma flowing from the Sun (as Alfvén's storm model required) but it also gave an intuitive way to see the formation of a current sheet or magnetopause between solar and terrestrial plasma (which Alfvén's storm model had ignored).

### 1.7. THE SPACE AGE BEGINS

The Chapman–Ferraro model made it appear too hard for solar plasma to enter the terrestrial magnetic environment and Alfvén's appeared to make it too easy. It was another twenty years before the seeds of what is now the generally accepted model were sown. By that time the space age had begun and much new information was emerging.

At the beginning of the 1950s, Biermann (1951) had deduced the presence of the solar wind from the behavior of comet tails. Parker (1958) further explained that not only was its flow supersonic but also it would be magnetized. In 1958 also, the magnetosphere received its name from Gold (1959). Gold's paper was motivated by the first major discovery of the space age, the Van Allen radiation belts (Van Allen and Frank, 1959). Despite the fact that retrospectively it was seen that Sputnik 2 had measured them (Dessler, 1984), the first reports were from the first US Earth orbiting spacecraft, Explorer 1. Out in space it was found that the distant magnetic dipole field of the Earth was adequate to trap a large amount of energetic charged particles. Gold (1959) introduced a very important concept, the interchange motion of flux tubes. Unfortunately, because he attributed the charged particles to a source near Earth [the cosmic ray albedo neutron decay theory, CRAND see e.g. Singer (1958), Vernov et al., (1959)], his paper was in error. He proposed that the creation of radiation belt particles near Earth would induce a

natural overturning motion in magnetospheric magnetic flux tubes wherein denser tubes move outwards and emptier tubes move in. The CRAND source can remain relevant to the highest energy particles (see e.g. Li et al., 2017). However, most of the radiation belt particles and the lower energy particles that are responsible for carrying the ring current originate from the solar environment. Kellogg (1959) first suggested a solar source for the Van Allen particles. The external source means that the particles are injected and energy must be supplied for the injection process. This is a driven interchange motion (cf. Southwood and Kivelson, 1989). The energy is in practice provided from the solar wind through part of the Birkeland current system discussed later.

Also in 1959, Dessler and Parker (1959) made a major breakthrough in understanding the main phase of geomagnetic storms. They proposed that solar plasma entry to the magnetosphere was enhanced following the initial compression of the magnetosphere at the start of a storm because the boundary of the magnetosphere would be unstable. They then derived a relation between the depression in the field and the energy of the charged particles trapped in the magnetospheric field for two special phase space distributions of particles, which was generalized by Scokopke (1966). The idea of enhanced solar particle entry during main phase producing a ring current around the Earth was right but the entry process remained to be identified.

We shall return to discuss particle injection and transport after introducing the open magnetosphere model next.

### 1.8. DUNGEY: THE OPEN MAGNETOSPHERE

Dungey freely admitted that his open magnetospheric model (Dungey 1961b) was inspired by the similarity between the ionospheric *DS* disturbed time current pattern and the motion in a stirred cup of coffee (Stern, 1986). As he stirred milk into the coffee by moving his spoon across the center of the cup he noted the circulation pattern resembled that in Figure 1.3.

Dungey had studied for a PhD ten years earlier working on an idea of Hoyle's that aurorae might originate from acceleration at magnetic neutral lines that would form between a terrestrial dipole field and a uniform exterior field (Stern, 1986). Crucially he realized in 1960 that the magnetic configuration would allow the solar wind to drive the familiar *DS* current system in the ionosphere.

By 1960, MHD was the way people thought; the frozen-field idea is built into Dungey's model. However, MHD is an approximation and will break down wherever the field is very small or varies rapidly on the scale of charged particle Larmor radii. Reconnection corresponds to one form of breakdown. Dungey's doctoral work (Dungey, 1950)

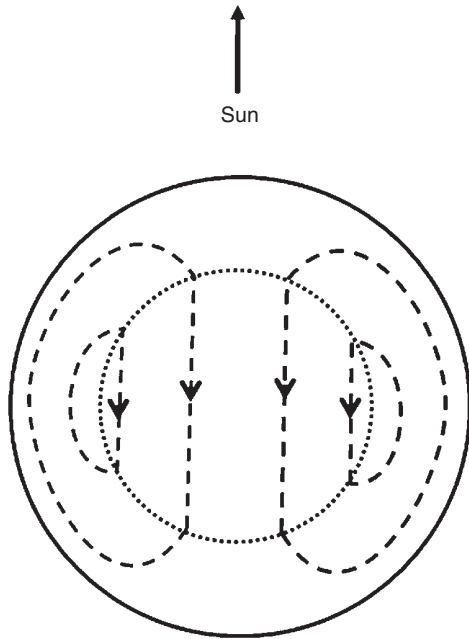
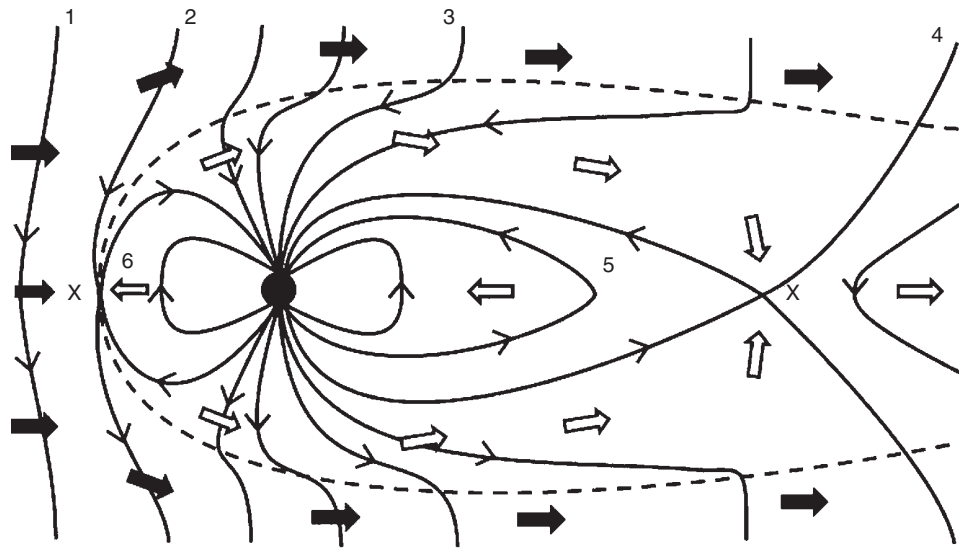


**Figure 1.3** The ionospheric DS flow pattern. The antisunward motion at high latitudes and the return at reminded Dungey of the pattern from stirring coffee.

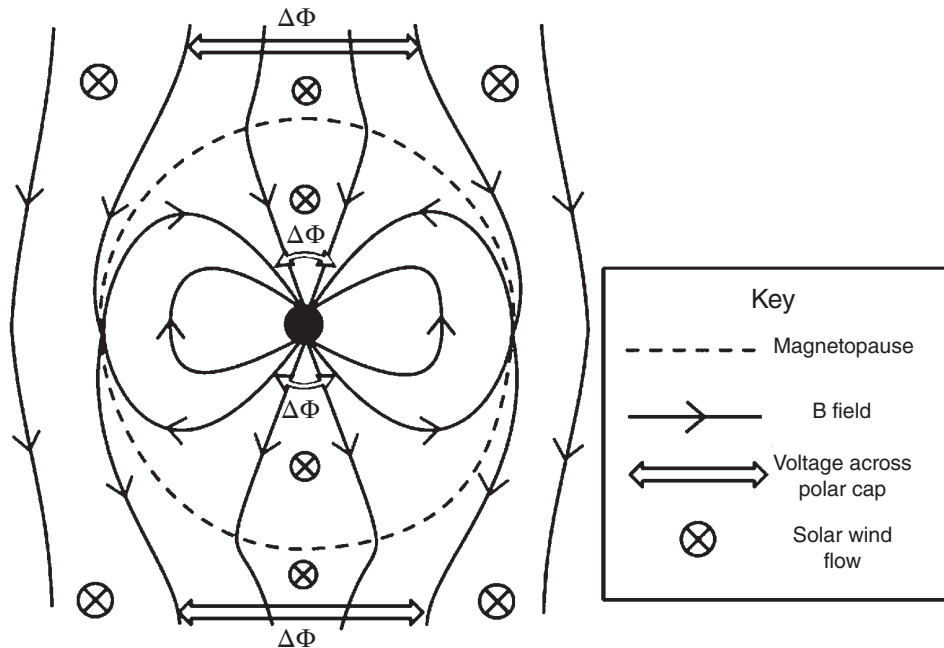
had introduced the idea of magnetic reconnection. Near neutral points in the magnetic field, the frozen-in field is no longer valid and field lines can be “broken.” The final element of the new model was magnetic reconnection.

Figure 1.3 reproduces an idealized form of the ionospheric flow showing the *DS* pattern. The sketch is a polar view of the northern hemisphere with the dashed lines representing the ionospheric plasma stream lines deduced from the magnetic perturbations measured at the Earth’s surface. There is a twin vortex flow. The dotted boundary marks where the flow switches from sunward on the equatorward side to antisunward poleward. Dungey suggested that sunward momentum was transferred along the magnetic field to drive the antisunward flow in the polar region. There would be a return sunward flow at low latitudes. The flow represents equipotentials of the ionospheric electric field. It is important to note that the electric field induced in the low latitude subauroral regions is opposite to that proposed by Alfvén (1940) and the flow is opposite to what would have been the overall pattern produced by the Gold (1959) mechanism.

Figure 1.4 shows the circulation of flux tubes in the noon–midnight meridian in the open model. The figure is shown with a southward interplanetary field component, the simplest case as it is symmetric. The magnetic field threads the magnetopause shown by the dashed line. Throughout the flow is marked by white arrows in the



**Figure 1.4** Dungey’s open magnetosphere. The simplest case of a purely southward interplanetary field (IMF) is assumed. The sketch is drawn in the noon–midnight meridian. The dashed curve represents the magnetopause. The dark arrows represent the solar wind flow, open arrows the flow induced in the terrestrial environment. Dayside and nightside magnetic reconnection occurs at the locations indicated by X. The numbers represent the envisaged field line motion sequence in steady state: solar wind (1), dayside reconnection (2), polar cap connection (3), tail reconnection (4), nightside inward motion (5), dayside outward motion to reconnection once more (6). The sketch is schematic as the tail on the nightside extends  $>100 R_E$  ( $R_E$  = Earth radius) (Dungey, 1965).



**Figure 1.5** Dawn–dusk meridian view of open magnetosphere with pure southward external field. The solar wind flow is into the page. The solar wind electric field voltage  $\Delta\Phi$  is projected down the (equipotential) field lines of the polar cap to the polar ionosphere.

interior of the magnetosphere. Field lines and plasma move as a whole as the field is frozen into the motion. The exception is in the two places marked by X where reconnection occurs. Here the field lines break and reconnect. Numbers on the figure outline how a single field line evolves in a steady configuration with reconnection occurring on the dayside (2), nightside (4) to dayside reconnection once more (6). Plasma inflow towards the center of the tail from each tail lobe is balanced by accelerated outflows towards the Earth and down tail. The antisolar flow is on the field in the polar cap. The black arrows represent the solar wind flow. The direct connection of the solar wind magnetic field to the polar cap magnetic field is what causes the polar cap antisolar flow. At lower latitudes the sunward flow returns magnetic flux to the dayside reconnection point.

The dawn–dusk elevation of the Dungey model is shown in Figure 1.5 in the simplest purely southward external field case. In this sketch, the electric field configuration is illustrated. In the steady state the flowing plasma and the southward field in the solar wind give rise to an eastward electric field and a potential drop along the neutral line where reconnection takes place. That potential is projected into the polar cap along the field lines as indicated in the sketch.

A further sketch is shown in Figure 1.6, which illustrates the resulting current system in the ionosphere due to the electric potential imposed across the ionosphere

at the feet of the flux tubes in the ionosphere. The continuous arrowed thin lines in Figure 1.6 represent the ionosphere Hall current. It is assumed, once again for simplicity, that the ionosphere has a uniform conductance. The Hall current is in precisely the opposite sense to the double vortex flow system that Dungey envisaged would be induced by momentum transfer from the solar wind in the ionosphere. The Hall current is nondissipative. However, there is also a dissipative current, the Pedersen current, in the direction of the imposed electric field. The Pedersen current flow is indicated by dashed arrowed lines. It can be seen from the arrows that the Pedersen current changes sense as one crosses the location represented by the thick oval curve. On magnetohydrodynamic time scales, electrical currents are divergence-free. Accordingly, the net inflow or outflow of horizontal current that occurs in the oval region means that there has to be current flow along (up or down) the magnetic field here. These are the currents postulated by Birkeland (1908) and are commonly called Birkeland currents. Localized magnetic perturbations were directly observed above the auroral zone in 1966 (Zmuda et al., 1967) and linked to Birkeland's original proposal by Cummings and Dessler (1967).

Comparison of Figures 1.5 and 1.6 shows that the Birkeland currents connect the voltage associated with the solar wind motion to an ionospheric load represented by the dissipative Pedersen conductance.

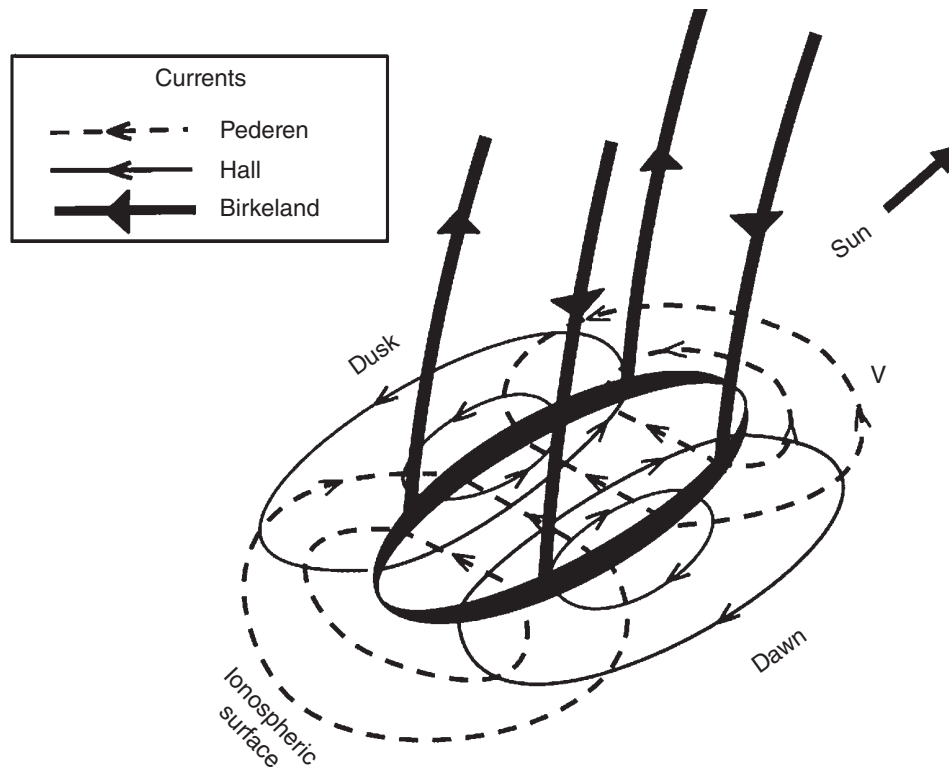


**Figure 1.6** Sketch of the currents induced in the ionosphere in the simple (southward IMF) open magnetosphere. The Pedersen currents are discontinuous at the oval curve, which corresponds to the auroral zone. The field aligned Birkeland current flow in/out at the discontinuity. The field lines poleward of the oval are open and extend into interplanetary space. Equatorward the field lines go from northern to southern hemisphere and so are closed. Comparing the configurations of Figures 1.5 and 1.6 shows that the ionosphere acts as a load on the solar wind.

MHD treats the electric field parallel to the background field as negligible, so the Birkeland currents might seem to be nondissipative. This is not necessarily so. The electrons everywhere would need to be infinitely mobile. Current (i.e. electrons) is drawn along the field simply to ensure that overall currents close. As long as there is a reservoir of cold electrons such as in the ionosphere, this can be achieved with very small voltages. However, where the large-scale current flow requires upward current and accordingly downward motion of electrons from a magnetospheric source, substantial voltages may be needed. The basic calculation was surprisingly late in coming (Knight, 1973). The acceleration of electrons down into the ionosphere provides aurora and also can excite radio waves (auroral kilometric radiation) (Gurnett, 1974).

### 1.9. PARTICLE TRANSPORT IN THE OPEN MODEL

In 1963 came the first detection of the boundary of the magnetosphere, the magnetopause (Cahill and

Amazeen, 1963). Dungey's sketch in the 1961 paper did not show a sharp boundary between solar and terrestrial regimes and there were those who saw the sharp boundary predicted by Chapman and Ferraro as evidence against an open model, regardless of the fact that it was clear that some form of particle entry had to occur. Of course, the interplanetary field is rarely purely southward. The simple symmetry of the internal magnetospheric circulation in the open model outlined in Figures 1.3–1.6 here is modified and skewed by addition of eastward, westward or radial external fields (see e.g. Cowley 1981a, 1981b). One should also note that the diagram in Figure 1.4 is schematic. It may be topologically correct but, in truth, the magnetic field is very distended on the nightside, a region known as the geomagnetic tail with a thin neutral sheet in the center. Nightside reconnection takes place in the sheet and plasma, which has entered by moving along the field in the polar cap, may be accelerated there.

The first evidence that Dungey's model magnetosphere was sound came in the mid-1960s from experimental evidence (Fairfield and Cahill, 1966) that geomagnetic activity increased with a southward interplanetary magnetic

field component. However, the reconnection model was slow in gaining wide acceptance.

The open magnetosphere provided a straightforward explanation for not only entry of plasma from the solar environment but also for acceleration and heating. In a steady-state picture of a circulation of plasma we have already described, the plasma contained on the closed flux tubes moving towards the Earth from the tail encounters flux tubes of decreasing volume. As a result, it is heated adiabatically i.e. because it is isolated thermally, its accessible phase space volume is constant; decreasing physical volume means increased thermal motion. The inward motion is the driven interchange motion referred to earlier and the adiabatic process was described by Gold (1959). Gold's envisaged motion was outward and spontaneous. The fact that the inward moving plasma is heated is the reason that the motion must be driven with energy ultimately coming from the solar wind. Because the motion of the plasma is collision-free, the energy gain as particles are moved towards the Earth is pitch angle dependent. Two adiabatic invariants, the magnetic moment and longitudinal invariant describe the motion transverse to the field and along the field respectively. The longitudinal invariant governs plasma motion along the field. The invariant appears misnamed in a magnetospheric context, as the corresponding particle motion is the bounce motion between magnetic mirrors back and forth in latitude along the magnetic field. It was originally derived in the controlled nuclear fusion program, where the corresponding motion was along the device. Detailed analysis of the adiabatic motion with the two invariants mentioned as well as a third, the flux invariant associated with drift around the Earth, was worked out in the 1950s. An excellent theoretical overview is given by Northrop and Teller (1960). Nakada et al. (1965) organized spacecraft energetic particle data to derive the phase space distribution using the first two invariants and showed explicitly that the source was external.

Each invariant has an associated periodic motion. In practice, solar wind magnetosphere coupling is not steady. The magnetospheric circulation proceeds in fits and starts, mostly on time scales short compared with the time charged particles take to move around the Earth. This means that the injection of particles from the tail in the closed field region takes place in a sporadic manner. As a result, within the closed field region the motion of many of the energetic particles that make up the ring current and the radiation belts is best described as a diffusion. Particle radial motion is a random walk as particles move in or out according to where they are in their drift phase as solar terrestrial coupling varies. An early comprehensive study is given in Schulz and Lanzerotti (1974).

If the field varies on a time or space scale comparable with the Larmor gyration the moment invariant is

violated and, similarly, variation on the bounce time scale will change the longitudinal invariant. It follows that plasma waves at frequencies near the electron or ion gyro-frequency can modify the magnetic moment and produce scattering in pitch angle. With a small enough pitch angle, energetic charged particles are lost as their mirror points become of low enough altitude that they collide with atmospheric neutrals. An early analysis of the coupling between pitch angle scattering and background wave instability was done by Kennel and Petschek (1966), who used the approach to derive a limit on stably trapped particle flux that fitted well with energetic particle data from the early Explorer 12 and 14 spacecraft.

In practice, the solar terrestrial interaction occurs on several time scales. A solar wind pressure increase will produce an increase in the Earth's field worldwide, known as a storm sudden commencement in minutes. Subsequently, changes in the direction of the interplanetary field will produce a series of bursts of magnetosphere wide flow driven by the solar wind from the polar cap, as described in the previous section. These are also the fits and starts referred to above. Akasofu and Chapman (1961) introduced the term substorm to describe this. They pointed out that the phenomenon whose time scale is typically around two hours had originally been identified by Birkeland (1908) as a polar elementary storm. Plasma injection and heating occur with each substorm, eventually building up a ring current around Earth over a day or two. The ring current carried by the injected particles provides the geomagnetic field depression which characterizes the storm main phase.

## 1.10. CONCLUDING REMARKS

By around 1970 or so, not only had the basic geography of the magnetosphere been established but also a lot of the ground work had been done for understanding how it worked. However, an honest history needs to note that there was still a large degree of controversy. Indeed, much of this was echoing the Scandinavian–Anglo-Saxon schism of the 1940s and 1950s. It was not generally seen that Dungey's open magnetosphere model brought critical aspects of both models together. For instance, a final important morphological discovery in 1971 was of magnetosheath plasma penetrating deep in the terrestrial field, the polar cusp (Heikkila and Winningham, 1971; Frank, 1971). Despite the known presence of an external field, many immediately identified the result with the likely entry of plasma through the Chapman–Ferraro neutral points (marked Q in Figure 1.2). Moreover, an early paper by Russell et al. (1971) even contained the tantalizing information that the cusp appeared to move up or down in latitude as the external field turned northward or southward. Nevertheless, the paper made no reference

to the Dungey model. Similarly, in the previous year a paper by Aubry et al. (1970) had shown the magnetopause eroding at low latitudes in the presence of a southward external field but also mentioned neither Dungey nor reconnection. Reconnection had become a controversial term in magnetospheric physics at this time (Southwood, 2015). The final denouement of the Dungey open reconnection model of the magnetosphere had to await the direct high resolution observations of heating and plasma acceleration in the magnetopause in conditions precisely consistent with reconnection by the ISEE (International Sun Earth Explorer) 1 and 2 spacecraft (Paschmann et al., 1979).

### ACKNOWLEDGMENTS

Work at Imperial College was supported by UK STFC Grants ST/K001051/1 and ST/N000692/1.

### REFERENCES

- Akasofu, S.-I., and S. C. Chapman (1961), The ring current, geomagnetic disturbance and the Van Allen radiation belts, *J. Geophys. Res.*, 66, 1321–1350.
- Alfvén, H. (1939), A theory of magnetic storms and of the aurorae, *K. Sven. Vetenskapakad. Handl., Ser. 3*, 18(3), 9. (Reprinted in part with comments by Alex Dessler and John Wilcox in *Eos*, 51, 180–194, 1970.)
- Alfvén, H. (1940), A theory of magnetic storms and of the aurorae, II, The aurorae; III, The magnetic disturbances. *K. Sven. Vetenskapakad. Handl., Ser. 3*, 18(9).
- Alfvén, H. (1942), Existence of electromagnetic-hydrodynamic waves, *Nature*, 150, 405, doi:10.1038/150405d0.
- Aubry, M. P., C. T. Russell, and M. G. Kivelson (1970), Inward motion of the magnetopause before a substorm, *J. Geophys. Res.*, 75, 7018–7031, doi: 10.1029/JA075i034p07018.
- Biermann L (1951), Kometenschweife und Korpuskularstrahlung, *Z. Astrophys.*, 29, 274–286.
- Birkeland, K. (1901), Expedition Norvegienne de 1899–1900 pour l'étude des aurores boréales, Videnskapsselskapets skrifter. 1, Matematisk Naturvidenskapelig Klasse, 1901, No.1, En Commission chez Jacob Dybwad, A. W. Brogger, Christiana, Norway.
- Birkeland, K., (1908), The Norwegian Aurora Polaris Expedition, 1902–1903, vol. I, section 1. H. Aschehoug, Oslo.
- Birkeland, K. (1913), The Norwegian Aurora Polaris Expedition, 1902–1903, vol. I, section 2. H. Aschehoug. Oslo.
- Cahill, L. J., Jr., and P. G. Amazeen (1963), The boundary of the geomagnetic field, *J. Geophys. Res.*, 68(7), 1835–1843, doi.org/10.1029/JZ068i007p01835.
- Carrington, R. C. (1860), Description of a singular appearance seen in the Sun on September I, 1859, *Mon. Not. R. Astron. Soc.*, 20, 13–15.
- Chapman, S. C. (1913), On the diurnal variations of the earth's magnetism produced by the moon and sun, *Phil. Trans. R. Soc. Lond. A*, 213, 279–321.
- Chapman, S. C. (1919), An outline of a theory of magnetic storms, *Proc. R. Soc. Lond. A*, 95, 61–83.
- Chapman, S. and V. C. A. Ferraro (1930), A new theory of magnetic storms, *Nature*, 126, 129–130.
- Chapman, S. and V. C. A. Ferraro (1931), A new theory of magnetic storms, I, The initial phase, *Terr. Magn. Atmos. Elect. (now J. Geophys. Res.)*, 36, 77–97, 171–186.
- Chapman, S. and V. C. A. Ferraro, (1932) A new theory of magnetic storms, I, The initial phase (continued), *Terr. Magn. Atmos. Elect. (now J. Geophys. Res.)*, 37, 147–156, 421–429.
- Chapman, S. and V. C. A. Ferraro (1933), A new theory of magnetic storms, II, The main phase, *Terr. Magn. Atmos. Elect. (now J. Geophys. Res.)*, 38, 79–96.
- Cowley, S. W. H., (1981a), Magnetospheric asymmetries associated with the Y-component of the IMF, *Planet. Space Sci.*, 29, 79.
- Cowley, S. W. H. (1981b), Asymmetry effects associated with the X-component of the IMF in a magnetically open magnetosphere, *Planet. Space Sci.*, 29, 809.
- Cummings, W. D., and A. J. Dessler (1967), Field-aligned currents in the magnetosphere, *J. Geophys. Res.*, 72(3), 1007–1013, doi: 10.1029/JZ072i003p01007.
- Daglis, I. A., R. M. Thorne, W. Baumjohann, and S. Orsini (1999), The terrestrial ring current: Origin, formation, and decay, *Rev. Geophys.*, 37(4), 407–438, doi: 10.1029/1999RG900009.
- Dessler, A.J. (1984), The Vernov Radiation Belt (Almost), *Science*, 226, 915.
- Dessler, A. J., and E. N. Parker, (1959), Hydromagnetic theory of geomagnetic storms, *J. Geophys. Res.*, 64, 2239–2252.
- Dungey, J. W. (1950), Some researches in cosmic magnetism. PhD thesis, Cambridge University.
- Dungey, J.W. (1961a), The steady state of the Chapman Ferraro problem in two dimensions, *J. Geophys. Res.*, 35, 1043.
- Dungey, J. W. (1961b), Interplanetary magnetic field and the auroral zones, *Phys. Rev. Lett.*, 6, 47–48.
- Dungey, J. W. (1965), The length of the magnetospheric tail, *J. Geophys. Res.*, 70(7), 1753–1753, doi: 10.1029/JZ070i007p01753.
- Egeland A., and W.J. Burke (2005), Kristian Birkeland, The First Space Scientist. Astrophysics and Space Science Library, Springer, Dordrecht.
- Fairfield, D.H., and L. J. Cahill Jr. (1966), Transition region magnetic field and polar magnetic disturbances, *J. Geophys. Res.*, 71, (1), 155–169, doi:10.1029/JZ071i001p00155.
- Ferraro, V. C. A. (1969), The birth of a theory. In S.-I. Akasofu, B. Fogle, and B. Haurwitz (Eds.), *Sidney Chapman, Eighty* (pp. 14–18). University of Colorado Press, Boulder.
- Fitzgerald, G. F. (1892), Sunspots and magnetic storms, *The Electrician*, 30, 48.
- Frank, L. A. (1971), Plasma in the earth's polar magnetosphere, *J. Geophys. Res.*, 76, 5202–5219.

- Fukushima, N. (1969) Equivalence in ground geomagnetic effect of Chapman-Vestine's and Birkeland-Alfvén electric current-systems for polar magnetic storms, *Rep. Ionos. Space Res. Jap.*, 23, 219–227.
- Fukushima, N. (1971), Electric current systems for polar substorms and their magnetic effect below and above the ionosphere, *Radio Science*, 6, 269–275, doi.org/10.1029/RS006i002p00269.
- Fukushima, N. (1994), Some topics and historical episodes in geomagnetism and aeronomy, *J. Geophys. Res.*, 99(A10), 19113–19142.
- Gold, T. (1959), Motions in the magnetosphere of the Earth, *J. Geophys. Res.*, 64, 1219–1224.
- Gurnett, D. A. (1974), The Earth as a radio source: Terrestrial kilometric radiation, *J. Geophys. Res.*, 79, 4227–4238.
- Heikkila, W. J. and J. D. Winningham (1971), Penetration of magnetosheath plasma to low altitudes through the dayside magnetospheric cusps, *J. Geophys. Res.*, 76, 883–891.
- Kellogg, P. J., (1959), Van Allen radiation of solar origin, *Nature*, 183, 1295–1297.
- Kelvin, Lord W. T. (1892), Royal Society Presidential Address, *Nature*, 47, 107–110.
- Kennel, C. F., and Petschek, H. E. (1966), Limit on stably trapped particle fluxes, *J. Geophys. Res.*, 71(1), 1–28.
- Knight, S. (1973), Parallel electric fields, *Planet. Space Sci.*, 21, 741–750.
- Li, X., R. Selesnick, Q. Schiller, K. Zhang, H. Zhao, D. N. Baker, and M. A. Temerin, (2017), Measurement of electrons from albedo neutron decay and neutron density in near-Earth space, *Nature*, 552, 382–385.
- Lindemann F A (1919), Note on the theory of magnetic storms, *Phil. Mag.*, 38 669–684.
- Matsushita S. (1968), Sq and L Current Systems in the Ionosphere, *Geophys. J. R. Astr. Soc.*, 15, 109–125.
- Nakada, M.P., J. W. Dungey and W.N. Hess (1965), On the origin of outer-belt protons, 1, *J. Geophys. Res.*, 70, 3529–3532.
- Northrop, T. G. and E. Teller (1960), Stability of the adiabatic motion of charged particles in the Earth's field, *Phys. Rev.*, 117, 215–225, doi/10.1103/PhysRev.117.215.
- Parker E. N., (1958), Dynamics of the interplanetary gas and magnetic fields, *Astrophys. J.*, 128, 664–676. doi: 10.1086/146579
- Parker, E. N. (1969), Geomagnetism and solar physics. In S.-I. Akasofu, B. Fogle, and B. Haurwitz (Eds.), *Sidney Chapman, Eighty*, pp. 24–26. University of Colorado Press, Boulder.
- Paschmann, G., B. U. Ö. Sonnerup, I. Papamastorakis, N. Scokopke, G. Haerendel, S. J. Bame, et al. (1979), Plasma acceleration at the Earth's magnetopause: Evidence for reconnection, *Nature*, 282, 243–246, doi:10.1038/282243a0.
- Russell, C. T., C. R. Chappell, M. D. Montgomery, M. Neugebauer, and F. L. Scarf (1971), Ogo 5 observations of the polar cusp on November 1, 1968, *J. Geophys. Res.*, 76, 6743–6764, doi: 10.1029/JA076i028p06743.
- Sabine, E. (1852), On periodical laws discoverable in the mean effect of the larger magnetic disturbances, *Phil. Trans. R. Soc. Lond.*, 142, 103–124.
- Sabine, E. (1861), On the lunar-diurnal variation of the magnetic declination obtained from the Kew photograms in the years 1858, 1859, and 1860, *Proc. Roy. Soc.*, 11, 73–80.
- Schmidt, A. (1917), *Erdmagnetismus in Enzyklopidie der Mathematischen Wissenschaften no. 1. VI*, Leipzig, Germany.
- Schulz, M., and L. J. Lanzerotti (1974) *Radial Diffusion in the Radiation Belts (Physics and Chemistry in Space Vol 7)*, pp 1–216. Springer-Verlag, N.Y.
- Schuster, A. (1911), On the origin of magnetic storms, *Proc. Roy. Soc. Lond.*, 85, 44–50, doi:10.1098/rspa.1911.0019.
- Schuster, A., and H. Lamb (1889), The diurnal variation of terrestrial magnetism, *Phil. Trans. R. Soc.*, A180, 467–512.
- Scokopke, N. (1966), A general relation between the energy of trapped particles and the disturbance field near the Earth, *J. Geophys. Res.*, 71, 3125–3130.
- Singer, S. F. (1958), Trapped albedo theory of the radiation belt, *Phys. Rev. Lett.*, 1, 181.
- Southwood, D.J. (2015) From the Carrington storm to the Dungey magnetosphere. In D. J. Southwood, S. W. H. Cowley, and S. Mitton (Eds.), *Magnetospheric plasma physics: The impact of Jim Dungey's research*. Springer, London, doi:10.1007/978-3-319-18359-6\_12.
- Southwood, D.J., and P. Brekke (2017), Norway's most celebrated scientist, *Astron. Geophys.*, 58, 5.28–5.31, doi.org/10.1093/astrogeof/atx174.
- Southwood, D.J., and M.G. Kivelson (1989), Magnetospheric interchange motions, *J. Geophys. Res.*, 94, 299–308.
- Spreiter, J. R., and B. R. Briggs (1962), Theoretical determination of the form of the boundary of the solar corpuscular stream produced by interaction with the magnetic dipole field of the Earth, *J. Geophys. Res.*, 67(1), 37–51, doi:10.1029/JZ067i001p00037.
- Stern, D. P. (1986), A conversation with Jim Dungey, *Eos*, 67, 1394–1395.
- Stewart, B. (1860), On the great magnetic disturbance of August 28 to September 7, 1859, as recorded by photography at the Kew Observatory, *Proc. Roy. Soc. Lond.*, 11, 407–410.
- Van Allen, J. A., and L. A. Frank (1959), Radiation around the earth to a radial distance of 107,400 km, *Nature*, 183(4659), 430–434.
- Vernov, A. N., N. L. Grigorov, I. P. Ivanenko, A. I. Lebedinskii, V. W. Murzin, and A. E. Chudakov (1959) Possible mechanism of production of terrestrial corpuscular radiation under the action of cosmic rays, *Sov. Phys. Dokl.*, 4, 154.
- Vestine, E. H., and S. Chapman (1938), The electric current-system of geomagnetic disturbance, *Terr. Magn. Atmos. Elec.*, 43, 351.
- Zmuda, A. J., J. H. Martin, and F. T. Heuring (1966), Transverse hydromagnetic disturbances at 1100 km in the auroral region, *J. Geophys. Res.*, 71, 5033–5045.



## 2

# Large-Scale Structure and Dynamics of the Magnetosphere

David G. Sibeck<sup>1</sup> and Kyle R. Murphy<sup>1,2</sup>

### ABSTRACT

Earth's magnetosphere is a dynamic system that responds to solar wind variations and exemplifies many of the physical processes that characterize the Heliophysics discipline. This chapter invokes the magnetic reconnection paradigm to describe the principle magnetospheric plasma and magnetic field regimes, first for steady state and then for time-dependent conditions, in a sequence that follows the flow of solar wind mass, energy, and momentum through the magnetosphere. This chapter provides extensive pointers to the more detailed reviews that can be found in the accompanying chapters of this volume.

### 2.1. INTRODUCTION

The Earth's magnetosphere and its immediate vicinity provide a readily accessible environment where both in situ and remote sensing observations can be used to study the fundamental physical processes governing Heliophysics. The Earth's magnetosphere, illustrated in Figure 2.1, exemplifies all of the features that distinguish the Heliophysics discipline: abrupt current sheets bound broad regions with uniform or smoothly varying parameters (Speiser, 1973); currents, magnetic flux tubes, and magnetic ropes facilitate teleconnections between widely separated regions (Crooker, 1990; Kivelson et al., 1996); shock fronts heat, decelerate, and divert plasma flows (Spreiter et al., 1966; Howe and Binsack, 1972); instability-driven waves interact with, energize, and redirect charged particles (Chapter 6, this volume); reconnection accelerates charged particles and changes global magnetic topologies (Chapter 4, this volume); energy is transferred across a broad range of spatial scales (Chapter 7, this volume); and turbulence releases energy on the smallest of spatial scales (Chapter 5, this volume), contrary to standard expectations for energy cascades.

Heliophysics itself draws upon nuclear physics, plasma physics, chemistry, spectroscopy, and other research areas to create a body of laws that describes the interaction of magnetized plasmas and neutrals with each other, with gravitating bodies and their atmospheres, and with magnetic fields (Siscoe and Schrijver, 2010). Many of the tools used to study Heliophysics, and in particular magnetospheric physics, have been borrowed from its sister disciplines, e. g. geophysics (meteorology, geomagnetism) and astrophysics. Many of the lessons learned from Heliophysics can be applied to research problems found in these sister disciplines.

Heliophysics and magnetospheric physics have practical applications for human endeavors (Song et al., 2001; Bothmer and Daglis, 2007). Earth's magnetic field shields its magnetosphere from hazardous galactic cosmic radiation and solar energetic particle events (Letaw et al., 1989) but the waves that appear in the Earth's Van Allen radiation belts deep within the magnetosphere (Horne and Thorne, 2003) as well as upstream in the foreshock (Wilson et al., 2016) can effectively energize charged particles to relativistic energies. These particles pose hazards to spacecraft operations via single event upsets, surface charging, and deep dielectric charging and discharging (Baker et al., 2018). Lower energy magnetospheric plasmas degrade solar panels and diminish power supplies.

<sup>1</sup>NASA Goddard Space Flight Centre, Greenbelt, MD, USA

<sup>2</sup>Department of Astronomy, University of Maryland, College Park, MD, USA

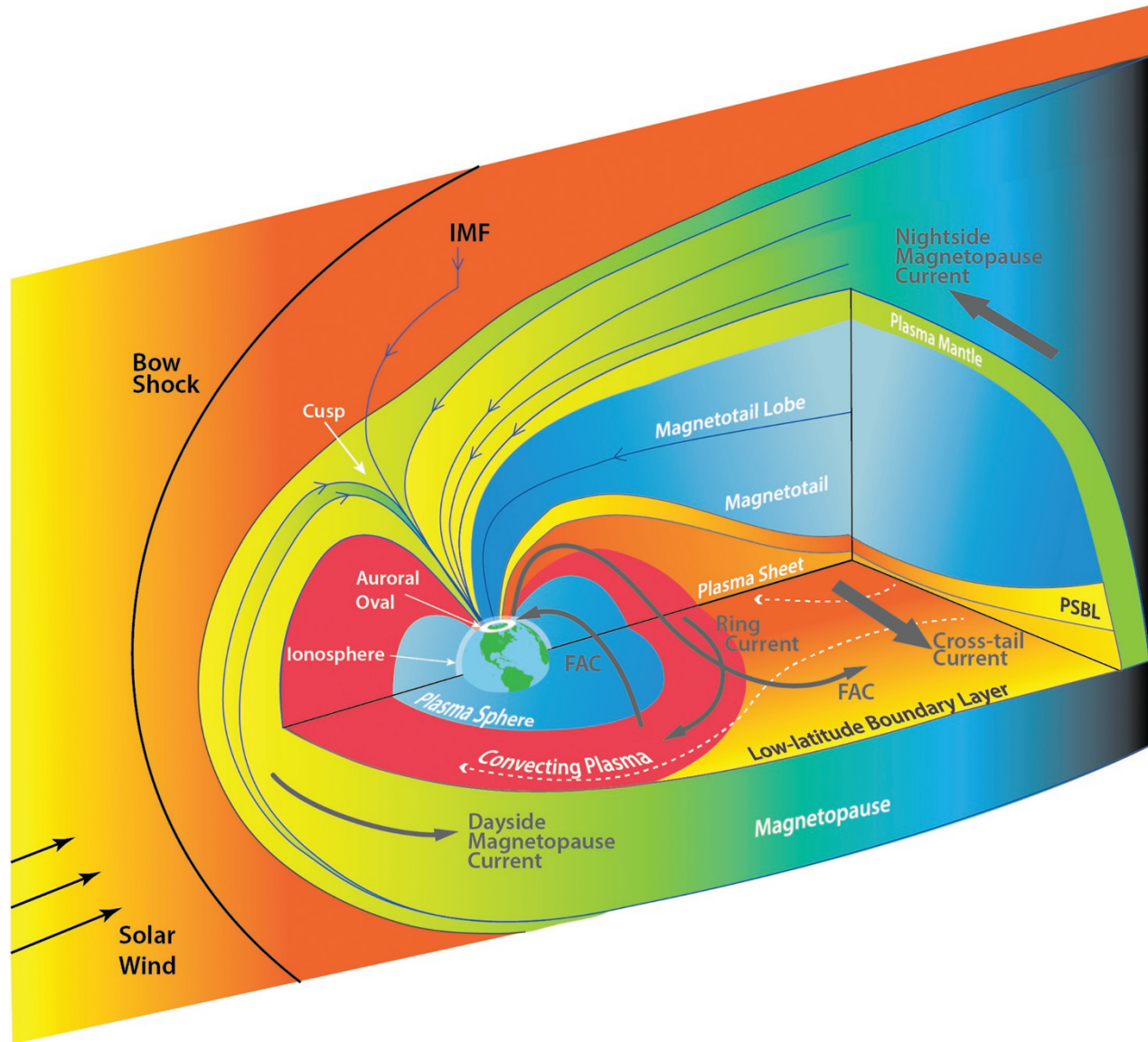


**Figure 2.1** Artist's conception of the Earth's magnetosphere showing plasma regimes, the thin boundaries that separate them, and electric currents (Adapted from National Research Council, 2003).

Geomagnetically-induced currents within the Earth driven by magnetospheric processes can disrupt electrical power grids. Predicting these phenomena, and mitigating their consequences, is an endeavor for Space Weather experts.

This chapter describes the various plasma, magnetic field, and energetic particle regimes found in the Earth's immediate vicinity during intervals of southward interplanetary magnetic field (IMF) and steady reconnection on the dayside magnetopause and in the nightside magnetosphere and provides a brief overview of the dynamic magnetosphere, including geomagnetic storms, magnetospheric and auroral substorms, the Kelvin–Helmholtz instability and dynamic pressure pulses. For an alternative view, the reader is referred to the excellent recent system science review by Borovsky and Valdivia (2018). Fear

(Chapter 19, this volume) describes quiet time interactions during intervals of northward interplanetary magnetic field (IMF) orientation. Nishimura (Chapter 18, this volume) describes the time-dependent storm and substorm interactions that occur primarily during intervals of southward IMF orientation and strong solar wind driving.

## 2.2. THE SOLAR WIND INPUT

The Earth's magnetic field, and the magnetospheric domain over which it predominates (Glassmeier, Chapter 24, this volume), lie within the solar wind. Within in this regime the magnetosphere responds both directly and indirectly to all solar wind variations; thus it is useful

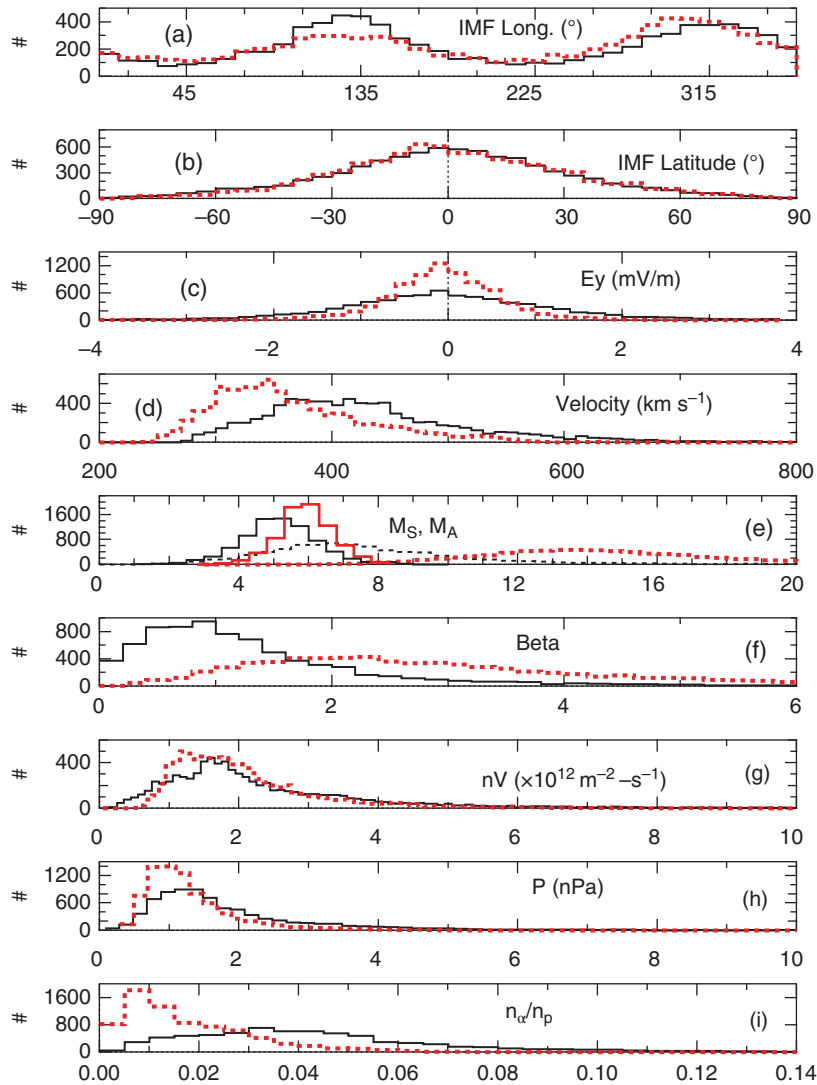


**Figure 2.2** Solar wind conditions at Earth during solar maximum in 2001 (black) and minimum in 2009 (red). From top to bottom, the figure shows histograms (a) of the geocentric solar ecliptic magnetic field longitude ( $0^\circ$  sunward,  $90^\circ$  in the direction opposite the Earth's motion around the Sun), (b) solar ecliptic magnetic field latitude ( $0^\circ$  equatorial,  $90^\circ$  northward), (c) the component of the electric field in the direction opposite the Earth's motion around the Sun, (d) the solar wind proton velocity, (e) the solar wind Alfvénic ( $M_A$ , dashed lines) and sonic ( $M_S$ , solid lines) Mach numbers, (f) plasma  $\beta$ , (g) the solar wind proton number flux, (h) the solar wind dynamic pressure, and (i) the ratio of alpha to proton number densities.

to begin by considering typical and unusual solar wind conditions at Earth's orbit. This review will frequently refer back to these characteristic solar wind parameters.

Figure 2.2 shows histograms of those solar wind parameters most important to the solar wind–magnetosphere interaction. The solar wind carries the Sun's magnetic field outward to Earth's orbit and beyond. Taking into account the Sun's rotation, the interplanetary magnetic field (IMF) typically exhibits a spiral ecliptic longitude of  $\sim 135^\circ$  or  $\sim 315^\circ$ , where  $0^\circ$  is sunward and  $270^\circ$  lies in the direction of Earth's motion around the Sun, as shown in Figure 2.2a. Figure 2.2b shows that the IMF typically lies

in or near the ecliptic (latitude =  $0^\circ$ ). Figure 2.2c shows that the solar wind carries an east/west electric field whose magnitude generally ranges from  $-1$  to  $1$  mV/m. Solar wind bulk velocities only rarely exceed their typical range from  $300$  to  $600$   $\text{km s}^{-1}$ . On average, the solar wind velocities increase from solar minimum to solar maximum (Figure 2.2d). The resulting sonic and Alfvénic Mach numbers range from  $4$  to  $6$  and  $6$  to  $15$ , respectively, decreasing from solar minimum to maximum (Figure 2.2e). Values for  $\beta$ , the ratio of proton thermal to magnetic pressures, range from near  $0$  to  $6$  or occasionally more, decreasing from solar minimum to maximum (Figure 2.2f). The solar wind proton

number flux typically ranges from 1 to  $3 \times 10^{12} \text{ m}^{-2} \text{ s}^{-1}$ . The magnetosphere is subjected to ion dynamic pressures that typically range from 0.5 to 2.5 nPa but occasionally exceed 8 nPa (Figure 2.2h). The solar wind composition varies greatly over the solar cycle, with ratios for alpha to proton densities increasing from 0.00 to 0.04 during solar minimum to 0.005 to 0.07 during solar maximum (Figure 2.2i).

### 2.3. BOW SHOCK, MAGNETOSHEATH, AND FORESHOCK

Thanks to the frozen-in condition (Alfvén, 1942), the Earth's magnetic field presents an obstacle to the oncoming solar wind plasma and therefore carves out a cavity within the heliosphere known as the magnetosphere (Chapman and Ferraro, 1930). As illustrated in Figure 2.1, a standing bow shock (Chapter 8, this volume) deflects and decelerates the supersonic and super Alfvénic solar wind flow, thereby enabling it to pass around the magnetosphere through the magnetosheath (Chapter 9, this volume). The subsolar bow shock is typically located some  $14.5 R_E$  upstream from the Earth (Fairfield, 1971), moving further outward for low solar wind Mach numbers but closer to Earth for high solar wind Mach numbers (Petrinec, 2002). Within the framework of magnetohydrodynamics, the shock jump conditions for quasi-perpendicular bow shocks in which the IMF lies perpendicular to the shock normal are consistent with a polytropic index of  $5/3$  (Winterhalter et al., 1984), which yields a ratio of downstream subsolar magnetosheath to upstream solar wind densities that approaches four.

Magnetosheath physicists have relied heavily upon the gasdynamic model of Spreiter et al. (1966) to time the motion of transients propagating across the magnetosheath (Freeman and Southwood, 1988) and determine magnetosheath plasma parameters just outside the magnetopause (Cooling et al., 2001), even though this model does not treat the magnetic field self-consistently. The model predicts the greatest magnetosheath densities and temperatures just outside the subsolar magnetopause, where magnetosheath velocities fall to zero.

Including the magnetic field has several important consequences. First, it enables kinetic effects associated with wave-particle interactions to occur within the foreshock (Blanco-Cano et al., 2009). Far upstream from the bow shock, these interactions generate weakly compressive waves that propagate at angles up to  $30^\circ$  away from the magnetic field. Nearer to the bow shock the interactions create fast magnetosonic waves that propagate at large angles to the magnetic field. In combination, the two categories of waves generate density and magnetic field strength cavities, which can grow to large amplitudes as spontaneous hot flow anomalies (Zhang et al., 2013). The density, velocity, and pressure variations associated with such upstream events

are invariably swept antisunward into the magnetosheath. They ultimately strike the magnetopause, drive large-amplitude magnetopause motion (Sibeck et al., 1999), and trigger reconnection (Hietala et al., 2018).

A population of backstreaming suprathermal and energetic ions and electrons produced by reflection and shock drift acceleration populate foreshock magnetic field lines that lie tangent to the Earth's bow shock, whilst intermediate and more diffuse (isotropic in the rest frame of the solar wind plasma) ion populations generated by Fermi acceleration between wave scattering centers upstream from the bow shock and the bow shock itself occur deeper within the foreshock (Burgess et al., 2012; Kempf et al., 2015). The source of the latter ions may be ions leaking out from the magnetosphere (Sarris et al., 1976; Kronberg et al., 2011), shocked solar wind ions within the magnetosheath (Edmiston et al., 1982), ions specularly-reflected from the bow shock (Sonnerup, 1969; Gosling et al., 1982), or ions energized by a single shock encounter (Scholer et al., 1998). Fermi acceleration may also populate some foreshock transient events with electrons (Liu et al., 2017). Intensities of the diffuse ions fall off exponentially with distance upstream from the bow shock with e-folding distances that vary from  $\sim 3$  to  $12 R_E$  as energies increase from 10 to 70 keV/e for both protons and alpha particles (Trattner et al., 1994).

From the perspective of the solar wind-magnetosphere interaction, the significance of the ions lies in the fact that their thermal pressure greatly depresses solar wind densities (Fairfield et al., 1990) and modestly depresses solar wind velocities (Bame et al., 1980) shortly prior to the solar wind's interaction with the bow shock and magnetosphere. The corresponding decrease in solar wind dynamic pressure enables the magnetopause to expand outward locally (Samsonov et al., 2017). Because the foreshock lies upstream from the pre-noon bow shock for the typical spiral IMF orientation, the prenoon magnetopause is bathed in lower solar wind dynamic pressure and greater wave activity than the postnoon magnetopause. The waves generated within the foreshock are transmitted through the magnetosheath, batter the magnetopause, and enter the magnetosphere (Engebretson et al., 1991; Lin et al., 1991), perhaps via the cusps (Yeoman et al., 2012).

Inclusion of a magnetic field has a second effect on predictions for magnetosheath characteristics. It enables the generation of both mirror mode and proton cyclotron waves in the magnetosheath (Schwartz et al., 1996). As noted by Soucek et al. (2008), the ion cyclotron instability should grow faster for low beta plasmas while the mirror instability should dominate for high beta plasmas. Turbulent conditions in the magnetosheath enable reconnection on electron scales decoupled from ion scales (Phan et al., 2018) and transient events in the magnetosheath may trigger local reconnection on the magnetopause (Laitinen et al., 2010).

The presence of a magnetic field has three other effects on the magnetosheath. First, a spiral IMF orientation

causes the thickness of the postnoon magnetosheath to exceed that of the prenoon magnetosheath, particularly for low solar wind Mach numbers (Chapman et al., 2004). Second, enhanced pressures associated with magnetic field lines draped against the magnetopause at orientations that depend on those in the IMF (Fairfield, 1967) result in the formation of a depletion layer with enhanced magnetic field strengths, depressed densities, greater ratios of perpendicular to parallel ion temperatures, and greater Alfvén velocities just outside the magnetopause (Zwan and Wolf, 1976), particularly during intervals of northward IMF orientation (Wang et al., 2004) when the presence of a depletion layer may enable steady reconnection at high latitudes (Fuselier et al., 2000). Finally, curvature forces associated with magnetic field lines draped against the magnetopause can accelerate the plasma just outside the flanks of the magnetopause to velocities greater than those in the ambient magnetosheath (Lavraud et al., 2007).

## 2.4. MAGNETOPAUSE

The Chapman–Ferraro magnetopause current layer separates the often-turbulent high beta plasmas and magnetic fields within the magnetosheath from the more stable low beta plasmas and magnetic fields within the magnetosphere. At rest, the magnetopause lies along the locus of points where the sum of thermal and magnetic pressures in the magnetosheath and magnetosphere balance (Soterelis and Meng, 1999). Magnetosheath pressures are proportional to the solar wind dynamic pressure (Martyn, 1951), while pressures within the tenuous outer dayside magnetosphere can readily be approximated by those of the magnetic field alone, which in turn is composed of contributions from the Chapman–Ferraro currents on the magnetopause, the Region 1 and 2 Birkeland currents within the magnetosphere (Chapter 13, this volume), the ring current (Chapter 20, this volume), and the cross-tail current (Tsyganenko and Sibeck, 1994) and the Earth’s dipole (Chapter 39, this volume). On average, the subsolar magnetopause lies some  $10.8 R_E$  from Earth (Fairfield, 1971).

Reconnection on the magnetopause enables the shocked solar wind mass, energy, and momentum within the magnetosheath to enter the magnetosphere (Chapter 10, this volume). Macroscale evidence for reconnection comes in the form of statistical studies indicating that the dayside magnetopause moves Earthward (Aubry et al., 1970), the cusps (Burch, 1973; Newell et al., 1989) and the auroral oval equatorward, and the magnetotail flanks outward (Maezawa, 1975) during the growth phase of geomagnetic substorms (Chapter 18, this volume) following southward IMF turnings, i.e. duskward (positive) solar wind electric field turnings.

These changes indicate that magnetic flux is removed from the dayside magnetosphere and added to the magnetotail. The largest geomagnetic disturbances, storms and substorms, tend to occur during intervals of southward IMF (Arnoldy, 1971; Burton et al., 1975), indicating that reconnection is the dominant mode of solar wind–magnetosphere interaction.

Reconnection on the magnetopause diverts dawn-to-dusk Chapman–Ferraro currents into the ionosphere, downward prior to local noon and upward after local noon (Maltsev and Lyatsky, 1975). Reconnection launches a fast rarefaction wave that depresses magnetic field strengths in the dayside magnetosphere (Coroniti and Kennel, 1979). Pressure gradient and magnetic curvature forces on newly reconnected magnetic field lines remove them from the dayside magnetosphere and transport them to the magnetotail (Dungey, 1961). From any of these perspectives, reconnection removes magnetic flux from the dayside magnetosphere, thereby allowing the dayside magnetopause to move earthward.

The location(s) where reconnection occurs on the magnetopause remain poorly understood. Component reconnection models predict reconnection to occur along a reconnection line passing through the subsolar point whose tilt depends upon the IMF orientation (Sonnerup, 1974; Gonzalez and Mozer, 1974). Antiparallel reconnection line models predict reconnection at locations where magnetosheath and magnetospheric magnetic fields lie nearly antiparallel (Crooker, 1979) or where current strengths peak (Alexeev et al., 1998), in which case reconnection occurs on the dayside equatorial magnetopause for southward IMF orientations, moves towards the flanks for the typical ecliptic IMF orientation, and moves poleward of the cusps during intervals of northward IMF orientation. Considerable evidence has now accumulated for a model in which reconnection occurs along lines across which the shear between magnetosheath and magnetospheric magnetic fields maximizes (Trattner et al., 2012). Reconnection may extend across the entire dayside magnetopause under some circumstances (Phan et al., 2000; Dunlop et al., 2011), or be spatially localized (Zou et al., 2018). It may occur steadily (Phan et al., 2004) or in bursts (Le et al., 1993) even for constant solar wind conditions.

In situ evidence for reconnection comes in the form of accelerated plasma flows that satisfy the Walén relationship, magnetic field components normal to the nominal rotational discontinuity magnetopause, and pitch angle distributions indicating the escape of suprathermal and energetic particles from the magnetosphere (Sonnerup et al., 1981). While reconnection may occur for a broad range of shear angles between the draped magnetosheath and magnetospheric magnetic fields during intervals when the jump between magnetospheric and magnetosheath plasma beta is small (i.e. when the magnetosheath plasma

beta is small), it only occurs for large shear angles when the jump is large (i.e. when the magnetosheath plasma beta is large) (Phan et al., 2013). Recent Magnetospheric Multiscale mission observations probe the waves and microscale electron particle distributions that enable reconnection to occur (Chapter 41, this volume).

The magnetic field rotates from magnetosheath to magnetospheric orientations across the magnetopause current layer, which on the dayside is generally 400–1000 km thick (Berchem and Russell, 1982). The depletion layer with depressed densities, enhanced magnetic field strengths, and enhanced flows perpendicular to the magnetosheath magnetic field appears just outside the magnetopause for low magnetic shears (Phan et al., 1994), but is generally absent for high shears except when the solar wind pressure is large (Anderson et al., 1997). A layer of magnetosheath-like plasma known as the low-latitude boundary layer or LLBL (Chapter 12, this volume) can be found just inside the magnetopause. The thickness of this layer ranges from  $\sim 0.1 R_E$  near the subsolar point (Eastman and Hones, 1979) to  $\sim 0.6 R_E$  on the flanks (Paschmann et al., 1993) and increases during intervals of northward IMF orientation (Mitchell et al., 1987), sometimes reaching  $1.4 R_E$  (Safrankova et al., 2007), suggesting that the layer forms via near simultaneous reconnection poleward of both cusps (Song and Russell, 1992). A layer of streaming energetic ions and electrons can almost always be found in the magnetosheath just outside the magnetopause (Meng and Anderson, 1970; Speiser et al., 1981). The similarity of the intensities and spectra within this layer to those in the outer magnetosphere and the location of the layer adjacent to the magnetopause suggest that these particles have generally escaped from the magnetosphere, whether along interconnected magnetic fields or by drifting to and scattering at the magnetopause, rather than originating via energization of solar wind particles at the bow shock (Sibeck and McEntire, 1988).

## 2.5. CUSPS

The footprints of newly reconnected magnetic field lines at the dayside magnetopause map to small regions in the high-latitude dayside ionosphere via the northern and southern cusps (Chapter 11, this volume). Consequently, the cusps afford magnetosheath plasma easy access down to ionospheric altitudes. Lavraud et al. (2004) reported a statistical survey of Cluster observations indicating the presence of a high density, low magnetic field strength, external cusp that is stagnant during intervals of northward IMF orientation but flowing during intervals of southward IMF orientation. The high-altitude cusp moves equatorward (and sunward) for southward IMF orientations (Zhou et al., 2000). Plasma

pressures within the cusp increase and magnetic field strengths diminish with increasing solar wind dynamic pressure and dipole tilt towards the sun (Zhou et al., 2001). Because the plasma on magnetic field lines within the cusp enters the magnetosphere via reconnection on the magnetopause, observations of energy dispersion signatures and precipitating and mirrored particle distributions in the mid- and low-latitude cusp can be used to infer the location, time, and time dependence of reconnection on the magnetopause (Onsager and Lockwood, 1997). The duskward and dawnward displacements of the low-altitude northern cusp for duskward and dawnward IMF orientations provide strong evidence for antiparallel reconnection on the magnetopause (Newell et al., 1989).

## 2.6. MAGNETOTAIL

The combined efforts of pressure gradient and magnetic curvature forces relentlessly transport one end of the newly reconnected dayside magnetic field lines antisunward. Since the other end of these magnetic field lines remains tied to the Earth's polar ionosphere, they stretch antisunward into magnetotail orientations with sunward pointing magnetic field lines within the northern lobe connected to the northern ionosphere and antisunward pointing magnetic field lines within the southern lobe connected to the southern ionosphere (Chapter 17, this volume).

The newly reconnected magnetic field lines enter the magnetotail at locations that depend upon the IMF orientation (Cowley, 1981). For a southward IMF orientation, the field lines enter the magnetotail at high northern and southern latitudes. For more typical duskward (dawnward) IMF orientations, field lines connected to the northern (southern) ionosphere enter at dawnside equatorial locations while those connected to the southern (northern) ionosphere enter at duskside equatorial locations. Since the newly entering magnetic field lines still contain an antisunward flowing plasma with densities lower than those in the magnetosheath, they can be readily distinguished from the older and nearly void magnetotail magnetic field lines from which this plasma has already drained. The newly deposited magnetic field lines can be found within a region known as the plasma mantle (Rosenbauer et al., 1975), located in the dawnside (duskside) northern lobe and duskside (dawnside) southern lobe for duskward (dawnward) IMF orientations (Hardy et al., 1979; Gosling et al., 1985). Magnetohydrodynamics interprets the transition from magnetosheath to magnetospheric densities, magnetic field strengths, and orientations in terms of standing rotational discontinuities and slow mode fans (Coroniti and Kennel, 1979). The depth to which the fan penetrates into the magnetotail increases with downstream distance (Siscoe and Sanchez, 1987).

As the newly reconnected magnetic field lines sink deeper into the magnetotail, the plasma on them drains outward in the antisunward direction, leaving magnetic field lines with very low densities within the lobes proper. Magnetic flux within the magnetotail cannot build up indefinitely. Reconnection at the cross-tail current sheet (Tsyganenko and Fairfield, 2004; Runov et al., 2006) closes the open lobe magnetic field lines and ejects them sunward towards the dayside magnetopause where the Dungey cycle is completed. Reconnection energizes the plasma on the reconnecting lobe magnetic field lines, sending field-aligned beams of ions and electrons Earthward towards the ionosphere, where they magnetically mirror, resulting in field lines with counterstreaming beams (Eastman et al., 1984). With time, the beams are pitch angle scattered, heated, and compressed (Tsyganenko, 1982), producing a plasma sheet with enhanced densities and temperatures (Bame et al., 1967) and more isotropic particles distributions (Eastman et al., 1984) that encompasses the much thinner current sheet. The plasma sheet cools and becomes denser when the IMF turns northward (Terasawa et al., 1997). The Earth's dipole tilt warps the location of both the plasma and current sheet (Dayeh et al., 2015).

Steady reconnection and convection models lead to a pressure balance or entropy inconsistency with models predicting nearly constant radial gradients in entropy that are not observed and inner plasma sheet magnetic field lines that are far more stretched than those observed (Erickson and Wolf, 1980; Kivelson and Spence, 1988; Spence et al., 1989). Predictions and observations can be reconciled if particles are lost via the combined effects of gradient-curvature drifts and plasma bubbles produced by bursty reconnection (Wolf et al., 2009). In fact, observations show that magnetotail reconnection is inherently unsteady (Baumjohann et al., 1990; Angelopoulos et al., 1992). On average, there is a curved reconnection line in the plasma sheet that bows outward and stretches anti-sunward from a  $\sim 130 R_E$  point of closest approach to Earth (Slavin et al., 1985). Transient reconnection lines can appear much nearer to the Earth.

Quasi stable steady magnetospheric convection events follow the onset of geomagnetic substorms (Kissinger et al., 2012) during intervals of enhanced solar wind-magnetosphere interaction when the IMF remains moderately southward (Tanskanen et al., 2005). They often contain a series of high-speed bursty bulk flows. The initial substorm onset produces a region of high pressure in the inner magnetosphere that deflects both fast transient and slow steady flows and magnetic fields towards the flanks. Flows slow in the near-Earth magnetotail at distances of 10–15  $R_E$  from Earth (Guild et al., 2018). Inner magnetospheric magnetic fields are not constant but rather grow stronger and more tail-like during intervals of steady magnetospheric convection (Pulkkinen et al.,

2013). The near-Earth plasma sheet thins, while the distant plasma sheet expands (Sergeev et al., 1996)

Theory (Michel and Dessler, 1970; Cowley, 1981) and global magnetohydrodynamic simulations (Berchem et al., 1998; Fedder and Lyon, 1995; Walker et al., 1999) predict that the magnetotail extends far downstream, is flattened in the direction perpendicular to the component of the IMF in the plane perpendicular to the solar wind flow, and twists in response to variations in the IMF orientation that determine where newly reconnected magnetic field lines are deposited within the magnetotail. The magnetotail remains readily identifiable at lunar distance (Meng and Anderson, 1974), 180  $R_E$  (Slavin et al., 1983), 500  $R_E$  (Mariani and Ness, 1969), 1000  $R_E$  (Walker et al., 1975), 1600  $R_E$  (Scarf, 1987), perhaps 3100  $R_E$  (Intriligator et al., 1979) and 5000  $R_E$  (Lagg et al., 2001) downstream, and possibly even 15 000  $R_E$  downstream (Ashford et al., 1998). The cross-section of the distant magnetotail might be elongated north/south (Behannon, 1970; Tsurutani et al., 1984), east/west (Sibeck et al., 1986a), or nearly circular (Maezawa et al., 1997), perhaps depending on whether or not the plasma mantle is included in the regions identified as the magnetotail (Sibeck and Lin, 2014). Observations confirm that the magnetotail twists in response to variations in IMF  $B_y$  (Sibeck et al., 1986b), particularly when the IMF has a northward component (Maezawa et al., 1997). Magnetotail magnetic field strengths diminish with downstream distances as the magnetopause boundary flares outward and flux closes across the magnetotail plasma and neutral sheets (Behannon, 1970).

## 2.7. INNER MAGNETOSPHERE: RING CURRENT, RADIATION BELTS, AND PLASMASPHERE

The ring current is comprised of ions with energies between 10 and 200 keV drifting westward around the Earth at distances of  $\sim 1.5$  to 9  $R_E$  (Chapter 20, this volume). While protons represent the dominant species in the quiet time ring current, oxygen ions originating in the ionosphere, probably from cusp outflow (Kistler et al., 2016), become increasingly important as geomagnetic activity increases (Chapter 23, this volume). During geomagnetic storms, the energy content of the particles within the ring current intensifies by a factor of 10–20, inflates the inner magnetosphere, and depresses magnetic field strengths nearer Earth, including those on the surface of the Earth (Dessler and Parker, 1959; Sckopke, 1966).

Traditionally, geomagnetic storms were thought to result from a series of substorms (Akasofu and Chapman, 1961) and the episodic enhanced electric fields associated with substorms certainly produce readily identifiable

discrete injections of energetic ions and electrons into the inner magnetosphere (Reeves et al., 1990). Whereas the ring current ion intensity enhancements associated with isolated substorms are transient, those associated with substorms during storms are more protracted (Reeves and Henderson, 2001). The sum of geomagnetic activity associated with substorms can be used to predict disturbances associated with storms (Davis and Parthasarathy, 1967) and the buildup of oxygen ions in storms can be related to ionospheric outflow during substorms (Daglis et al., 1994). Simulations indicate that the combined effects of impulsive plasma injections and large-scale convection electric fields can result in the development of a strong ring current (Yu et al., 2014).

However, simulations also indicate that enhanced steady convection alone can suffice to strengthen the ring current (Chen et al., 1993; Fok et al., 1996), as observed with the aid of energetic neutral atom images of the ring current during steady convection (Lui et al., 2001). The development of at least some storms can then be more closely tied to enhanced magnetospheric convection than to impulsive reconnection and energy unloading within the magnetotail (Zhou et al., 2001). Small-scale ion injections incrementally contribute to the buildup of the Earth’s ring current during steady magnetospheric convection (Gkioulidou et al., 2014). Adiabatic convection of plasma sheet plasma inward can account for the observed increase in ring current plasma pressure and the predominance of  $O^+$  pressure seen at those distances nearest Earth during geomagnetic storms (Menz et al., 2017). This process may be further enhanced by ultra-low frequency (ULF) wave radial diffusion (Murphy et al., 2014a).

The sum of gradient-curvature and convection drifts determines the final destination of particles injected from the magnetotail into the near-Earth region. Particles with the greatest energies ( $\sim 1$  MeV or more) move primarily under the influence of gradient-curvature drifts, which divert the incoming ions azimuthally westward into the duskside magnetosphere and the electrons eastward into the dawnside magnetosphere. Subject solely to gradient-curvature drifts, the ions would encircle the Earth creating the ring current. However, the convection electric field pushes them deeper into the magnetosphere on the nightside, but outward to the magnetopause on the dayside. Under the influence of this electric field, ions with ring current energies (10–200 keV) may strike the magnetopause at postnoon or even earlier local times and be lost to the magnetosheath (Sorathia et al., 2017), contributing to a partial ring current in the postnoon magnetosphere.

The convection electric fields, and both ions and electrons, penetrate deeper into the magnetosphere as geomagnetic activity increases, peaking within the ring current at distances of about  $4 R_E$  from Earth

(Rowland and Wygant, 1998; Califf et al., 2014). Particles with ring current energies can be pushed deep into the nightside magnetosphere under the influence of the strongest electric fields. Electron injections have been observed only  $\sim 2.5 R_E$  from Earth, although injections at these distances may correspond to the adiabatic energization of a preexisting population by a fast magnetosonic wave rather than an injection of new particles (Turner et al., 2015). Even during intervals of small convection electric field, the azimuthally limited transient injections corresponding to bursty bulk flows that occur during intervals of steady magnetospheric convection can be particularly effective at trapping, energizing, and injecting particles into the inner magnetosphere (Ukhorskiy et al., 2017).

Whether the plasma sheet ion and electron populations injected into the inner magnetosphere begin as isotropic or anisotropic distributions, the combined effects of gradient-curvature and convection drifts send them to different locations within the magnetosphere with different arrival times, resulting in populations that exhibit significant anisotropies. One consequence of this is magnetopause shadowing. Whereas particles with low pitch angles follow nearly circular paths as they gradient-curvature drift around the Earth, drift-shell splitting causes those with  $90^\circ$  pitch angles to move radially outward in the dayside magnetosphere and be preferentially lost or ‘shadowed’ to the magnetosheath upon encountering the magnetopause. Since ions drift westward and electrons eastward, “butterfly” pitch angle distributions of electrons and ions are common in the outer postnoon and prenoon dayside magnetospheres, respectively (West et al., 1973; Sibeck et al., 1987a).

A second, and as we shall shortly see arguably more consequential, effect of drift shell splitting lies in the fact that ring current ion populations exhibiting much greater fluxes perpendicular than parallel to the magnetic field are susceptible to ULF electromagnetic ion cyclotron (EMIC) (Cornwall, 1965) and short-wavelength mirror-mode instabilities (Cheng and Qian, 1994), while suprathermal electron distributions exhibiting the same anisotropy are susceptible to the generation of very-low frequency (VLF) whistler-mode chorus at much higher frequencies (Sazhin and Hayakawa, 1992). By the time they reach the dawnside and duskside magnetosphere (Figure 2.3a), the electron and ion populations injected from the magnetotail, whether steadily or unsteadily, often exhibit such anisotropies, leading to the frequent occurrence of EMIC (Anderson et al., 1992) and mirror mode (Constantinescu et al., 2009) waves in the duskside magnetosphere and whistler mode chorus in the dawnside magnetosphere (Li et al., 2009). Chorus waves from outside the plasmopause can propagate Earthward into the plasmasphere, where they become the embryonic source

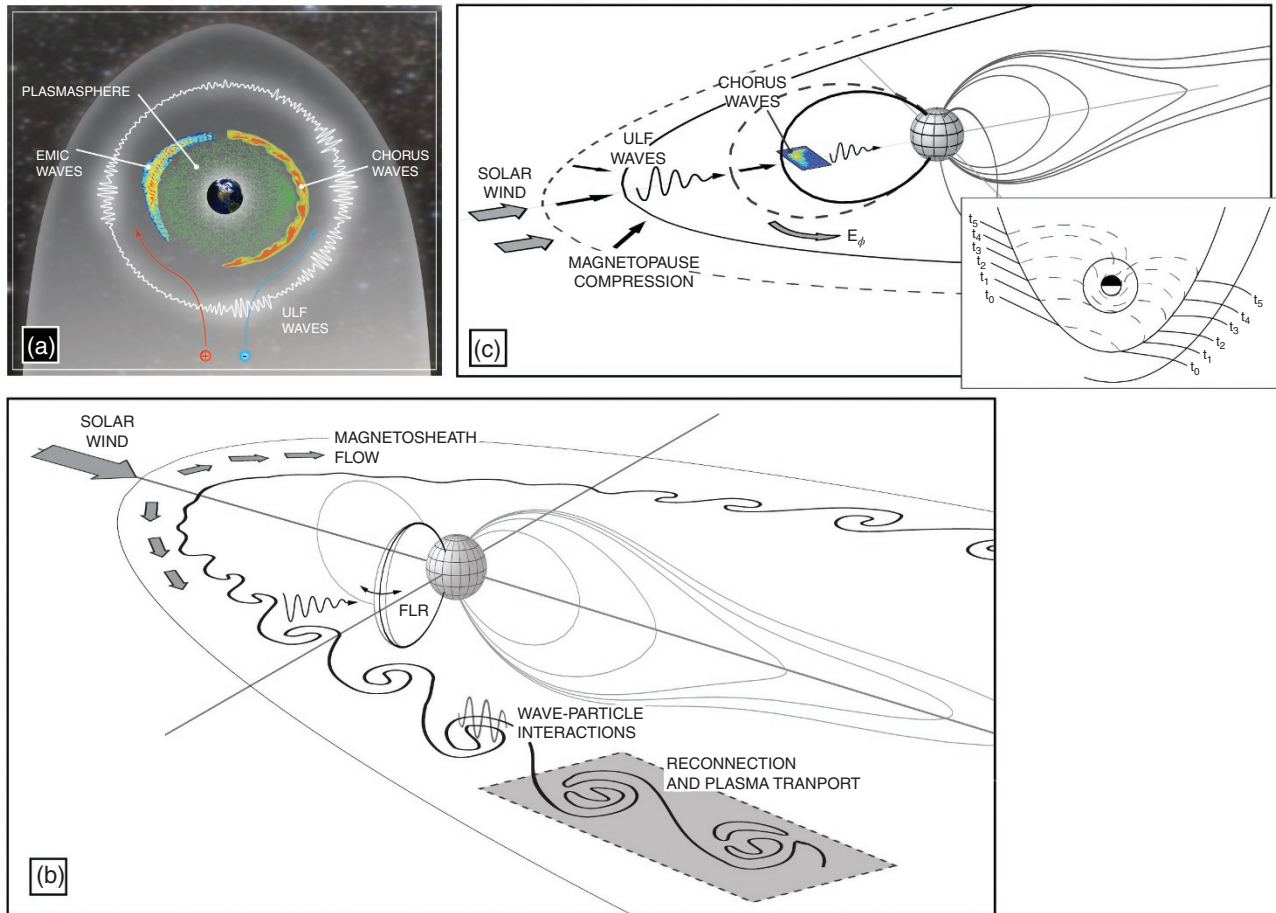


**Figure 2.3** (a) Energetic ions and electrons injected from the tail drift westward and eastward around providing a source of particles for both the ring current and outer radiation belt, respectively. The injection of both ions and electrons can lead to the growth of EMIC waves, typically in the dusk magnetosphere, and VLF chorus waves, in the dawn magnetosphere, and just outside the dense plasmapause, respectively. During active times enhanced ULF wave power is observed throughout the magnetosphere (Thorne, 2010; Reproduced with permission of John Wiley & Sons). (b) The Kelvin-Helmholtz instability excites toroidal field line resonances and ULF waves within the magnetosphere. Within the vortices of the instability localized, wave particle interactions and reconnection can occur. (c) An interplanetary shock impacts the dayside magnetosphere, compressing the magnetopause and inner magnetosphere, launching fast mode ULF waves throughout the magnetosphere and generating a strong azimuthal electric field and plasma anisotropies that can interact with magnetospheric plasma and generate VLF chorus wave (respectively) (Wilken et al., 1982; Reproduced with permission of John Wiley & Sons). The inset shows the propagation of the interplanetary shock through the magnetospheric system. Wave fronts in the outer magnetosphere advance ahead of those in the magnetosheath and solar wind thanks to the high fast mode magnetosonic wave mode speeds in the outer magnetosphere. The presence of the plasmasphere deep within the magnetosphere slows wave fronts and causes them to be concave around the Earth.

of plasmaspheric hiss (Bortnik et al., 2009; Meredith et al., 2013).

There are two Van Allen electron radiation belts (Chapter 21, this volume). Inner belt electrons with energies up to  $\sim 1$  MeV are stably trapped at radial distances of  $1.2\text{--}2 R_E$  from the center of the Earth in the equatorial plane. Outer belt electrons with similar energies exhibit highly variable intensities at distances ranging from 3 to

$7 R_E$  from the center of the Earth (Ganushkina et al., 2011 and references therein). A slot region of low electron intensities separates the two belts. Very energetic (10s of MeV) protons can be found within the inner belt. The intensities of protons with lower energies peak at greater radial distances, extend outward beyond geosynchronous orbit, and do not exhibit a slot (Garcia and Spjeldvik, 1985).

The inner proton belt forms via a combination of cosmic ray albedo neutron decay and slow inward diffusion of trapped solar protons (Selesnick et al., 2007). Losses are caused by ionization of the neutral atmosphere, energy transfer to plasma electrons, and inelastic nuclear scattering. Electrons with energies from 0.05 to 1.0 MeV in this region have generally been thought to originate via slow inward radial diffusion, cosmic ray albedo neutral decay, and the transient effects of interplanetary shocks, but more recently have been attributed to transient enhancements in the inner edges of the outer radiation penetrating through the slot region (see below) into the inner radiation belt (Turner et al., 2017). Careful inspection has revealed the persistent presence of  $\sim 1$  MeV electrons accompanying the inner belt protons (Selesnick, 2015) and large geomagnetic storms can introduce  $\sim 1$  MeV electrons into the inner belt for periods of at least 1.5 years (Claudepierre et al., 2017).

The slot region lies some 2–3  $R_E$  from the center of the Earth, separating the inner and outer electron radiation belts. It is a location where whistler mode waves associated with plasmaspheric hiss emissions pitch angle scatter energetic electrons, causing them to precipitate into the ionosphere (Lyons and Thorne, 1973). The slot region moves outward during solar maximum, inward during solar minimum (Fung et al., 2006).

The Earth's outer radiation belt exhibits a population of electrons with energies ranging from several hundreds of keV to several MeV (Mauk et al., 2013). Substorm-driven inward convection of the suprathermal tail of the plasma sheet electron population provides the source population for these electrons (Foster et al., 2016). Further energization can occur via adiabatic diffusive processes that move the electrons radially inward (Schulz and Lanzerotti, 1974; Shprits et al., 2008a), perhaps in response to ULF waves driven by solar wind pressure variations (Ukhorskiy et al., 2005), the Kelvin–Helmholtz instability on the magnetopause (Elkington et al., 1999), or internal magnetospheric instabilities (Ozeke and Mann, 2008; Ukhorskiy et al., 2009). The interaction of the electrons with the ULF waves can also be coherent, leading to much more rapid acceleration and transport (Mann et al., 2013). Ozeke et al. (2014) provide analytic expressions for ULF wave radiation belt radial diffusion coefficients.

While steady magnetospheric convection following some substorms may supply the seed population of electrons needed for adiabatic radial diffusion and acceleration by ULF waves to relativistic energies (Kissinger et al., 2014), it cannot explain every feature of the outer radiation belts. Fox et al. (2006) reported that nonadiabatic processes were required to account for electrons with energies greater than  $\sim 1$  MeV at radial distances ranging from 5 to 7  $R_E$ . Reeves et al. (2013) and Boyd et al. (2018) reported case and statistical surveys of radial gradients in

phase space density profiles showing that local acceleration, and not inward diffusion from a source located further radially outward, is the predominant mechanism governing enhancements in  $\sim 1$  MeV radiation belt electrons. Interactions with chorus mode waves can account for this enhancement (Shprits et al., 2008b).

Loss processes play just as an important role in defining the outer radiation belt as processes that energize and transport electrons (Millan and Thorne, 2007). The energetic electrons in the outer radiation belt can be lost via outward diffusion and loss to the magnetosheath when their drift paths strike the magnetopause (West et al., 1972; Shprits et al., 2006), by drift shell bifurcation, scattering, and loss to the magnetosheath or atmosphere when they drift through the dayside magnetosphere and in particular the cusps (Ukhorskiy et al., 2011), or by pitch angle scattering and precipitation into the atmosphere via interaction with chorus (Bortnik and Thorne, 2007) or EMIC (Lorentzen et al., 2000) waves.

The Earth's plasmasphere is a cold (1 eV), dense ( $10\text{--}10^4\text{ cm}^{-3}$ ), torus of  $H^+$  ( $\sim 80\%$ ),  $He^+$  ( $10\text{--}20\%$ ), and  $O^+$  (several per cent) centered upon the Earth (Goldstein, 2006; Chapter 22, this volume). Plasma within the plasmasphere originates in the Earth's dayside ionosphere, corotates with the Earth's magnetic field, and can extend outward beyond geosynchronous orbit during quiet times. The outer boundary of the plasmasphere, the plasmopause, lies along the streamline passing through the dusk-side stagnation point where steady-state corotational and externally imposed dawn–dusk electric fields balance within the magnetosphere (Grebowsky, 1970). Plasma outside this closed streamline lies on open trajectories that intercept the magnetopause.

The location of the plasmopause varies with time in response to the electric fields imposed by reconnection at the dayside magnetopause and in the magnetotail. Reconnection on the magnetopause launches fast mode expansion waves deep into the dayside magnetopause that carry duskward electric fields. These electric fields drive a sunward bulge in the dayside plasmopause (Grebowsky, 1970; Katus et al., 2015). The resulting broad dayside plume narrows with time to a plume stretching outward away from Earth towards the postnoon magnetopause while the dayside plasmopause erodes Earthward. When reconnection ceases at the magnetopause, the strength of the duskward electric field diminishes and the plume corotates duskward with the remainder of the plasmasphere. The plasmasphere refills and the plasmopause moves outward. The onset of reconnection within the Earth's magnetotail launches sunward-moving fast compressional waves that apply duskward electric fields to the nightside inner magnetosphere. These electric fields drive indentations on the plasmopause that propagate sunward (both eastward and westward) from the site of

reconnection, leaving behind a nightside plasmopause that lies closer to Earth (Goldstein et al., 2005). Plumes primarily occur during intervals of enhanced solar wind–magnetosphere interaction but can be observed for all levels of geomagnetic activity (Moldwin et al., 2004).

The cold plasma within the plasmasphere plays an important role within the solar wind–magnetosphere interaction. Intermingled plasmaspheric and ring current plasmas favor the growth of the EMIC waves responsible for radiation belt electron energization and loss (Gary et al., 1995). Hiss waves within the outer plasmasphere scatter energetic electrons on the inner edge of the outer radiation belt, resulting in the formation of the slot region (Lyons et al., 1972). As a consequence, the observed locations of the inner edge of the outer radiation belt electrons track those of the innermost plasmopause as determined empirically as a function of the Dst index, which measures the strength of the ring current (Li et al., 2006). Finally, plumes reaching the magnetopause may locally throttle reconnection (Walsh et al., 2013, 2014).

## 2.8. THE RESPONSE OF THE MAGNETOSPHERE TO A DYNAMIC SOLAR WIND

The previous section described the typical properties of the magnetosphere and the various regions that develop as a result of the solar wind–magnetosphere interaction. This section briefly reviews the magnetospheric response to a dynamic and varying solar wind leading to geomagnetic storms, magnetospheric and auroral substorms, the Kelvin–Helmholtz instability, magnetopause motion, wave generation, and plasma dynamics. The response of the magnetosphere to intense and dynamic solar wind driving is referred to as Space Weather. Additional details regarding Space Weather, storms, substorms, and geomagnetic activity can be found in subsequent chapters (e.g., Chapter 18, this volume).

### 2.8.1. Geomagnetic Storms

Geomagnetic storms are the result of intense solar wind driving, and a complex interplay and cross-coupling between, the various plasma populations and regions of the magnetosphere leading to increased geomagnetic activity. This activity is manifested as enhanced magnetic reconnection at the magnetopause and in the magnetotail, large-amplitude electromagnetic waves, and electron and ion acceleration, loss, and transport across a range of energies spanning over six orders of magnitude (eV–MeV) that can last from a fraction of a day up to a week. The intense solar wind driving leading to geomagnetic storms is typically the result of large scale solar wind features such as coronal mass ejections (CMEs), corotating

interaction regions (CIRs) or high-speed solar wind streams (HSSs) impacting the Earth’s magnetosphere (Murphy et al., 2018a). Differences exist between each of these large-scale solar wind structures and specifically their temporal profiles (Hutchinson et al., 2011); however, each of these structures is associated initially with a period of enhanced number density and dynamic pressure, and intense southward IMF, lasting for about a day and an extended period of sustained high-speed solar wind, typically exceeding 500 km/s, lasting on the order of days (Kataoka and Miyoshi et al., 2006; Murphy et al., 2018a).

The initial impact of the large-scale solar wind feature at the onset of a geomagnetic storm is typically associated with enhanced dynamic pressure and southward IMF. Force balance between the enhanced dynamic pressure and magnetic pressure of the magnetosphere, coupled with enhanced dayside reconnection resulting from southward IMF, causes the magnetopause to rapidly move toward Earth and compresses the dayside magnetosphere (Sibeck et al., 1991; Shue et al., 1998). Enhanced dayside reconnection transfers energy from the solar wind to the nightside magnetotail, increasing magnetospheric convection, intensifying substorm activity, and rapidly enhancing the ring current (Murphy et al., 2018a). The plasmopause erodes and plasmaspheric plumes form (Walsh et al., 2013), there is a rapid increase in the auroral electrojet current and AE index, a decrease in the storm time disturbance index Dst, and an increase in the equatorial electrojet intensity at the start of the geomagnetic storm, respectively (Hutchinson et al., 2011). This initial phase of the geomagnetic storm is referred to as the storm main phase.

The compressed dayside magnetic field and stretched magnetic field of the magnetotail during the main phase enhance drift shell splitting. Drift shell splitting results in higher pitch angle particles moving away from the Earth and lower pitch angle particles moving toward the Earth as they drift into the dayside magnetosphere (Sibeck et al., 1987b). The enhanced ring current diminishes magnetic field strengths near the Earth. Conservation of the third adiabatic invariant via the so-called Dst effect also causes particles, in particular energetic outer radiation belt electrons, to move outward (Kim and Chan, 1997). The outward motion of plasma and inward motion of the magnetopause results in rapid loss of magnetospheric particles via the magnetopause during the early stages of geomagnetic storms (Turner et al., 2012a; Ukhorskiy et al., 2009). Dramatic losses of electrons from the outer radiation belt referred to as radiation belt dropouts (Turner et al., 2012b) result from magnetopause shadowing abetted by rapid outward radial transport by ultra-low frequency waves (Mann et al., 2016), the Dst effect, and drift shell splitting. Finally, the initial increase in dynamic pressure triggers a variety of

electromagnetic wave activity including EMIC, VLF and ULF waves that can couple to the local plasma population, driving additional dynamics including loss via precipitation to the Earth's upper atmosphere (Halford et al., 2015; Murphy et al., 2015; Saikin et al., 2016).

The geomagnetic storm transitions from the main phase to the recovery phase as the Dst index begins to recover and solar wind dynamic pressure and southward IMF return to nominal quiet time values. The decay in the ring current strength as measured by the Dst index is the direct result of ring current particles flowing outward through the dayside magnetopause and charge exchange with exospheric neutrals (Liemohn et al., 1999, 2001). During the recovery phase the solar wind velocity remains enhanced for several days providing a source of ULF wave energy in the magnetosphere (Rae et al., 2005). Substorm activity is also sustained during the early recovery phase introducing new low-medium energy plasma via substorm injections (Jaynes et al., 2015; Murphy et al., 2018a). These injections provide the source population of low energy  $\sim 10$  KeV electrons capable of generating VLF Chorus waves as well as the seed population of  $\sim 100$ s KeV electrons. The presence of ULF and VLF wave activity and a seed population of  $\sim 100$  KeV electrons provides a pathway to replenish energetic electron in the outer electron radiation belt via VLF wave local acceleration (Li et al., 2014) and inward ULF wave radial diffusion (Ozeke et al., 2017) during the recovery phase of geomagnetic storms.

Geomagnetic storms represent the most dynamic of Space Weather events and significant progress has been made in understanding these dynamics and the physical processes controlling them. Despite this, the effect that geomagnetic storms and Space Weather have on space- and ground-based infrastructure and the ability to model both the global and local dynamics of the magnetosphere during geomagnetic storms remains limited. This includes our ability to forecast storm-time magnetosphere dynamics as well as our understanding of storm-time geomagnetically induced currents (GICs), the effects of space-based radiation on spacecraft charging and single event upsets, increased satellite drag during storms and even the effect that enhanced storm-time energetic particle precipitation has on climate.

### 2.8.2. Substorms

Substorms are one of the most common, readily observed, and recognizable Space Weather events. In the magnetosphere a substorm is characterized by the transition from a high energy state to a lower energy state, whereby energy stored in the stretched magnetotail, the result of the solar wind-magnetosphere interaction described in section 2.6, is explosively released (Cummings et al., 1968). In the ionosphere this release

of energy is manifested by a rapid expansion and brightening of the auroral oval in both the northern and southern hemispheres (Akasofu 1964). These vibrant auroral displays, readily observed on the Earth, make substorms the most recognizable Space Weather event.

As described in section 2.3, dayside magnetic field lines reconnect with the solar wind and are dragged antisunward and into the nightside of the Earth. A buildup of magnetic flux in the nightside magnetosphere leads to the formation of the highly stretched and compressed magnetic topology known as the magnetotail. This buildup of flux cannot be sustained indefinitely, eventually the magnetotail becomes unstable and reconnection is triggered causing the nightside magnetotail to dipolarize and in the process explosively release energy stored in the stretched magnetic field configuration. This explosive release of energy is the magnetospheric substorm; the storage of energy pre-onset is referred to as the substorm growth phase and the period following onset is the substorm expansion phase (McPherron, 1979). Following the release of energy in the nightside magnetosphere, bursty bulk flows (BBFs) are launched toward the Earth (Angelopoulos et al., 1992), the tail dipolarizes, and plasma is injected into the inner magnetosphere (Baker, 1984). This dipolarization leads to the disruption of the cross-tail current system into the ionosphere and subsequently the formation of the substorm current wedge (SCW) (McPherron et al., 1973) and increased ultra-low frequency wave activity, observed both in the nightside magnetosphere (Kepko et al., 2001) and the ionosphere (Rae and Watt, 2016). In the ionosphere the dipolarization corresponds to a rapid poleward and azimuthal expansion and brightening of the auroral oval and an enhancement in the ionospheric electrojets. The increased auroral activity is referred to as the auroral substorm. Prolonged magnetotail activity can lead to continued magnetotail activity in the form of steady magnetospheric convection intervals (SMCs) (Kissinger et al., 2011) and periodic substorms (Walach et al., 2017). SMCs result from continued reconnection on the dayside, or balanced reconnection rates on both the day and night side (DeJong et al., 2009), leading to prolonged magnetotail and auroral activity. Periodic substorms are generally observed at geosynchronous orbit (Borovsky et al., 1993; Cai et al., 2006) and may develop as the result of enhanced oxygen outflow from the ionosphere following a substorm (Ouellette et al., 2013). Note that periodic substorms are less well understood than SMCs and isolated substorms.

The process or processes that trigger magnetospheric substorms are one of the most controversial topics in space physics (Angelopoulos et al., 2008a, 2008b; Lui 2009). A dedicated NASA mission, the Time History of Events and Macroscale Interactions during Substorms (THEMIS) (Angelopoulos et al., 2008b) was launched

specifically to determine how energy was released in the magnetotail during substorms and differentiate between the prevailing near-Earth neutral line (Baker et al., 1996) and current disruption (Lui, 1996) paradigms. However, observations from a dense array of auroral imagers and conjugate magnetospheric spacecraft during the THEMIS era have led to the development of a third paradigm, the auroral streamer paradigm (Nishimura et al., 2010). Rather than providing science closure the introduction of a new paradigm has added to the substorm controversy and remains a highly debated topic within space physics community (Frey et al., 2010; Rae et al., 2013).

The controversy surrounding substorm onset has spurred significant scientific discoveries and advances, often facilitated by the launch of the THEMIS mission and new arrays with both high spatial and temporal resolution providing observations of the aurora, magnetic field perturbations, and ionosphere dynamics during substorms. In particular, auroral beads, azimuthal auroral structures developing during the late growth phase and early expansion phase of a substorm, have been shown to be a key component of the substorm process (Donovan et al., 2006; Liang et al., 2008; Sakaguchi et al., 2009; Rae et al., 2009; Kataoka et al., 2011; Murphy et al., 2014b; Kalmoni et al., 2017). Detailed analysis of the spatial and temporal scales of these auroral forms suggests they are the ionospheric manifestation of a plasma instability in the nightside magnetotail (Rae et al., 2010; Kalmoni et al., 2015, 2018). Multipoint observations from low-altitude spacecraft demonstrate the three-dimensional structure of the substorm current wedge (Murphy et al., 2013; Forsyth et al., 2014). Multipoint magnetospheric observations have revealed how the magnetotail plasma and magnetic field environments evolve during magnetospheric substorms (Miyashita et al., 2009; Runov et al., 2011; Gabrielse et al., 2014; Machida et al., 2014) and the effects that magnetotail substorms have on the inner magnetosphere (Turner et al., 2015; Jaynes et al., 2015; Murphy et al., 2018a).

### 2.8.3. The Kelvin–Helmholtz Instability

The Kelvin–Helmholtz instability occurs in response to velocity shears across boundaries separating fluids. At Earth, the Kelvin–Helmholtz instability can develop along the magnetopause when the magnetosheath velocity is sufficiently high (Mann and Wright, 1999; Hasegawa et al. 2004). The Kelvin–Helmholtz instability can generate large-scale surface waves and vortices along the magnetopause boundary that facilitate localized activity (Nykyri and Otto, 2001) and energy transport along the magnetopause boundary and as well as more global activity along the magnetospheric flanks and deeper into the inner magnetosphere (Wright and Mann, 2006).

Locally, the Kelvin–Helmholtz instability can abet the transport of plasma across the magnetopause boundary (Nykyri and Otto 2001). Recent multipoint observations from the Magnetospheric Multiscale (MMS) mission have also demonstrated localized plasma heating via wave–particle interactions (Moore et al., 2016) and reconnection (Eriksson et al., 2016) can occur within the vortices and rolled up plasma and magnetic fields that develop as a result of the Kelvin–Helmholtz instability, as illustrated in Figure 2.3b. Globally, surface waves driven by the Kelvin–Helmholtz instability transport energy away from the magnetopause boundary as ultra-low frequency waves and excite field line resonances in the inner magnetosphere (Southwood 1974) (Figure 2.3b). This energy can further couple to radiation belt electrons via resonant wave–particle interactions (Claudepierre et al., 2013) and may be a key component of radiation belt energization during geomagnetic storms and high-speed solar wind (Paulikas and Blake, 1979; Murphy et al., 2018b).

While reconnection is undoubtedly the dominant process in solar wind–magnetosphere coupling and energy transfer (Dungey, 1961), recent work has shown the Kelvin–Helmholtz instability at Earth to be ubiquitous along the dayside magnetopause developing during all IMF and solar wind conditions (Kavosi and Reader, 1995) and not just periods of high-speed solar wind (Mann and Wright, 1999). This suggests that the Kelvin–Helmholtz instability may be an ever-present component of the solar wind–magnetosphere interaction.

### 2.8.4. Dynamic Pressure Pulses

Dynamic pressure pulses are abrupt step-like increases in the solar wind dynamic pressure. Pressure pulses attend solar wind shocks (Cattell et al., 2017) and frequently occur near stream interfaces (Morley et al., 2010). The enhanced pressures transmit compressional fast magnetohydrodynamic waves into the magnetosphere, as shown in Figure 2.3c, cause the magnetopause to move Earthward rapidly and compress the Earth’s magnetic field. The inward motion stops when the enhanced solar wind pressure is balanced by an increased magnetic pressure closer to the Earth. Gradients in the pressure applied to the current sheets at the magnetopause and inner edge of the low-latitude boundary layer generate field-aligned currents that flow into the high-latitude ionosphere and produce transient swirls of current and flow that can be observed by ground magnetometers and radars (Sibeck et al., 2003).

The magnetopause compression can lead to a rapid loss of inner magnetosphere plasma via magnetopause shadowing and can also drive enhanced ULF wave activity that furthers the loss of inner magnetospheric plasma via outward radial diffusion (Murphy et al., 2015). The compression enhances plasma temperature anisotropies,

providing a source of free energy for VLF waves (Halford et al., 2015), which then drive further dynamics via wave–particle interactions (Horne and Thorne, 1998). The compression of the magnetopause also launches an antisunward pulse and large-amplitude azimuthal electric field that can interact with inner magnetospheric plasmas via drift resonances; this is especially true with dynamic pressure pulses associated with shocks (Foster et al., 2015; Hudson et al., 2017; Kanekal et al., 2016). Overall, solar wind dynamic pressure pulses have drastic effects on the Earth’s magnetosphere, driving various wave modes throughout the inner magnetosphere as well as particle transport, energization, and loss.

## 2.9. CONCLUSION

Sixty years ago we knew little to nothing about the solar wind and its interaction with the Earth’s magnetosphere. The ten years that followed the advent of the first scientific spacecraft in 1958 saw the discovery of the Earth’s ring current and radiation belts, the magnetopause, magnetosheath and bow shock, the magnetotail, the cusps, and the plasmasphere (Stern, 1996; Chapter 1, this volume). The following years saw an intense effort to specify the characteristics of the various plasma and magnetic field regimes that comprise the magnetosphere and its environs. The locations of the often-sharp boundaries that separate them were identified, and the properties of both regions and boundaries were determined as functions of solar wind conditions. Reconnection was found to play a key role in governing the flow of solar wind, mass energy, and momentum into and through the magnetosphere, as evidenced by the dependence of many magnetospheric phenomena, such as storms and substorms, on the north/south component of the IMF. The magnetospheric current systems that both connect and flow on the boundaries between regions were identified and quantified as a function of solar wind conditions. Recent years have seen renewed interest in the role of the bow shock and its foreshock in energizing particles and modifying the solar wind–magnetosphere interaction. Surveys of plasma waves throughout geospace demonstrated the crucial roles they play in particle energization, transport, and loss. Cross-scale coupling occurs at the bow shock, magnetopause, and in the magnetotail, often resulting in turbulence.

And yet, many questions remain unanswered. While we can predict when substorms are likely to occur, we cannot predict exactly when, where, or how strong they will be. While the north/south component of the interplanetary magnetic field (IMF  $B_z$ ) controls the flow of energy into the magnetosphere, the solar wind velocity may control the burstiness of its release during substorms (Newell et al., 2016), and we do not know whether geomagnetic

storms will enhance, diminish, or leave the intensities of radiation belt electrons unchanged (Reeves et al., 2003).

Observations from single well-instrumented spacecraft, in particular low-cost CubeSats, will continue to play an important role in answering these and other questions. In recent years, constellation missions have increasingly been used to address both global and local questions such as the nature of magnetic reconnection (Chapter 40, this volume). The multi-agency missions of the International Solar–Terrestrial Program (Acuña et al., 1995; Sibeck and Kudela, 1999) and the THEMIS mission (Angelopoulos et al., 2008b) provide good examples of the former, while the closely-spaced spacecraft of the Cluster (Escoubet et al., 2001) and MMS (Burch et al., 2016) missions provide examples of the latter. Arrays of ground-based magnetometers (Gjerloev, 2012), ELF/VLF radio receivers (Barr et al., 2000), riometers (Honary et al., 2011), all-sky imagers, and radars place the spacecraft observations in context and help evaluate the global significance of individual mechanisms. Global imagers, such as the IMAGE, TWINS, and forthcoming SMILE mission will play an increasingly important role in exploring the solar wind–magnetosphere interaction (Chapter 42, this volume). Increasingly elaborate magnetohydrodynamic, hybrid, and particle-in-cell code simulations (Chapter 37, this volume; Chapter 38, this volume; Chapter 44, this volume) encapsulate our best understanding of the basic physics. We will truly understand nature of the solar wind–magnetosphere interaction when these simulations accurately predict the wide range of magnetospheric phenomena as a function of the ever-varying solar wind.

## ACKNOWLEDGMENTS

Research at GSFC was funded by NASA’s THEMIS and Van Allen Probes projects. KRM is partially funded by NSF grant 162403, NASA ROSES Guest Investigator 18-HGIO18/2-0122 and Space Weather Operations to Research 18-HSWO2R18-0010. The solar wind observations shown in Figure 2.1 were obtained from omniweb. [gsfc.nasa.gov](http://gsfc.nasa.gov).

## REFERENCES

- Acuña, M. H., et al. (1995), The global geospace science program and its investigations. In C. T. Russell (Ed.), *The Global Geospace Mission* (p. 5). Kluwer, Norwell, MA.
- Akasofu, S. I. (1964), The development of the auroral substorm, *Planet. Space Sci.*, 12(4), 273–282, [https://doi.org/10.1016/0032-0633\(64\)90151-5](https://doi.org/10.1016/0032-0633(64)90151-5).
- Akasofu, S.-I., and S. Chapman (1961), The ring current, geomagnetic disturbance and the Van Allen radiation belts, *J. Geophys. Res.*, 66, 1321–1350.

- Alexeev, I. I., D. G. Sibeck, and S. Y. Bobrovnikov (1998), Concerning the location of magnetopause merging as a function of the magnetopause current strength, *J. Geophys. Res.*, 103, 6675–6684.
- Alfvén, H. (1942), Existence of electromagnetic-hydrodynamic waves, *Nature*, 150, 405–406.
- Anderson, B. J., R. E. Erlandson, and L. J. Zanetti (1992), A statistical study of Pc1-2 magnetic pulsations in the equatorial magnetosphere: 1. Equatorial occurrence distributions, *J. Geophys. Res.*, 97, 3075–3088.
- Anderson, B. J., T.-D. Phan, and S. A. Fuselier (1997), Relationships between plasma depletion and subsolar reconnection, *J. Geophys. Res.*, 102, 9531–542.
- Angelopoulos, V., et al., (1992), Bursty bulk flows in the inner central plasma sheet, *J. Geophys. Res.*, 97, 4027–4039.
- Angelopoulos, V., et al. (2008a), Tail reconnection triggering substorm onset, *Science*, 321 (5891), 931–935, doi:10.1126/science.1160495.
- Angelopoulos, V., et al. (2008b), First results from the THEMIS mission, *Space Sci. Rev.*, 141, 453–476.
- Arnoldy, R. L. (1971), Signature in the interplanetary medium for substorms, *J. Geophys. Res.*, 76, 5189–5201.
- Ashford, S. M., et al. (1998), Energetic solar particle dropouts detected at 1.63 AU: A possible encounter with the Earth's distant magnetotail, *J. Geophys. Res.*, 103, 9535–9544.
- Aubry, M. P., C. T. Russell, and M. G. Kivelson (1970), Inward motion of the magnetopause before a substorm, *J. Geophys. Res.*, 75, 7018–7031.
- Baker, D. N. (1984), Particle and field signatures of substorms in the near magnetotail. In E. W. Hones (Ed.), *Magnetic reconnection in space and laboratory plasmas, Geophysical Monograph Series* (Vol. 30, pp. 193–202). American Geophysical Union, <https://doi.org/10.1029/GM030p0193>.
- Baker, D. N., T. I. Pulkkinen, V. Angelopoulos, et al. (1996), Neutral line model of substorms: Past results and present view, *J. Geophys. Res.*, 101(A6), 12975–13010, doi:10.1029/95JA03753.
- Baker, D. N., et al. (2018), Space weather effects in the Earth's radiation belts, *Space Sci. Rev.*, 214, doi:10.1007/s11214-017-0452-7.
- Bame, S. J., et al. (1967), Characteristics of the plasma sheet in the Earth's magnetotail, *J. Geophys. Res.*, 113–129, 1967.
- Bame, S. J., et al. (1980), Deceleration of the solar wind upstream from the Earth's bow shock, *J. Geophys. Res.*, 85, 281–2990.
- Barr, R., D. Llanwyn Jones, and C. J. Rodger (2000), ELF and VLF radio waves, *J. Atmo. Solar-Terr. Phys.*, 62, 1689–1718.
- Baumjohann, W., G. Paschmann, and H. Lühr (1990), Characteristics of high-speed ion flows in the plasma sheet, *J. Geophys. Res.*, 95, 3801–3809.
- Behannon, K. W. (1970), Geometry of the geomagnetic tail, *J. Geophys. Res.*, 75, 743–753.
- Berchem, J., et al. (1998), The distant tail at 200 RE: Comparison between Geotail observations and the results from a global magnetohydrodynamic simulation, *J. Geophys. Res.*, 103, 9121–9142.
- Berchem, J., and C. T. Russell (1982), The thickness of the magnetopause current layer: ISEE 1 and 2 observations, *J. Geophys. Res.*, 87, 2108–2114.
- Blanco-Cano, X., N. OMidi, and C. T. Russell (2009), Global hybrid simulations: Foreshock waves and cavitons under radial interplanetary magnetic field geometry, *J. Geophys. Res.* 114, doi:10.1029/2008JA013406.
- Borovsky, J. E., R. J. Nemzek, and R. D. Belian (1993), The occurrence rate of magnetospheric-substorm onsets: Random and periodic substorms, *J. Geophys. Res.*, 98, 3807–3813.
- Borovsky, J. E., and J. A. Valdivia (2018), The Earth's magnetosphere: A systems science overview and assessment, *Surveys in Geophysics*, 39, 817–859, doi:10.1007/s10712-018-9487-x, 2018.
- Bortnik, J., and R. M. Thorne (2007), The dual role of ELF/VLF chorus waves in the acceleration and precipitation of radiation belt electrons, *J. Atmo. Sol. Terr. Phys.*, 69, 378–386.
- Bortnik, J., et al. (2009), An observations linking the origin of plasmaspheric hiss to discrete chorus emissions, *Science*, 324, 775–778.
- Bothmer, V., and I. A. Daglis (2007), *Space Weather: Physics and Effects*, Springer, New York.
- Boyd, A. J., et al. (2018), What causes radiation belt enhancements: A survey of the Van Allen Probes era, *Geophys. Res. Lett.*, 45, doi:10.1029/2018GL077699.
- Burch, J. L. (1973), Rate of erosion of dayside magnetic flux based on a quantitative study of the dependence of polar cusp latitude on the interplanetary magnetic field, *Radio Sci.*, 8, 55–961.
- Burch, J. L., et al. (2016), Magnetospheric Multiscale overview and science objectives, *Space Sci. Rev.*, 199, 5–21.
- Burgess, D., E. Möbius, and M. Scholer (2012), Ion acceleration at the Earth's bow shock, *Space Sci. Rev.*, 173, 5–47, 2012.
- Burton, R. K., R. L. McPherron, and C. T. Russell (1975), An empirical relationship between interplanetary conditions and Dst, *J. Geophys. Res.*, 80, 4204–4214.
- Cai, X., M. G. Henderson, and C. R. Clauer (2006), A statistical study of magnetic dipolarization for sawtooth events and isolated substorms at geosynchronous orbit with GOES data, *Ann. Geophys.*, 24, 3481–3490, doi:10.5194/angeo-24-3481-2006.
- Califf, S., et al (2014), THEMIS measurements of quasi-static electric fields in the inner magnetosphere, *J. Geophys. Res.*, 11, 939–9951.
- Cattell, C., et al. (2017), Dayside response of the magnetosphere to a small shock compression: Van Allen Probes, Magnetospheric MultiScale, and GOES-13, *Geophys. Res. Lett.*, 44, 8712–8720, doi:10.1002/2017GL074895.
- Chapman, J. F., et al. (2004), MHD simulations of Earth's bow shock: Interplanetary magnetic field orientation effects on shape and position, *J. Geophys. Res.*, 109(A4), doi:10.1029/2003JA010235.
- Chapman, S., and V. C. A. Ferraro (1930), *A new theory of magnetic storms, Nature*, 126, 129–130.
- Chen, M. W., et al. (1993), Stormtime transport of ring current and radiation-belt ions, *J. Geophys. Res.*, 98, 3835–3849.
- Cheng, C. Z., and Q. Qian (1994), Theory of ballooning-mirror instabilities for anisotropic pressure plasmas in the magnetosphere, *J. Geophys. Res.*, 99, 1113–11209.

- Claudepierre, S. G., et al. (2013), Van Allen Probes observation of localized drift resonance between poloidal mode ultra-low frequency waves and 60 keV electrons, *Geophys. Res. Lett.*, 40 (17), 4491–4497, doi:10.1002/grl.50901.
- Claudepierre, S. G., et al. (2017), The hidden dynamics of relativistic electrons (0.7–1.5 MeV) in the inner zone and slot region, *J. Geophys. Res.*, 122, 3127–3144.
- Constantinescu, O. D., et al. (2009), THEMIS observations of duskside compressional Pc5 waves, *J. Geophys. Res.*, 114, doi:10.1029/2008JA013519.
- Cooling, B. M. A., C. J. Owen, and S. J. Schwartz (2001), Role of the magnetosheath flow in determining the motion of open flux tubes, *J. Geophys. Res.*, 106, 18763–18775.
- Cornwall, J. M. (1965), Cyclotron instabilities and electromagnetic emission in the ultra-low frequency and very low frequency ranges, *J. Geophys. Res.*, 70, 612–619.
- Coroniti, F. V., and C. F. Kennel (1979), Magnetospheric reconnection, substorms, and energetic particle acceleration. In J. Arons, C. Max, and C. McKee (Eds.) *Particle acceleration mechanisms in astrophysics* (pp. 169–178). American Institute of Physics, New York.
- Cowley, S. W. H. (1981), Magnetospheric asymmetries associated with the y-component of the IMF, *Planet. Space Sci.*, 2, 79–96.
- Crooker, N. U. (1979), Dayside merging and cusp geometry, *J. Geophys. Res.*, 4, 951–959.
- Crooker, N. U. (1990), On mapping flux transfer events to the ionosphere, *J. Geophys. Res.*, 95, doi:10.1029/JA05iA04p0375.
- Cummings, W., J. Barfield, and P. Coleman Jr. (1968), Magnetospheric substorms observed at the synchronous orbit, *J. Geophys. Res.*, 73(21), 6687–6698.
- Daglis, I. A., et al. (1994), Energy density of ionospheric and solar wind origin ions in the near-Earth magnetotail during substorms, *J. Geophys. Res.*, 9, 5691.
- Davis, T. N., and R. Parthasarathy (1967), The relationship between polar magnetic activity DP and growth of the geomagnetic ring current, *J. Geophys. Res.*, 72, 5825.
- Dayeh, M. A., et al. (2015), Shape of the terrestrial plasma sheet in the near-Earth magnetospheric tail as imaged by the Interstellar Boundary Explorer, *Geophys. Res. Lett.*, 21150–2122.
- DeJong, A. D., A. J. Ridley, X. Cai, and C. R. Clauer (2009), A statistical study of BRIs (SMCs), isolated substorms, and individual sawtooth injections, *J. Geophys. Res.*, 114, A08215, doi:10.1029/2008JA013870.
- Dessler, A. J., and E. N. Parker (1959), Hydromagnetic theory of geomagnetic storms, *J. Geophys. Res.*, 24, 2239–2252.
- Donovan, E., et al. (2006), The azimuthal evolution of the substorm expansive phase onset aurora. In M. Syrjäsuo and E. Donovan (Eds.), *Proceedings of ICS-8* (pp. 55–60). University of Calgary, Alberta, Canada.
- Dungey, J. W. (1961), Interplanetary magnetic field and the auroral zone, *Phys. Rev. Lett.*, 6, 47.
- Dunlop, M. W., et al. (2011), Magnetopause reconnection across wide local time, *Ann. Geophys.*, 19, 1683–1697.
- Eastman, T. E., and E. W. Hones, Jr. (1979), Characteristics of the magnetospheric boundary layer and magnetopause layer as observed by Imp 6, *J. Geophys. Res.*, 4, 2019–2028.
- Eastman, T. E., L. A. Frank, W. K. Peterson, and W. Lennartson (1984), The plasma sheet boundary layer, *J. Geophys. Res.*, 89, doi:10.1029/JA089iA03p01553.
- Edmiston, J. P., C. F. Kennel, and D. Eichler (1982), Escape of heated ions upstream of quasi-parallel shocks, *Geophys. Res. Lett.*, 9, 531–534.
- Elkington, S. R., M. K. Hudson, and A. A. Chan (1999), Interaction with toroidal-mode Pc-5 ULF oscillations, *Geophys. Res. Lett.*, 26, 3273–3276.
- Engbretson, M. J., et al. (1991), A comparison of ULF fluctuations in the solar wind, magnetosheath, and dayside magnetosphere: 1. Magnetosheath morphology, *J. Geophys. Res.*, 6, 3441–3454.
- Erickson, G. M., and R. A. Wolf (1980), Is steady convection possible in the Earth's magnetotail? *Geophys. Res. Lett.*, 7, 897–900.
- Eriksson, S., et al. (2016), Magnetospheric Multiscale observations of magnetic reconnection associated with Kelvin-Helmholtz waves, *Geophys. Res. Lett.*, 43(11), 5606–5615, <https://doi.org/10.1002/2016GL068783>.
- Escoubet, C. P., M. Fehringer, and M. Goldstein (2001), The Cluster mission, *Ann. Geophys.*, 19, 1197–1200.
- Fairfield, D. H. (1967), The ordered magnetic field of the magnetosheath, *J. Geophys. Res.*, 72, 5865–5877.
- Fairfield, D. H. (1971), Average and unusual locations of the Earth's magnetopause and bow shock, *J. Geophys. Res.*, 76, 6700–6716.
- Fairfield, D. H., et al. (1990), Upstream pressure variations associated with the bow shock and their effects on the magnetosphere, *J. Geophys. Res.*, 95, 3773–3786.
- Fedder, J. A., and J. G. Lyon (1995), The Earth's magnetosphere is 165 RE long: Self-consistent currents, convection, magnetospheric structures and processes for northward interplanetary magnetic field, *J. Geophys. Res.*, 100, 3623–3635.
- Fok, M.-C., T. E. Moore, and M. E. Greenspan (1996), Ring current development during storm main phase, *J. Geophys. Res.*, 101, 15311–15322.
- Fox, N. J., B. H. Mauk, and J. B. Blake (2006), Role of non-adiabatic processes in the creation of the outer radiation belts, *Geophys. Res. Lett.*, 33, doi:10.1029/2006GL02658.
- Forsyth, C., et al. (2014), In situ spatiotemporal measurements of the detailed azimuthal substructure of the substorm current wedge, *J. Geophys. Res.: Space Phys.*, 119(2), 927–946, <https://doi.org/10.1002/2013JA019302>.
- Foster, J. C., et al. (2015), Shock-induced prompt relativistic electron acceleration in the inner magnetosphere, *J. Geophys. Res.: Space Phys.*, 120, 1661–1674, doi:10.1002/2014JA020642.
- Foster, J. C., P. J. Erickson, Y. Omura, et al. (2016), Van Allen Probes observations of prompt MeV radiation belt electron acceleration in nonlinear interactions with VLF chorus, *J. Geophys. Res.*, 121, doi:10.1002/2016JA023429.

- Freeman, M. P., and D. J. Southwood (1988), The correlation of variations in the IMF with magnetosheath field variations, *Adv. Space Sci.*, 8, 217–220.
- Frey, H. U. et al. (2010), Comment on “Substorm triggering by new plasma intrusion: THEMIS all-sky imager observations” by Y. Nishimura et al. *J. Geophys. Res.*, 115, A12232, doi:10.1029/2010JA016113.
- Fung, S. F., X. Shao, and L. C. Tan (2006), Long-term variations of the electron slot region and global radiation belt structure, *Geophys. Res. Lett.*, 33, doi:10.1029/2005GL024891.
- Fuselier, S. A., S. M. Petriner, and K. J. Trattner (2000), Stability of the high-latitude reconnection site for steady northward IMF, *Geophys. Res. Lett.*, 27, doi:10.1029/1999GL003706.
- Gabrielse, C., V. Angelopoulos, A. Runov, and D. L. Turner (2014), Statistical characteristics of particle injections throughout the equatorial magnetotail, *J. Geophys. Res.: Space Phys.*, 119, 2512–2535, doi:10.1002/2013JA019638.
- Ganushkina, N. Y. et al. (2011), Locations of boundaries of outer and inner belts as observed by Cluster and Double Star, *J. Geophys. Res.*, 116, doi:10.1029/2010JA016376.
- Garcia, H. A., and W. N. Spjeldvik (1985), Anisotropy characteristics of geomagnetic trapped ions, *J. Geophys. Res.*, 90, 347–358.
- Gary, S. P., M. F. Thomsen, L. Yin, and D. Winske (1995), Electromagnetic proton cyclotron instability: Interactions with magnetospheric protons, *J. Geophys. Res.*, 100, 21961–21972.
- Gjerloev, J. W. (2012), The SuperMAG data processing technique, *J. Geophys. Res.*, 117, doi:10.1029/2012JA017683, 2012.
- Gkioulidou, M., et al. (2014), The role of small-scale ion injections in the buildup of Earth’s ring current pressure: Van Allen Probes observations of the 17 March 2013 storm, *J. Geophys. Res.*, 119, 7327–7342.
- Goldstein, J. (2006), Plasmasphere response: Tutorial and review of recent imaging results, *Space Sci. Rev.*, 124, 203–216, doi:10.1007/s11214-006-105-y.
- Goldstein, J., et al. (2005), Coupled response of the inner magnetosphere and ionosphere on 17 April 2002, *J. Geophys. Res.*, 110, doi:10.1029/2004JA010712, 2005.
- Gonzalez, W. D., and F. S. Mozer (1974), A quantitative model for the potential resulting from reconnection with an arbitrary interplanetary magnetic field, *J. Geophys. Res.*, 79, 4186–4194.
- Gosling, J. T., et al. (1982), Evidence for specularly reflected ions upstream from the quasi-parallel bow shock, *Geophys. Res. Lett.*, 9(12), 1333–1336.
- Gosling, J. T., et al. (1985), North–south and dawn–dusk plasma asymmetries in the distance tail lobes: ISEE 3, *J. Geophys. Res.*, 90, 6354–6360.
- Grebowsky, J. M. (1970), Model study of plasmopause motion, *J. Geophys. Res.*, 75, 4329–4333.
- Guild, T. B., et al. (2008), Geotail and LFM comparisons of plasma sheet climatology: 1. Average values, *J. Geophys. Res.*, 113, doi:10.1029/2007JA012611.
- Halford, A. J., et al. (2015), BARREL observations of an ICME-shock impact with the magnetosphere and the resultant radiation belt electron loss, *J. Geophys. Res.: Space Phys.*, 91, https://doi.org/10.1002/2014JA020873.
- Hardy, D. A., H. K. Hills, and J. W. Freeman (1979), Occurrence of the lobe plasma at lunar distance, *J. Geophys. Res.*, 84, 72–77.
- Hasegawa, et al. (2004), Transport of solar wind into Earth’s magnetosphere through rolled-up Kelvin–Helmholtz vortices, *Nature*, 430(7001), 755–758, doi:10.1038/nature02799.
- Hietala, H., et al. (2018), In situ observations of a magnetosheath high-speed jet triggering magnetopause reconnection, *Geophys. Res. Lett.*, 45, 1732–1740, 2018.
- Honary, F., S. R. Marple, K. Barratt, P. Chapman, M. Grill, and E. Nielsen (2011), Digital beam-forming imaging riometer systems, *Rev. Sci. Instrum.*, 82, 031301, doi:10.1063/1.356730.
- Horne, R. B., and Thorne, R. M. (1998), Potential waves for relativistic electron scattering and stochastic acceleration during magnetic storms, *Geophys. Res. Lett.*, 25(15), 3011–3014, https://doi.org/10.1029/98GL01002.
- Horne, R. B., and R. M. Thorne (2003), Relativistic electron acceleration and precipitation during resonant interactions with whistler-model chorus, *Geophys. Res. Lett.*, 30, doi:10.1029/2003GL01673.
- Howe, H. C., Jr., and J. H. Binsack (1972), Explorer 33 and 35 plasma observations of magnetosheath flow, *J. Geophys. Res.*, 77, doi:10.1029/JA077i01p033334.
- Hudson, M., et al. (2017), Simulated prompt acceleration of multi-MeV electrons by the 17 March 2015 interplanetary shock, *J. Geophys. Res.*, 122, doi:10.1002/2017JA024445.
- Hutchinson, J. A., Wright, D. M., and Milan, S. E. (2011), Geomagnetic storms over the last solar cycle: A superposed epoch analysis, *J. Geophys. Res.: Space Phys.*, 116(A9), https://doi.org/10.1029/2011JA016463.
- Intriligator, D. S., et al. (1979), Evidence for magnetospheric tail associated phenomena at 3100 RE, *Geophys. Res. Lett.*, 6, 585–588.
- Jaynes, A. N., et al. (2015), Source and seed populations for relativistic electrons: Their roles in radiation belt changes, *J. Geophys. Res.: Space Phys.*, 120, 7240–7254, https://doi.org/10.1002/2015JA021234.
- Kalmoni, N. M. E., et al. (2015), Statistical characterization of the growth and spatial scales of the substorm onset arc, *J. Geophys. Res.: Space Phys.*, 120(10), 1–14, https://doi.org/10.1002/2015JA021470.
- Kalmoni, N. M. E. et al. (2017), Statistical azimuthal structuring of the substorm onset arc: Implications for the onset mechanism, *Geophys. Res. Lett.*, 44(5), 2078–2087, https://doi.org/10.1002/2016GL071826.
- Kalmoni, N. M. E. et al. (2018), A diagnosis of the plasma waves responsible for the explosive energy release of substorm onset, *Nat. Commun.*, 9, Art. 4806, https://doi.org/10.1038/s41467-018-07086-0.
- Kanekal, S. G., et al. (2016), Prompt acceleration of magnetospheric electrons to ultrarelativistic energies by the 17 March 2015 interplanetary shock, *J. Geophys. Res.: Space Phys.*, 121, 7622–7635.
- Kataoka, R., and Y. Miyoshi (2006), Flux enhancement of radiation belt electrons during geomagnetic storms driven

- by coronal mass ejections and corotating interaction regions. *Space Weather*, 4, S09004, <https://doi.org/10.1029/2005SW000211>.
- Kataoka, R., Y. Miyoshi, T. Sakanoi, et al. (2011), Turbulent microstructures and formation of folds in auroral breakup arc, *J. Geophys. Res.*, 116, A00K02, doi:10.1029/2010JA016334.
- Katus, R. M., et al. (2015), Statistical storm time examination of MLT-dependent plasmopause location derived from IMAGE EUV, *J. Geophys. Res.*, 120, 5545–5559.
- Kavosi, S., and J. Raeder (2015), Ubiquity of Kelvin–Helmholtz waves at Earth’s magnetopause, *Nat. Commun.*, 6, 7019, doi:10.1038/ncomms8019.
- Kempf, Y., et al. (2015), Ion distributions in the Earth’s foreshock: Hybrid-Vlasov simulation and THEMIS observations, *J. Geophys. Res.*, 120(5), doi:10.1002/2014JA020519, 2015.
- Kepko, L., Kivelson, M. G., and Yumoto, K. (2001), Flow bursts, braking, and Pi2 pulsations. *J. Geophys. Res.*, 106 (A2), 1903, <https://doi.org/10.1029/2000JA000158>.
- Kim, H. J., and Chan, A. A. (1997). Fully adiabatic changes in storm time relativistic electron fluxes. *J. Geophys. Res.*, 102 (A10), 22107–22116, <https://doi.org/10.1029/97JA01814>.
- Kissinger, J., R. L. McPherron, T.-S. Hsu, and V. Angelopoulos (2011), Steady magnetospheric convection and stream interfaces: Relationship over a solar cycle, *J. Geophys. Res.*, 116, A00I19, doi:10.1029/2010JA015763.
- Kissinger, J., R. L. McPherron, T.-S. Hsu, et al. (2012), Necessity of substorm expansions in the initiation of steady magnetospheric convection, *Geophys. Res. Lett.*, 3, doi:10.1029/2012GL052599.
- Kissinger, J. et al. (2014), The importance of storm time steady magnetospheric convection in determining the final relativistic electron flux level, *J. Geophys. Res.*, 11, 7433–7443.
- Kistler, L. M., et al. (2016), The source of O<sup>+</sup> in the storm time ring current, *J. Geophys. Res.*, 121, 5333–534.
- Kivelson, M. G., and H. E. Spence (1988), On the possibility of quasi-static convection in the quiet magnetotail, *Geophys. Res. Lett.*, 15, 1541–1544.
- Kivelson, M. G., et al. (1996), Flux ropes, interhemispheric conjugacy, and magnetospheric current closure, *J. Geophys. Res.*, 101, 27341–27350.
- Kronberg, E. A., et al. (2011), On the origin of the energetic ion events measured upstream of the Earth’s bow shock by STEREO, Cluster, and Geotail, *J. Geophys. Res.*, 116, doi:10.1029/2010JA015561.
- Lagg, A., et al. (2001), Energetic particle measurements during the earth swing-by of the Cassini spacecraft in August 1999, *J. Geophys. Res.*, 106, 3020–3022.
- Laitinen, T. V., et al. (2010), Local influence of magnetosheath plasma beta fluctuations on magnetopause reconnection, *Ann. Geophys.*, 28, 1053–1063.
- Lavraud, B., et al. (2004), Cluster survey of the high-altitude cusp properties: A three-year statistical study, *Ann. Geophys.*, 22, 3009–3019.
- Lavraud, B., et al. (2007), Strong bulk plasma acceleration in Earth’s magnetosheath: A magnetic slingshot effect? *Geophys. Res. Lett.*, 34, doi:10.1029/2007GL030024.
- Le, G., C. T. Russell, and H. Kuo (1993), Flux transfer events—Spontaneous or driven? *Geophys. Res. Lett.*, 20, 71–794.
- Letaw, J. R., R. Siberberg, and C. H. Tsao (1989), Radiation hazards on space missions outside the magnetosphere, *Adv. Space Res.*, 9, 285–21.
- Li, W., et al. (2009), Global distribution of whistler-mode chorus waves observed on the THEMIS spacecraft, *Geophys. Res. Lett.*, 36, doi:10.1029/2009GL037595.
- Li, W., et al. (2014), Radiation belt electron acceleration by chorus waves during the 17 March 2013 storm, *J. Geophys. Res.: Space Phys.*, 119, 4681–4693, doi: 10.1002/2014JA019945.
- Li, X., D. N. Baker, T. P. O’Brien, L. Xie, and Q. G. Zong (2006), Correlation between the inner edge of outer radiation belt electrons and the innermost plasmopause location, *Geophys. Res. Lett.*, 33, doi:10.1029/2006GL026294.
- Liang, J., E. F. Donovan, W. W. Liu, et al. (2008), Intensification of preexisting auroral arc at substorm expansion phase onset: Wave-like disruption during the first tens of seconds, *Geophys. Res. Lett.*, 35, L17S19, doi:10.1029/2008GL033666.
- Liemohn, M. W., J. U. Kozyra, V. K. Jordanova, et al. (1999), Analysis of early phase ring current recovery mechanisms during geomagnetic storms, *Geophys. Res. Lett.*, 26, 2845–2848.
- Liemohn, M. W., J. U. Kozyra, M. F. Thomsen, et al. (2001), Dominant role of the asymmetric ring current in introducing the stormtime Dst\*, *J. Geophys. Res.*, 106, 10883–10904.
- Lin, N., et al. (1991), Comparison of ULF fluctuations in the solar wind, magnetosheath, and dayside magnetosphere: 2. Field and plasma conditions in the magnetosheath, *J. Geophys. Res.*, 96, 3455–3464.
- Liu, T. Z., et al. (2017), Fermi acceleration of electrons inside foreshock transient event cores, *J. Geophys. Res.*, 122, doi:10.1002/2017JA024480.
- Lorentzen, K. R., et al. (2000), Precipitation of relativistic electrons by interaction with electromagnetic ion cyclotron waves, *J. Geophys. Res.*, 105, 5381–5390.
- Lui, A. T. Y. (1996), Current disruption in the Earth’s magnetosphere: Observations and models, *J. Geophys. Res.*, 101(A6), 13067–13088, doi:10.1029/96JA00079.
- Lui, A. T. Y. (2009), Comment on “Tail reconnection triggering substorm onset,” *Science*, 324(5933), 1391, doi:10.1126/science.1167726.
- Lui, A. T. Y., R. W. McEntire, and K. B. Baker (2001), A new insight on the cause of magnetic storms, *Geophys. Res. Lett.*, 28, 3413–3416.
- Lyons, L. R., and R. M. Thorne (1973), Equilibrium structure of radiation belt structure, *J. Geophys. Res.*, 78, 2142–2149.
- Lyons, L. R., R. M. Thorne, and C. F. Kennel (1972), Pitch-angle diffusion of radiation belt electrons within the plasmasphere, *J. Geophys. Res.*, 77, 3455–3474.
- Machida, S., Y. Miyashita, A. Ieda, et al. (2014), Statistical visualization of the Earth’s magnetotail and the implied mechanism of substorm triggering based on superposed-epoch analysis of THEMIS data, *Ann. Geophys.*, 32, 99–111.
- Maezawa, K. (1975), Magnetotail boundary motion associated with geomagnetic substorms, *J. Geophys. Res.*, 80, 3543–354.
- Maezawa, K., et al. (1997), Structure of the distant magnetotail and its dependence on the IMF by component: Geotail observations, *Adv. Space Res.*, 20, 949–959.

- Maltsev, Yu. P., and W. B. Lyatsky (1975), Field-aligned currents and erosion of the dayside magnetopause, *Planet. Space Sci.*, 23, 1257–1260.
- Mann, I. R., and A. N. Wright (1999), Diagnosing the excitation mechanisms of Pc5 magnetospheric flank waveguide mode and FLRs, *Geophys. Res. Lett.*, 26, 2609.
- Mann, I. R., et al. (2013), Discovery of the action of a geophysical synchrotron in the Earth's Van Allen radiation belts, *Nat. Comm.*, 4, doi:10.1038/ncomms3795.
- Mann, I. R., Ozeke, L. G., Murphy, et al. (2016). Explaining the dynamics of the ultra-relativistic third Van Allen radiation belt, *Nat. Phys.*, 12, 978–983, <https://doi.org/10.1038/nphys3799>.
- Mariani, F., and N. F. Ness (1969), Observations of the geomagnetic tail at 500 Earth radii by Pioneer 8, *J. Geophys. Res.*, 74, 5633–5641.
- Martyn, D. F. (1951), The theory of magnetic storms and auroras, *Nature*, 167, 92–94.
- 1, et al. (2013), Science objectives and rationale for the Radiation Belt Storm Probes mission, *Space Sci. Rev.*, 179, 3–27.
- McPherron, R. L. (1979). Magnetospheric substorms, *J. Geophys. Res.: Space Phys.*, 17(4), 657–681.
- McPherron, R. L., C. T. Russell, and M. P. Aubry (1973), Satellite studies of magnetospheric substorms on August 15, 1968: 9. Phenomenological model for substorms, *J. Geophys. Res.*, 78(16), 3131–3149, doi:10.1029/JA078i016p03131.
- Meng, C. I., and K. A. Anderson (1970), A layer of energetic electrons (>40 keV near the magnetopause), *J. Geophys. Res.*, 75, 1827.
- Meng, C. I., and K. A. Anderson (1974), Magnetic field configuration in the magnetotail near 60 earth radii, *J. Geophys. Res.*, 79, 5143–5153.
- Menz, A. M., et al. (2017), The role of convection in the buildup of the ring current pressure during the 17 March 2013 storm, *J. Geophys. Res.*, 122, 475–492.
- Meredith, N. P., et al. (2013), Global statistical evidence for chorus as the embryonic source of plasmaspheric hiss, *Geophys. Res. Lett.*, 40, 281–896.
- Michel, F. C., and A. J. Dessler (1970), Diffusive entry of solar-flare particles into geomagnetic tail, *J. Geophys. Res.*, 75, 6061–6072.
- Millan, R.M., and R. M. Thorne (2007), Review of radiation belt relativistic electron loss, *J. Atmo. Sol. Terr. Phys.*, 6, 362–377, doi:10.1016/j.jastp.2006.06.01.
- Mitchell, D. G., et al. (1987), An extended study of the low-latitude boundary layer on the dawn and dusk flanks of the magnetopause, *J. Geophys. Res.*, 92, 734–7404.
- Miyashita, Y., et al. (2009), A state-of-the-art picture of sub-storm-associated evolution of the near-Earth magnetotail obtained from superposed epoch analysis, *J. Geophys. Res.*, 114, A01211, doi:10.1029/2008JA013225.
- Moldwin, M. B., J. Howard, J. Sanny, et al. (2004), Plasmaspheric plumes: CRRES observations of enhanced density beyond the plasmopause, *J. Geophys. Res.*, 1099, doi:10.102/2003JA010310.
- Moore, T. W., Nykyri, K., and Dimmock, A. P. (2016), Cross-scale energy transport in space plasmas, *Nat. Phys.*, 12, 1–23, <https://doi.org/10.1038/nphys3869>.
- Morley, S. K., et al. (2010), Dropouts of the outer electron radiation belt in response to solar wind stream interfaces: Global positioning system observations, *Proc. R. Soc. A*, 466(2123), 3329–3350, <https://doi.org/10.1098/rspa.2010.0078>.
- Murphy, K. R., et al. (2013), The detailed spatial structure of field-aligned currents comprising the substorm current wedge, *J. Geophys. Res.: Space Phys.*, 118(12), 7714–7727, <https://doi.org/10.1002/2013JA018979>.
- Murphy, K. R., et al. (2014a), A ULF wave driver of ring current energization, *Geophys. Res. Lett.*, 41(19), 6595–6602, <https://doi.org/10.1002/2014GL061253>.
- Murphy, K. R., et al. (2014b), Inner magnetospheric onset preceding reconnection and tail dynamics during substorms: Can substorms initiate in two different regions? *J. Geophys. Res.: Space Phys.*, 119(12), 9684–9701, <https://doi.org/10.1002/2014JA019795>.
- Murphy, K. R., Mann, I. R., and Sibeck, D. G. (2015), On the dependence of storm-time ULF wave power on magnetopause location: Impacts for ULF wave radial diffusion, *Geophys. Res. Lett.*, 42(22), 9676–9684, <https://doi.org/10.1002/2015GL066592>.
- Murphy, K. R., et al. (2018a), The global statistical response of the outer radiation belt during geomagnetic storms, *Geophys. Res. Lett.*, 45(9), 3783–3792, <https://doi.org/10.1002/2017GL076674>.
- Murphy, K. R., et al. (2018b), Determining the mode, frequency, and azimuthal wave number of ULF waves during a HSS and moderate geomagnetic storm, *J. Geophys. Res.: Space Phys.*, 123, <https://doi.org/10.1029/2017JA024877>.
- National Research Council (2003), *The Sun to the Earth – and Beyond: A Decadal Research Strategy in Solar and Space Physics*. National Academies Press, Washington, DC.
- Newell, P. T., et al. (1989), Some low-altitude cusp dependencies on the interplanetary magnetic field, *J. Geophys. Res.*, 4, 8921–8927.
- Newell, P. T., et al. (2016), Substorm probabilities are best predicted from solar wind speed, *J. Atmo. Solar-Terr. Phys.*, 1436, 28–37.
- Nishimura, Y., et al. (2010), Substorm triggering by new plasma intrusion: THEMIS all-sky imager observations, *J. Geophys. Res.*, 115, A07222, doi:10.1029/2009JA015166.
- Nykyri, K., and A. Otto (2001), Plasma transport at the magnetospheric boundary due to reconnection in Kelvin–Helmholtz vortices, *Geophys. Res. Lett.*, 28, 3565–3568, doi:10.1029/2001GL013239.
- Onsager, T. G., and M. Lockwood (1997), High-latitude particle precipitation and its relationship to magnetospheric source regions, *Space Sci. Rev.*, 80, 77–107.
- Ouellette, J. E., O. J. Brambles, J. G. Lyon, et al. (2013), Properties of outflow-driven sawtooth substorms, *J. Geophys. Res.: Space Phys.*, 118, 3223–3232, doi:10.1002/jgra.50309.
- Ozeke, L. G., and I. R. Mann (2008), Energization of radiation belt electrons by ring current ion driven ULF waves, *J. Geophys. Res.*, 113, doi:10.102/2007JA012468.
- Ozeke, L. G., et al. (2014), Analytic expressions for ULF radiation belt radial diffusion coefficients, *J. Geophys. Res.*, 119, 1587–1605.

- Ozeke, L. G., Mann, I. R., Murphy, et al. (2017). Ultra-relativistic radiation belt extinction and ULF wave radial diffusion: Modeling the September 2014 extended dropout event. *Geophys. Res. Lett.* (September), 1–10, <https://doi.org/10.1002/2017GL072811>.
- Paschmann, G., et al. (1993), Structure of the dayside magnetopause for low magnetic shear, *J. Geophys. Res.*, 98, 13409–13422.
- Paulikas, G. A., and J. B. Blake (1979), Effects of the solar wind on magnetospheric dynamics: Energetic electrons at the synchronous orbit. In W. P. Olson (Ed.) *Quantitative modeling of magnetospheric processes, Geophysics Monograph Series* (Vol. 21, pp. 180–202). American Geophysical Union, Washington, DC, doi:10.1029/GM021p0180.
- Petrinec, S. M. (2002), The location of the Earth's bow shock, *Planet. Space Sci.*, 50, 541–547.
- Phan, T.-D., et al. (1994), The magnetosheath region adjacent to the dayside magnetopause: AMPTE/IRM observations, *J. Geophys. Res.*, 99, 121–141.
- Phan, T. D., et al. (2000), Extended magnetic reconnection at the Earth's magnetopause from detection of bi-directional jets, *Nature*, 404, 848–850.
- Phan, T. D., et al. (2004), Cluster observations of continuous reconnection at the magnetopause under steady interplanetary magnetic field conditions, *Ann. Geophys.*, 22, 2355–2367.
- Phan, T. D., et al. (2013), Dependence of magnetic reconnection on plasma  $\beta$  and magnetic shear: Evidence from magnetopause observations, *Geophys. Res. Lett.*, 40(1), doi:10.1029/2012GL05428.
- Phan, T. D., et al. (2018), Electron magnetic reconnection without ion coupling in Earth's turbulent magnetosheath, *Nature*, 557, 202–206.
- Pulkkinen, T. I., et al. (2013), Plasma sheet magnetic fields and flows during steady magnetospheric convection events, *J. Geophys. Res.*, 118, 6136–6144.
- Rae, I. J., and C. E. J. Watt (2016). ULF waves above the nightside auroral oval during substorm onset. In A. Keiling, D.-H. Lee, and V. Nakariakov (Eds.) *Low-frequency waves in space plasmas* (pp. 99–120). American Geophysical Union, Washington, DC, <https://doi.org/10.1002/9781119055006.ch7>.
- Rae, I. J., et al. (2005). Evolution and characteristics of global Pc5 ULF waves during a high solar wind speed interval, *J. Geophys. Res.: Space Phys.*, 110(A12), 1–16, <https://doi.org/10.1029/2005JA011007>.
- Rae, I. J., et al. (2009) Near-Earth initiation of a terrestrial substorm, *J. Geophys. Res.*, 114, A07220, doi:10.1029/2008JA013771.
- Rae, I. J., et al. (2010). Optical characterization of the growth and spatial structure of a substorm onset arc, *J. Geophys. Res.: Space Phys.*, 115(10), 1–10, <https://doi.org/10.1029/2010JA015376>.
- Rae, I. J., et al. (2013), Comment on “Formation of substorm Pi2: A coherent response to auroral streamers and currents” by Y. Nishimura et al., *J. Geophys. Res.: Space Phys.*, 118, 3488–3496, doi:10.1002/jgra.50336.
- Reeves, G. D., and M. G. Henderson (2001), The storm-substorm relationship: Ion injections in geosynchronous measurements and composite energetic neutral atom images, *J. Geophys. Res.*, 106, 5833–5844.
- Reeves, G. D., et al. (1990), Multi-satellite measurements of the substorm injection region, *Geophys. Res. Lett.*, 17, 2015.
- Reeves, G. D., K. L. McAdams, R. H. W. Friedel, and T. P. O'Brien (2003), Acceleration and loss of relativistic electrons during geomagnetic storms, *Geophys. Res. Lett.*, 30(10), doi:10.1029/2002GL016513.
- Reeves, G. D., et al. (2013), Electron acceleration in the heart of the Van Allen radiation belts, *Science*, 341, 991–994.
- Rosenbauer, H., et al. (1975), Heos 2 plasma observations in the distant polar magnetosphere: The plasma mantle, *J. Geophys. Res.*, 80, doi:10.1029/JA00i019p02723.
- Rowland, D. E., and J. R. Wygant (1998), Dependence of the large-scale, inner magnetospheric electric field on geomagnetic activity, *J. Geophys. Res.*, 103, 14959–14694.
- Runov, A., et al. (2006), Structure of the magnetotail current sheet: 2001 Cluster observations, *Ann. Geophys.*, 24, 247–262.
- Runov, A., V. Angelopoulos, X.-Z. Zhou, et al. (2011), A THEMIS multicase study of dipolarization fronts in the magnetotail plasma sheet, *J. Geophys. Res.*, 116, A05216, doi:10.1029/2010JA016316.
- Safrankova, J., et al. (2007), Variations of the flank LLBL thickness as response to the solar wind dynamic pressure and IMF orientation, *J. Geophys. Res.*, 112, doi:10.1029/2006JA01189.
- Saikin, A. A., et al. (2016), The dependence on geomagnetic conditions and solar wind dynamic pressure of the spatial distributions of EMIC waves observed by the Van Allen Probes, *J. Geophys. Res.: Space Phys.*, 121, 4362–4377, doi:10.1002/2016JA022523.
- Sakaguchi, K., et al. (2009), Fine structures and dynamics in auroral initial brightening at substorm onsets, *Ann. Geophys.*, 27(2), 623–630, doi:10.5194/angeo-27-623-2009.
- Samsonov, A. A., et al. (2017), A method to predict magnetopause expansion in radial IMF events by MHD simulations, *J. Geophys. Res.: Space Phys.*, 122(3), doi:10.1002/2016JA023301.
- Sarris, E. T., S. M. Krimigis, and T. P. Armstrong (1976), Observations of magnetospheric bursts of high-energy protons and electrons at approximately 35 earth radii with Imp 7, *J. Geophys. Res.*, 81, doi:10.1029/JA081i013p02341.
- Sazhin, S. S., and M. Hayakawa (1992), Magnetospheric chorus emissions: A review, *Planet. Space Sci.*, 40, 681–697.
- Scarf, F. L. (1987), Pioneer 8 traversal of the geomagnetic tail at 1600 RE, *J. Geophys. Res.*, 2, 11201–11204.
- Scholer, M., H. Kucharek, and K. J. Trattner (1998), Injection and acceleration of energetic particles at collisionless shocks, *Adv. Space Res.*, 21, 533–542.
- Schulz, M., and L. J. Lanzerotti (1974), *Particle Diffusion in the Radiation Belts, Physics and Chemistry in Space*, vol. 7, Springer, New York.
- Schwartz, S. J., D. Burgess, and J. J. Moses (1996), Low-frequency waves in the Earth's magnetosheath: present status, *Ann. Geophys.*, 14, 1134–1150.
- Scokopke, N. (1966), A general relation between the energy of trapped paricles and the disturbance field near the Earth, *J. Geophys. Res.*, 71, 3125–3130.

- Selesnick, R. S. (2015), Measurement of inner radiation belt electrons with kinetic energy above 1 MeV, *J. Geophys. Res.*, 120, doi:10.1002/2015JA021387.
- Selesnick, R. S., M. D. Looper, and R. A. Mewaldt (2007), A theoretical model of the inner proton radiation belt, *Space Weather*, 5(4), doi:10.1029/2006SW000275.
- Sergeev, V. A., R. J. Pellinen, and T. I. Pulkkinen (1996), Steady magnetic convection: A review of recent results, *Space Sci. Rev.*, 75, 551–604.
- Shprits, Yu. Y., et al. (2006), Radial diffusion driven by losses at magnetopause, *J. Geophys. Res.*, 111, doi:10.1029/2006JA011657.
- Shprits, Yu. Y., et al. (2008a), Review of modeling of losses and sources of relativistic electrons in the outer radiation belt I: Radial transport, *J. Atmo. Solar-Terr. Phys.*, 70, 1679–1693.
- Shprits, Yu., et al. (2008b) Review of modeling of losses and sources of relativistic electrons in the outer radiation belt II: Local acceleration and loss, *J. Atmo. Solar-Terr. Phys.*, 70, 1694–1713.
- Shue, J.-H., et al. (1998). Magnetopause location under extreme solar wind conditions. *J. Geophys. Res.*, 103(A8), 17691, <https://doi.org/10.1029/98JA01103>.
- Sibeck, D. G., and K. Kudela (1999), *Interball in the ISTP Program*. Kluwer, Dordrecht.
- Sibeck, D. G., and R.-Q. Lin (2014), Size and shape of the distant magnetotail, *J. Geophys. Res.*, 119, 1029–1043.
- Sibeck, D. G., and R. W. McEntire (1988), Multiple satellite observations of leakage of particles from the magnetosphere, *Adv. Space Res.*, 8, 201–216.
- Siscoe, G. L., and E. Sanchez (1987), An MHD model for the complete open magnetotail boundary, *J. Geophys. Res.*, 92, 7405–7412.
- Sibeck, D. G., et al. (1986a), Major flattening of the distant geomagnetic tail, *J. Geophys. Res.*, 91, 4223–4237.
- Sibeck, D. G., et al. (1986b), Twisting of the geomagnetic tail. In Y. Kamide and J. A. Slavin (Eds.), *Solar wind–magnetosphere coupling* (pp. 717–730). Terra, Tokyo.
- Sibeck, D. G., R. W. McEntire, A. T. Y. Lui, and S. M. Krimigis (1987a), A statistical study of ion pitch angle distributions. In A. T. Y. Lui (Ed.), *Magnetotail physics* (pp. 225–230). Johns Hopkins Press.
- Sibeck, D. G., R. W. McEntire, A. T. Y. Lui, et al. (1987b), Magnetic field drift shell splitting: Cause of unusual dayside particle pitch angle distributions during storms and substorms, *J. Geophys. Res.*, 92(A12), 13485–13497, doi:10.1029/JA092iA12p13485.
- Sibeck, D. G., Lopez, R. E., and Roelof, E. C. (1991). Solar wind control of the magnetopause shape, location, and motion. *J. Geophys. Res.*, 96(A4), 5489, <https://doi.org/10.1029/90JA02464>.
- Sibeck, D. G., et al. (1999), Comprehensive study of the magnetospheric response to a hot flow anomaly, *J. Geophys. Res.*, 104, 4577–4594.
- Sibeck, D. G., N. B. Trivedi, E. Zesta, et al. (2003), Pressure-pulse interaction with the magnetosphere and ionosphere, *J. Geophys. Res.*, 108, doi:10.1029/2002JA00675.
- Siscoe, G. L., and C. J. Schrijver (2010), Perspectives on heliophysics. In C. J. Schrijver and G. L. Siscoe (Eds.), *Heliophysics: Space Storms and radiation: Causes and effects* (pp. 1–14). University Press, Cambridge.
- Slavin, J. A., et al. (1983), Average configuration of the distant (less than 220-earth-radii) magnetotail – Initial ISEE-3 magnetic field results, *Geophys. Res. Lett.*, 10, 973–976.
- Slavin, J. A., et al. (1985), An ISEE-3 study of average and sub-storm conditions in the distant magnetotail, *J. Geophys. Res.*, 90, 10875–10895.
- Song, P., and C. T. Russell (1992), Model of the formation of the low-latitude boundary layer for strongly northward interplanetary magnetic field, *J. Geophys. Res.*, 7, 1411–1420.
- Song, P., H. J. Singer, and G. L. Siscoe (2001), *Space Weather. Geophysical Monograph 125*, American Geophysical Union, Washington, DC.
- Sonnerup, B. U. Ö. (1969), Acceleration of particles reflected at a shock front, *J. Geophys. Res.*, 74(5), 1301–1304.
- Sonnerup, B. U. Ö. (1974), Magnetopause reconnection rate, *J. Geophys. Res.*, 79, 1546–1549.
- Sonnerup, B. U. Ö., et al. (1981), Evidence for magnetic field reconnection at the Earth's magnetopause, *J. Geophys. Res.*, 6, 10049–10067.
- Sorathia, K. A., et al. (2017), Energetic particle loss through the magnetopause: A combined global MHD and test-particle study, *J. Geophys. Res.*, 122, 9329–9343.
- Soterelis, T., and C.-I. Meng (1999), Magnetopause from pressure balance, *J. Geophys. Res.*, 104, 6889–6898.
- Soucek, J., E. Lucek, and I. Dandouras (2008), Properties of magnetosheath mirror modes observed by Cluster and their response to change in plasma parameters, *J. Geophys. Res.*, 113, doi:10.1029/2007JA012649.
- Southwood, D. J. (1974), Some features of field line resonances in the magnetosphere, *Planet. Space Sci.*, 22(3), 483–491. doi:10.1016/0032-0633(74)90078-6.
- Speiser, T. W. (1973), Magnetospheric current sheets, *Radio Sci.*, 8, doi:10.1029/RS008i011p00973.
- Speiser, T. W., D. J. Williams, and H. A. Garcia (1981), Magnetospherically trapped ions as a source of magnetosheath energetic ions, *J. Geophys. Res.*, 86, 723–732.
- Spence, H. E., M. G. Kivelson, R. J. Walker, and D. J. McComas (1989), Magnetospheric plasma pressures in the midnight meridian – Observations from 2.5 to 35 R<sub>E</sub>, *J. Geophys. Res.*, 4, 5264–5272.
- Spreiter, J. R., A. L. Summers, and A. Y. Alksne (1966), Hydro-magnetic flow around the magnetosphere, *Planet. Space Sci.*, 14, 251–250.
- Stern, D. P. (1996), A brief history of magnetospheric physics during the space age, *Rev. Geophys.*, 34, 1–31.
- Tanskanen, E. I., et al. (2005), Magnetotail response to prolonged southward IMF B<sub>z</sub> intervals: Loading, unloading, and continuous magnetospheric dissipation, *J. Geophys. Res.*, 110, doi:10.1029/2004JA010561.
- Terasawa, T., et al. (1997), Solar wind control of density and temperature in the near-Earth plasma sheet: Wind-Geotail collaboration, *Geophys. Res. Lett.*, 24, 935–938.

- Thorne, R. M. (2010), Radiation belt dynamics: The importance of wave-particle interactions, *Geophys. Res. Lett.*, 37, doi:10.1029/2010GL044990.
- Trattner, K. J., et al. (1994), Statistical analysis of diffuse ion events upstream of the Earth's bow shock, *J. Geophys. Res.*, 99, doi:10.1029/94JA00576.
- Trattner, K. J., S. M. Petrinec, S. A. Fuselier, and T. D. Phan (2012), The location of reconnection at the magnetopause: Testing the maximum magnetic shear model with THEMIS observations, *J. Geophys. Res.*, 117, doi:10.1029/2011JA016959.
- Tsurutani, B. T., D. E. Jones, and D. G. Sibeck (1984), The two-lobe structure of the magnetotail, from  $x = -60$  to  $-240 R_e$ , *Geophys. Res. Lett.*, 11, 1066–1069, doi:10.1029/GL011i010p01066.
- Tsyganenko, N. A. (1982), On the convective mechanism for formation of the plasma sheet in the magnetospheric tail, *Planet. Space Sci.*, 30, 1007–1012.
- Tsyganenko, N. A., and D. H. Fairfield (2004), Global shape of the magnetotail current sheet as derived from Geotail and Polar data, *J. Geophys. Res.*, 109, doi:10.1029/2003JA010062.
- Tsyganenko, N. A., and D. G. Sibeck (1994), Concerning flux erosion from the dayside magnetosphere, *J. Geophys. Res.*, 99, 13425–13436.
- Turner, D. L., Shprits, Y., Hartinger, M., and Angelopoulos, V. (2012a), Explaining sudden losses of outer radiation belt electrons during geomagnetic storms. *Nature Phys.*, 8(3), 208–212, <https://doi.org/10.1038/nphys2185>.
- Turner, D. L., et al. (2012b), Outer radiation belt flux dropouts: Current understanding and unresolved questions. In D. Summers, I. R. Mann, D. N. Baker, and M. Schulz (Eds.), *Dynamics of the Earth's radiation belts and inner magnetosphere*, *Geophysical Monograph Series* (Vol. 199, pp. 195–212), <https://doi.org/10.1029/2012GM001310>.
- Turner, D. L., et al. (2015), Energetic electron injections deep into the inner magnetosphere associated with substorm activity, *Geophys. Res. Lett.*, 42, 2079–2087.
- Turner, D. L., et al. (2017), Investigating the source of near-relativistic and relativistic electrons in Earth's inner radiation belt, *J. Geophys. Res.*, 123, 695–710.
- Ukhorskiy, A. Y., et al. (2005), Impact of toroidal ULF waves on the outer radiation belt electrons, *J. Geophys. Res.*, 110, doi:10.1029/2005JA011017.
- Ukhorskiy, A. Y., M. I. Sitnov, K. Takahashi, and B. J. Anderson (2009), Radial transport of radiation belt electrons due to stormtime Pc5 waves, *Ann. Geophys.*, 27, 2173–2181.
- Ukhorskiy, A. Y., M. I. Sitnov, R. M. Millan, and B. T. Kress (2011), The role of drift orbit bifurcations in energization and loss of electrons in the outer radiation belt, *J. Geophys. Res.*, 116, doi:10.1029/2011JA016623.
- Ukhorskiy, A. Y., M. I. Sitnov, V. G. Merkin, M. Gkioulidou, and D. G. Mitchell (2017), Ion acceleration at dipolarization fronts in the inner magnetosphere, *J. Geophys. Res.: Space Phys.*, 122(3), 3040–3054, doi: 10.1002/2016JA023304.
- Walach, M. T., et al. (2017), Comparative study of large-scale auroral signatures of substorms, steady magnetospheric convection events, and sawtooth events. *J. Geophys. Res.: Space Phys.*, 122(6), <https://doi.org/10.1002/2017JA023991>.
- Walker, R. C., U. Villante, and A. J. Lazarus (1975), Pioneer 7 observations of plasma flow and field reversal regions in the distant geomagnetic tail, *J. Geophys. Res.*, 80, 1238–1244.
- Walker, R. J., R. L. Richard, T. Ogino, and M. Ashour-Abdalla (1999), The response of the magnetotail to changes in the IMF orientation: The magnetotail's long memory, *Phys. Chem. Earth, Part C*, 24, 221–227.
- Walsh, B. M. et al. (2013), Statistical analysis of the plasmaspheric plume at the magnetopause, *J. Geophys. Res.*, 118, 4844–4851.
- Walsh, B. M., et al. (2014), The plasmaspheric plume and magnetopause reconnection, *Geophys. Res. Lett.*, 41, 223–228.
- Wang, Y., J. Raeder, and C. Russell (2004), Plasma depletion layer: its dependence on solar wind conditions and the Earth's dipole tilt, *Ann. Geophys.*, 22, 4273–4290.
- West, H. I., Jr., R. M. Buck, and J. R. Walton (1972), Shadowing of electron azimuthal-drift motions near the noon magnetopause, *Nature Phys. Sci.*, 240, 6–7.
- West, H. I., Jr., R. M. Buck, and J. R. Walton (1973), Electron pitch angle distributions throughout the magnetosphere as observed on Ogo 5, *J. Geophys. Res.*, 78, 1064–1081.
- Wilken, B., C. K. Goertz, D. N. Baker, P. R. Higbie, and T. A. Fritz (1982), The SSC on July 29, 1977 and its propagation within the magnetosphere, *J. Geophys. Res.*, 87, 5901–5910.
- Wilson, L. B., III, et al. (2016), Relativistic electrons produced by foreshock disturbances observed upstream of Earth's bow shock, *Phys. Rev. Lett.*, 117, 215101.
- Winterhalter, D., et al. (1984), The MHD Rankine-Hugoniot jump conditions and the terrestrial bow shock – A statistical comparison, *Adv. Space Res.*, 4, 287–292.
- Wolf, R. A., et al. (2009), Entropy and plasma sheet transport, *J. Geophys. Res.*, 114, doi:10.1029/2009JA014044.
- Yeoman, T. K., et al. (2012), Upstream-generated Pc3 ULF wave signatures observed near the Earth's cusp, *J. Geophys. Res.*, 117, doi:10.1029/2011JA017327.
- Yu, Y., et al. (2014), The role of ring current particle injections: Global simulations and Van Allen Probes observations during 17 March 2013 storm, *Geophys. Res. Lett.*, 41, 1126–1132.
- Zhang, H., et al. (2013), Spontaneous hot flow anomalies at quasi-parallel shocks: 1. Observations, *J. Geophys. Res.*, 118, 3357–3363.
- Zhou, X.-W., et al. (2000), Solar wind control of the polar cusp at high altitude, *J. Geophys. Res.*, 105, 245–252.
- Zhou, X.-W., et al. (2001), Factors controlling the diamagnetic pressure in the polar cusp, *Geophys. Res. Lett.*, 28, 915–918.
- Zou, Y., et al. (2018), Spreading speed of magnetopause reconnection X-lines using ground-satellite coordination, *Geophys. Res. Lett.*, 45, 80–89.
- Zwan, B. J., and R. A. Wolf (1976), Depletion of solar wind plasma near a planetary boundary, *J. Geophys. Res.*, 81, 1636–1648.

# 3

## The Equations of the Magnetosphere

Herbert Gunell

### ABSTRACT

The use of equations and mathematical modelling in magnetospheric and space physics is reviewed. First, the basic equations are discussed. Then, kinetic and fluid theory are treated. The role of approximations and the applicability of the theories in practice are emphasized.

### 3.1. THOUGHTS ON EQUATIONS

The topic of equations in magnetospheric science is vast. It involves the fundamental equations of electromagnetics, Newton's laws for particle motion, and the theory of relativity; these are crucial not only to the understanding of our field but, indeed, also to most if not all of physics. At the other end of the scale, we have equations that are used by researchers to explain a particular observation that cannot be generalized to other situations. In between we find equations that apply to a particular problem, such as the current–voltage relationship of the aurora, that while not fundamental are, nevertheless, often used by many scientists in the field.

The vast majority of the magnetosphere, at least in terms of volume, is a collisionless plasma that it can be described by the equations governing collisionless plasma physics. However, the interface toward the ionosphere at the magnetosphere's inner boundary is not collisionless at all. In fact, it is through collisions that we can see the aurora, the only magnetospheric phenomenon that is observable with the naked eye and without scientific instrumentation.

Speaking of equations, it may also be worthwhile to reflect upon why we use them and how best we can accomplish what we want with, or perhaps without, the use of

equations. Biot–Savart's law, which in modern textbooks is written as (Cheng, 1989):

$$\vec{B} = \frac{\mu_0 I}{4\pi} \oint_{C'} \frac{d\vec{l}' \times \vec{a}_R}{R^2} \quad (3.1)$$

was published by Biot and Savart (1820) in an article, about one page long, that contained no equations and no figures. In this case, a single equation combined with a small figure defining the quantities involved would more efficiently convey the relationship between the current and the magnetic field. Thus, we can talk about nature in the language of mathematics, which is understood also by those who are unfamiliar with the language in which the original publication is written. This being said, one must also acknowledge that mathematical language sometimes is not always readily comprehended even by colleagues in the field and that a physical understanding often may be easier to convey by other means, particularly when the study itself involves lengthy derivations of equations.

Furthermore, describing our findings mathematically allows for quantitative predictions. The ability to make predictions is necessary in developing science-based technical applications, and also to understand science itself when we move beyond simple relationships between a small number of variables. For example, the plasma waves that appear in the various parts of the magnetosphere are derived mathematically, and we would hardly be able to understand the physics behind them without

---

*Department of Physics, Umeå University, Umeå, Sweden;*  
*Royal Belgian Institute for Space Aeronomy, Brussels, Belgium*

that mathematical description. When analyzing satellite data it is by comparison to theoretical predictions of wavelengths, frequencies, and directions of propagation that we can identify wave modes and, in turn, generation mechanisms and energy flows. Thus, the mathematical description is more than a language used for efficiency in lieu of other languages. It is an integral part of modern magnetospheric physics, and we cannot do without it.

In spite of the above example of an equationless publication from 1820, the need for quantitative predictions was already realized at the time and the mathematical treatment of the natural sciences was emerging, as can be seen by the example of Poisson's equation, which is of great importance in our field (Poisson, 1813). The field of numerical simulations is entirely based on the numerical treatment of equations, and experiments can be conducted completely in the computer with no connection to reality. Once the equations that are used have been established, when their limitations are known and how initial and boundary conditions are put in relation to observations, these computer experiments can be conducted much like laboratory experiments. It is then possible to publish scientific papers that, although they rely completely on the mathematical description, contain no equations at all (Gunell et al., 2007, my own paper – not to embarrass anybody else). Thus, what existed first as a purely theoretical field of study has created a new field that is essentially experimental.

Computer simulations can be very successful in advancing our understanding of magnetospheric physics. In addition to the purely numerical challenges of the field, it is imperative to know the limitations of the numerical models used, to establish the validity of the models to the problem under study, and to confirm as much as possible that the numerical results agree with observations. There is not always a clear answer to the question of which model is the most suitable to a particular problem. A model may describe some aspects of a phenomenon well, while failing to describe others, and then the choice of model depends not only on the physics of the object of study but also on the question one endeavors to answer.

The aim of this chapter is to review, briefly, some of the techniques in common use in magnetospheric and space physics; to shed some light on the regimes of applicability of these models, and to provide a few examples of how these methods are used today. For a complete treatment with detailed derivations of the equations one has to turn to textbooks, for example the book by Krall and Trivelpiece (1973), which has been a useful source of information to the author of this chapter. I have endeavored to provide examples of mathematical modelling of various phenomena from the parts of magnetospheric physics

with which I am familiar. The list is not exhaustive nor restricted to Earth's magnetosphere, since the underlying principles that govern the behavior of our planet are shared with other solar system objects. In other words, in this chapter, the author goes on and on about stuff. The examples mentioned here do not cover the complete history of the field and it is very likely that important works have been forgotten. Hopefully, those that have been remembered will be able to illustrate the successes and challenges of mathematical modelling in magnetospheric physics today.

### 3.2. BASIC EQUATIONS

In magnetospheric physics, like everywhere else, the electric and magnetic fields can be found as solutions to Maxwell's equations:

$$\left\{ \begin{array}{l} \nabla \times \vec{E} = -\frac{\partial \vec{B}}{\partial t} \end{array} \right. \quad (3.2)$$

$$\left\{ \begin{array}{l} \nabla \times \vec{B} = \mu_0 \vec{J} + \varepsilon_0 \mu_0 \frac{\partial \vec{E}}{\partial t} \end{array} \right. \quad (3.3)$$

$$\left\{ \begin{array}{l} \nabla \cdot \vec{E} = \frac{\rho}{\varepsilon_0} \end{array} \right. \quad (3.4)$$

$$\left\{ \begin{array}{l} \nabla \cdot \vec{B} = 0 \end{array} \right. \quad (3.5)$$

The notation is explained in Table 3.1. In a plasma, the sources,  $\rho$  and  $\vec{J}$ , to the electromagnetic fields are given by the particle positions and velocities. For a complete description we thus need to model the motion of all charged particles. We may define a function that specifies the positions and velocities for the  $\bar{N}_\alpha$  particles of species  $\alpha$  (Klimontovich, 1958; Dupree, 1963):

$$N_\alpha(\vec{x}, \vec{v}, t) = \sum_{1 \leq j \leq \bar{N}_\alpha} \delta(\vec{x} - \vec{x}_j(t)) \delta(\vec{v} - \vec{v}_j(t)) \quad (3.6)$$

Integrating equation 3.6 over all phase space we obtain the total number of particle of species  $\alpha$ :

$$\bar{N}_\alpha = \int N_\alpha(\vec{x}, \vec{v}, t) d\vec{x} d\vec{v}. \quad (3.7)$$

The charge density in equation (3.4) and the current density in equation (3.3) are found by integration:

$$\rho = \sum_\alpha q_\alpha \int N_\alpha(\vec{x}, \vec{v}, t) d\vec{v} \quad (3.8)$$

$$\vec{J} = \sum_\alpha q_\alpha \int \vec{v} N_\alpha(\vec{x}, \vec{v}, t) d\vec{v} \quad (3.9)$$

Assuming that there is no particle production nor any losses and that only electric and magnetic forces

**Table 3.1** The quantities represented by the symbols used in this chapter

$\vec{E}$	Electric field	$\mu_0$	Permeability of free space
$\vec{B}$	Magnetic flux density	$\epsilon_0$	Permittivity of free space
$\vec{J}$	Current density	$c_0$	Speed of light in vacuum
$\rho$	Charge density	$\alpha$	Particle species
$\rho_m$	Mass density	$\vec{x}$	Particle position
$\sigma$	Conductivity	$\vec{v}$	Particle velocity
$f$	Distribution function	$\lambda_D$	Debye length
$n$	Plasma density	$\omega$	Angular frequency
$n_e$	Electron density	$\bar{P}$	Pressure tensor
$n_i$	Ion density	$e$	elementary charge
$k$	Wave number	$N_\alpha(\vec{x}, \vec{v}, t)$	Klimontovich–Dupree distribution function
$\nu$	Collision frequency	$\bar{N}_\alpha$	Total number of particles of species $\alpha$

act on the particles, the equations of motion for particle  $j$  are:

$$\frac{d\vec{x}_j}{dt} = \vec{v}_j \quad (3.10)$$

$$\frac{d\vec{v}_j}{dt} = \frac{q_j}{m_j} (\vec{E} + \vec{v}_j \times \vec{B}) \quad (3.11)$$

Due to the conservation of particles in phase space,  $dN_\alpha(\vec{x}, \vec{v}, t)/dt = 0$ , which using the equations of motion becomes:

$$\begin{aligned} \frac{\partial N_\alpha(\vec{x}, \vec{v}, t)}{\partial t} + \vec{v} \cdot \frac{\partial N_\alpha(\vec{x}, \vec{v}, t)}{\partial \vec{x}} \\ + \frac{q_\alpha}{m_\alpha} (\vec{E} + \vec{v} \times \vec{B}) \cdot \frac{\partial N_\alpha(\vec{x}, \vec{v}, t)}{\partial \vec{v}} = 0 \end{aligned} \quad (3.12)$$

The fields in equation 3.12 are the microscopic fields that each particle feels from all the other particles. For convenience it has not been explicitly stated in equation 3.12 that, when evaluating the fields at the particle position, the contributions from the particle itself must be removed (Dupree, 1963). Equation 3.12 looks conspicuously like the Vlasov equation, which we shall meet in section 3.3, but, unlike that equation, equation 3.12 includes the interaction between individual particles and can therefore describe fluctuations due to particle discreteness that are otherwise ignored in kinetic theory. Because this description requires modelling the motion of all particles it is not practical beyond very small systems. Nevertheless, there are practical applications where the effects of particle discreteness are important. Scattering of electromagnetic radiation is a single particle effect and incoherent scattering radars (Gordon, 1958) rely on it, because without the discrete particles there would be no scattering centers.

Thermal fluctuations in the plasma are caused by the motion of individual particles, which gives rise to collective wave modes. Power spectra of these thermal fluctuations can be computed through superposition of dressed test particles (Rostoker, 1964a, 1964b). In the dressed test particle model, each particle is treated as a Debye-shielded, dressed, test particle; the waves it generates as it moves through the plasma are computed and the contributions from all such test particles are added to yield the final spectrum. A plasma is often defined as an ionized gas that exhibits collective properties. In the dressed test particle method, the particles are – one by one – taken out of the plasma and its response to their presence is examined. In incoherent scattering radars, it is the width of the ion fluctuation spectrum that determines the width of the scattered power spectrum and not, as one naively could believe, the thermal spread of the electron distribution (Bowles, 1958; Fejer, 1960; Hagfors, 1961; Rosenbluth & Rostoker, 1962). This shows the importance of always remembering that the kinetic and fluid descriptions are approximations and that there are phenomena that can be understood only by going back to the most basic equations.

### 3.3. KINETIC THEORY

Kinetic theory is a statistical description of the plasma, where one considers the distribution function  $f(\vec{x}, \vec{v}, t)$ , which is defined so that the number of particles in an element  $d\vec{x} d\vec{v}$  of the six-dimensional phase space at time  $t$  is:

$$f(\vec{x}, \vec{v}, t) d\vec{x} d\vec{v}$$

As there are almost always more than one particle species in the plasma, separate distribution functions  $f_\alpha$  are defined for each species. Under the influence of electromagnetic forces, the distribution function satisfies the

Vlasov equation (Vlasov, 1968, translated from (Vlasov, 1938))

$$\frac{\partial f_\alpha}{\partial t} + \vec{v} \cdot \frac{\partial f_\alpha}{\partial \vec{x}} + \frac{q_\alpha}{m_\alpha} (\vec{E} + \vec{v} \times \vec{B}) \cdot \frac{\partial f_\alpha}{\partial \vec{v}} = 0 \quad (3.13)$$

Vlasov was the first to use this equation in plasma physics but equations of this form were known a full century earlier, when Liouville (1838) examined purely mathematical equation properties. In gas dynamics, the Boltzmann equation (Boltzmann, 1896) is an equation of the same kind which includes a collision term, and Jeans (1915) used an equation of this form to study the motion of stars. Henon (1982) argued that, because of this history, a better name for the equation would be “collisionless Boltzmann equation”, but the name for equation 3.13 that stuck – at least in this field – is the Vlasov equation.

The Vlasov equation, equation 3.13, is the zeroth order kinetic equation describing the plasma, in which all particle to particle interactions have been neglected. By assuming each particle interacts directly with one other particle, the first order kinetic equation can be derived. By including interactions between each particle and two others, one obtains the second order kinetic equation, and so on (Krall and Trivelpiece, 1973). The condition that allows us to neglect binary interactions is that there are many particles in a Debye cube:

$$\frac{1}{n\lambda_D^3} \ll 1 \quad (3.14)$$

This can be understood by considering two particles that occupy the same small volume within the Debye sphere, or cube. The motion of one of these particles will be more influenced by the many particles in the Debye sphere than by the only one other particle within the small volume. Thus, if equation 3.14 is satisfied, collective effects dominates over single particle effects, and that is how we usually define a plasma. For practical purposes, this sets the lower limit to the length scales for which conclusions can be drawn from zeroth order kinetic theory to approximately the Debye length. For shorter length scales, the word plasma may no longer be the most accurate description. For time scales, the Vlasov equation is valid for times shorter than typical collision times.

In space, collision frequencies are often very low, and the Vlasov equation and Maxwell’s equations together provide an excellent description of the plasma. When the collision times are longer than other relevant time scales, for example the plasma period and the electron and ion cyclotron periods, the distributions do not always thermalize into Maxwellian distributions, and space plasmas often have non-Maxwellian distributions, exhibiting suprathermal tails that can be modelled using, for example, Kappa distributions (Pierrard & Lazar, 2010) or simple pole expansions (Löfgren & Gunell, 1997; Gunell & Skiff,

2001, 2002). One application of kinetic theory is to compute dispersion relations for waves. In the electrostatic case, equations 3.13 and (3.4) are linearized and Fourier transformed, and a relationship between  $\omega$  and  $k$  can be found. A consequence of linearizing is that the results are only accurate for small amplitudes. For ion time scale waves in plasmas with non-Maxwellian distributions, Skiff et al. (2002) found that kinetic modes, that is to say, modes not well described by fluid theory, become important.

Another way in which kinetic theory can be used is to perform computer simulations to find how the plasma develops with time, given specific initial and boundary conditions. The two major classes of kinetic simulation methods are Vlasov simulations and particle simulations. In Vlasov simulations phase space is discretized, so that the distribution function is known at the nodes of a grid. With knowledge of the distribution function, the fields can be computed at the grid points. Then, with knowledge of the fields, the phase space fluxes are computed, the distribution function is updated and this processes is repeated over and over, advancing the distribution function in time. The methods used usually build on the splitting scheme (Cheng & Knorr, 1976). In particle simulations, the distribution function is represented by a number of particles, often several orders of magnitude fewer than the number of particles in the real plasma. The charge and current densities are transferred to a grid, and the fields are calculated on that grid. Then the particles are moved under influence of these fields and the process is repeated (Birdsall & Langdon, 1991). Even though particle in cell (PIC) simulations are using particles, they are not including particle to particle interactions and should be seen as a method for solving the Vlasov equation. Numerical kinetic modelling is described in more detail in Chapter 38.

In recent years, Vlasov simulations have been used in magnetospheric physics to study, for example, electrostatic acceleration of auroral electrons in the upward (Gunell et al., 2013) and downward (Gunell et al., 2015) current regions, and large-scale simulations of the magnetosphere have been performed of both the nightside (Palmroth et al., 2017) and dayside (Palmroth et al., 2018) regions. Those large-scale simulations employed a hybrid scheme where only the ions were modelled kinetically; the electrons are there as a mere neutralizing fluid. Such hybrid schemes are necessary as one cannot achieve the spatial and temporal resolutions required to simulate both electrons and ions in a simulation that includes the whole magnetosphere. The same idea is often employed in hybrid particle simulations, where the ions are treated as particles and the electrons as a fluid, and such hybrid models have been used extensively to study planets and other solar system objects (for example Kallio and Janhunen, 2001; Müller et al., 2011). There are also implicit

methods (Markidis et al., 2010; Chapter 35, this volume), where the electrons are included as particles but the electron plasma period is not resolved. In all these methods some of the physics is lost. That is the price one has to pay for the ability to perform global simulations, and it is the responsibility of the modeler to make sure that what is lost is not important to the problem that is being addressed.

### 3.4. FLUID THEORY AND MAGNETOHYDRODYNAMICS

A set of fluid equations can be obtained by taking moments of the Vlasov equation, combining these with Maxwell's equations, and closing the system of equations with a suitable equation of state. Depending on the assumptions that are made, widely differing phenomena can be described. Dispersion relations for waves in plasmas, such as Langmuir waves and ion acoustic waves, are often derived in this way in textbooks.

One particular theory of some interest in magnetospheric physics is magnetohydrodynamics (MHD). Alfvén (1942) used this set of equations:

$$\left\{ \begin{array}{l} \nabla \times \vec{B} = \mu_0 \vec{J} \\ \nabla \times \vec{E} = -\frac{\partial \vec{B}}{\partial t} \\ \vec{J} = \sigma(\vec{E} + \vec{v} \times \vec{B}) \\ \rho_m \frac{\partial \vec{v}}{\partial t} = \vec{J} \times \vec{B} - \nabla p \end{array} \right. \quad (3.15)$$

$$(3.16)$$

$$(3.17)$$

$$(3.18)$$

for a magnetized fluid, assuming the plasma to be incompressible and  $\sigma = \infty$  to derive the “electromagnetic-hydrodynamic” wave that propagates along the background magnetic field with phase speed:

$$v_A = \frac{B_0}{\sqrt{\mu_0 \rho}}. \quad (3.19)$$

Now these waves are known as Alfvén waves and  $v_A$  the Alfvén speed. Equations (3.15)–(3.18) are known as the MHD equations; when  $\sigma = \infty$  is assumed we have ideal MHD. These equations predicted the Alfvén waves, which subsequently were observed in experiments with liquid metals (Lehnert, 1958) and in the magnetosphere (Cummings et al., 1969). While the use of ideal MHD in space physics relies on many simplifying assumptions, this treatment is able to predict phenomena that do exist and have been observed. It is important to consider what the limitations are. The approach of Alfvén (1942) was to assume a perfectly conducting incompressible fluid and examine the consequences. If we instead start with a kinetic description and derive the fluid equations by

computing the moments of equation 3.13 – with a collision term on the right-hand side, making it a Boltzmann equation – we may be able to determine when certain assumptions are valid. In a single-fluid model the momentum equation then becomes:

$$\rho_m \frac{\partial \vec{v}}{\partial t} + \rho_m (\vec{v} \cdot \nabla) \vec{v} = \rho \vec{E} + \vec{J} \times \vec{B} - \nabla \cdot \vec{P}, \quad (3.20)$$

where  $\vec{P}$  is the plasma pressure tensor. The generalized Ohm's law is obtained by multiplying the equations for the first moment by  $q_\alpha/m_\alpha$  for electrons and ions and adding the two equations to form:

$$\begin{aligned} \frac{\partial \vec{J}}{\partial t} + \nabla \cdot (\vec{v} \vec{J} + \vec{J} \vec{v} - \vec{v} \vec{v} \rho) &= \left( \frac{n_e e^2}{m_e} + \frac{n_i e^2}{m_i} \right) \vec{E} \\ &+ \left( \frac{e^2}{m_e} + \frac{e^2}{m_i} \right) \frac{\rho_m \vec{v} \times \vec{B}}{m_e + m_i} - \left( \frac{em_i}{m_e} - \frac{em_e}{m_i} \right) \frac{\vec{J} \times \vec{B}}{m_e + m_i} \\ &- \frac{e}{m_e} \nabla \cdot \left( \vec{P}_i \frac{m_e}{m_i} - \vec{P}_e \right) - \nu \vec{J}. \end{aligned} \quad (3.21)$$

For simplicity a plasma constituted of electrons and one singly charged ion species ( $q_\alpha = e$ ) has been assumed, and the collision term has been approximated using the average collision frequency,  $\nu$ . We also need equations of continuity for the mass and charge densities:

$$\frac{\partial \rho_m}{\partial t} + \nabla \cdot (\rho_m \vec{v}) = 0 \quad (3.22)$$

$$\frac{\partial \rho}{\partial t} + \nabla \cdot \vec{J} = 0. \quad (3.23)$$

Equations 3.20–3.23 form a set of single fluid equations, which in order to be solved need be closed by an equation of state relating the pressure and density, for example  $p \propto \rho_m$  for an isothermal fluid;  $p \propto \rho_m^\gamma$ , where  $\gamma = C_p/C_V$  is the specific heat ratio, for an adiabatic fluid or  $\nabla \cdot \vec{v} = 0$  for an incompressible fluid.

In going from equations (3.15)–(3.18) to equations 3.20–3.23 a number of approximations have been made. Observing that  $m_e \ll m_i$  will simplify equation 3.21 somewhat. Quasi neutrality will make  $\rho = 0$ , and if small perturbations around an equilibrium are considered the term  $\nabla \cdot (\vec{v} \vec{J} + \vec{J} \vec{v} - \vec{v} \vec{v} \rho)$  in equation 3.21 can be neglected, since it is of second order. The term containing  $\vec{J} \times \vec{B}$  in equation 3.21 is negligible in comparison to the term containing  $\vec{v} \times \vec{B}$ , if characteristic length scales over which the quantities involved change are long enough, because according to equation (3.15)  $\vec{J}$  is proportional  $\nabla \times \vec{B}$ . If also the temporal changes are slow enough, the  $\partial \vec{J} / \partial t$  term can be neglected. Similarly, the

pressure gradient can be neglected for large length scales and for low-pressure plasmas in strong magnetic fields.

In equation (3.18) the divergence of the pressure tensor has been approximated by a pressure gradient. The off-diagonal terms of  $\bar{P}$  may be neglected if the Reynolds number is large so that viscosity is unimportant. Furthermore, the use of a scalar pressure means that pressure isotropy has been assumed. In a collision-dominated plasma, isotropy is ensured, and even in collisionless plasmas this approximation is often used successfully. If the collision frequency is low, other processes on faster time scales act as effective collisions to isotropize the plasma. Thus, MHD, under the assumption of an isotropic pressure, can be applicable to large and slow scales, even though it cannot say anything about the processes on small and fast scales that are necessary to maintain that applicability.

By assuming quasi neutrality (Schottky, 1924) the space charge density is taken to be zero, that is to say  $\rho = 0$ , without placing the corresponding restriction on the divergence of the electric field. Thus, equation (3.4) is violated in this approximation and we may very well have  $\nabla \cdot \vec{E} \neq 0$ . If we find  $\vec{E}$  in quasi neutral theory, equation (3.4) can be used to compute the charge density,  $\rho$ , that gave rise to that field. The plasma is not neutral – only quasi neutral. Even though this paragraph is in the section about fluid theory, quasi neutrality is used in kinetic theory too. For example, Chiu and Schulz (1978) used a quasi neutral kinetic model of an auroral field line to find that significant electric fields parallel to the magnetic field exist over distances of several Earth radii due to the magnetic mirror configuration. When does quasi neutrality not apply? The electric field around a test particle that is placed in a plasma falls off on a typical spatial scale of a Debye length. However, while the spatial scale over which the plasma can sustain a deviation from quasi neutrality is related to the Debye length,  $1 \lambda_D$  is not an upper limit to it. In electric double layers, space charge effects are generating a potential drop, and these structures can be “some tens of plasma Debye lengths” (Torvén and Andersson, 1979).

Global numerical modelling is discussed in Chapter 37. Here, let us briefly consider one example of a situation where considerations of the approximations made matter, namely magnetic reconnection. If the plasma truly obeyed the ideal MHD equations, the field lines would always be frozen to the plasma and reconnection would be impossible. Of course, the plasma is not an ideal MHD fluid and field lines reconnect all the time. In resistive MHD, reconnection is possible in principle, but it has been found that it is necessary to include Hall effects to obtain realistic reconnection rates (Birn et al., 2001). Moreover, two-fluid effects have been shown to be important for a more detailed description of the physics involved (Yamada et al.,

2010). Also, pressure anisotropy and kinetic effects (Egedal et al., 2013) influence the reconnection process. At Jupiter’s moon Ganymede (Chapter 35, this volume), Hall MHD has proved better than resistive MHD at predicting a configuration of field aligned currents that agree with observations of auroral emissions (Dorelli et al., 2015).

### 3.5. TEST PARTICLE MODELS

Both kinetic and fluid models, described in sections 3.3 and 3.4 respectively, are self-consistent. They account for both how the fields affect the particles and how the particles affect the fields. Test particle simulations is a class of simplified models that are not self-consistent. Instead the fields are prescribed and the particle trajectories that result from those given fields are calculated by integrating the equation of motion with the Lorentz force acting on the particles. This can be useful in cases where the particles do not affect the fields to a significant extent. For example, in Earth’s radiation belts that were discovered at the dawn of the space age (Van Allen et al., 1958) have been modelled in this way (Roederer, 1967; Chapter 21, this volume).

Another example of the use of test particle models is to study a minor species that does not affect the behavior of the plasma. For example, charge-exchange X-rays are caused when highly charged ions ( $O_6^+$ ,  $C_6^+$ ,  $Ne_8^+$ , etc.), which constitute a small fraction of the solar wind, undergo charge-exchange collisions with neutrals in the exosphere of a planet. The X-ray emissions can be modelled by first using a self-consistent hybrid model of the interaction between the planet and the solar wind to find the electric and magnetic field. Then a test particle model can be used to compute the trajectories of the highly charged ions and the resulting emissions (Gunell et al., 2004, 2007).

The test particle simulation can be useful for specific purposes as shown by these examples, but not being self-consistent it remains an incomplete description of the plasma.

### 3.6. SUMMARY

Now that we have reached the end of the last section before the concluding words, let us examine whether it is possible to draw a simple picture that makes sense of it all. An attempt at that is shown in Figure 3.1, which illustrates how the main classes of plasma theory described in this chapter are related to each other. With Maxwell’s equations, Newton’s laws of motion, and the Lorentz force we can model how all particles move and how the particles, in turn, affect the electric and magnetic fields. As following all particles is impractical in most

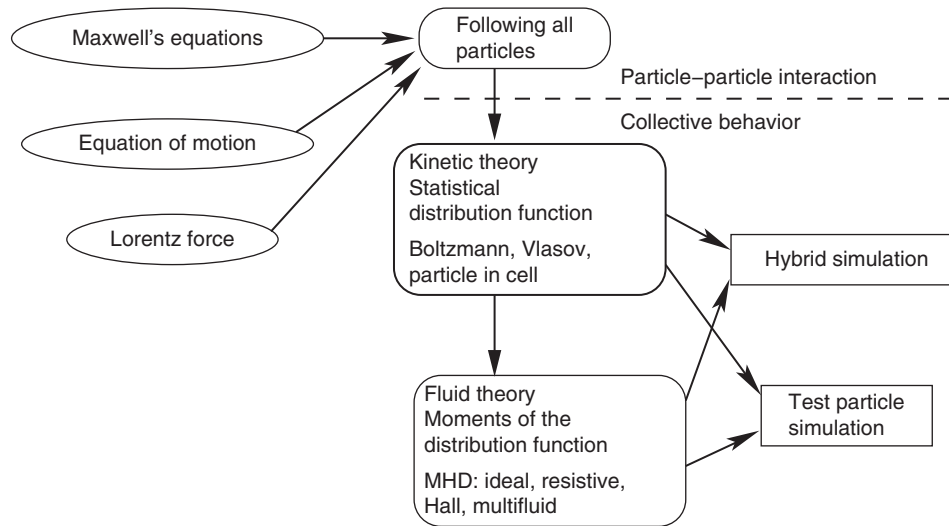


**Figure 3.1** Schematic figure designed to illustrate the relationship between classes of plasma models in common use.

cases, one can instead use a statistical model where the development of the distribution function is considered; this is known as kinetic theory. By forming moments of the distribution function, fluid theory is obtained. It does not end there. Combinations of both fluid and kinetic theory can be used in hybrid models and the fields found in either fluid or kinetic theory can be used to compute particle trajectories in test particle simulations. Can we also make a figure that illustrates under what conditions the different theories should be used? This turns out to be much more difficult. When deciding on what model to use there are many choices to be made. Can the plasma be described by one or several fluids? Is the problem electrostatic or electromagnetic? How many dimensions are required in configuration space and in velocity space? It is not unusual that two different models can be used to study the same plasma, depending on what aspects of it are emphasized.

### 3.7. CONCLUSIONS

The equations of magnetospheric physics are much the same as those of electromagnetic theory, collisionless plasma physics, the kinetic theory of gases, and fluid dynamics. In any practical application of mathematics in space physics, approximations have to be made, and it is imperative to know the limitations of the models one intends to apply to a particular problem. Even when these limitations are known, assessing whether a model is applicable to a problem is no trivial task. If we, for example, study a phenomenon using a model that includes ions but not electrons, that model itself cannot tell us whether electron physics is important also on ion length and time

scales. Ultimately, it is comparing model results to observations that must provide the answer to the question of model applicability, and it is the combined use of experiments and mathematical modelling that will advance space science in the future.

### ACKNOWLEDGMENTS

This work was supported by the Swedish National Space Agency contract 108/18 and by the Belgian Science Policy Office through the Solar Terrestrial Centre of Excellence and by BRAIN-Be contract BR/175/A2/MOMA.

### REFERENCES

- Alfvén, H. (1942), Existence of electromagnetic-hydrodynamic waves, *Nature*, 150, 405–406, doi:10.1038/150405d0.
- Biot, J.-B., and F. Savart (1820), Note sur le magnétisme de la pile de Volta, *Annales de chimie et de physique*, 15, 222–223.
- Birdsall, C. K., and A. B. Langdon (1991), *Plasma physics via computer simulation*, IOP Publishing Ltd, Bristol, UK.
- Birn, J., J. F. Drake., M. A. Shay, et al. (2001), Geospace environmental modeling (GEM) magnetic reconnection challenge, *J. Geophys. Res.*, 106, 3715–3720, doi:10.1029/1999JA900449.
- Boltzmann, L. (1896), Vorlesungen über Gastheorie, I. Theil: Theorie der Gase mit einatomigen Molekülen, deren Dimensionen gegen die mittlere Weglänge verschwinden (Bd. 1 von 2), Barth, Leipzig.
- Bowles, K. L. (1958), Observation of vertical-incidence scatter from the ionosphere at 41 Mc/sec, *Physical Review Letters*, 1, 454–455, doi:10.1103/PhysRevLett.1.454

- Cheng, C. Z., and G. Knorr (1976), The integration of the Vlasov equation in configuration space, *Journal of Computational Physics*, 22, 330–351, doi:10.1016/0021-9991(76)90053-X.
- Cheng, D. K. (1989), *Field and wave electromagnetics*, World Student Series, 2nd edn., Addison-Wesley Publishing Company Inc.
- Chiu, Y. T., and M. Schulz (1978), Self-consistent particle and parallel electrostatic field distributions in the magnetospheric-ionospheric auroral region, *J. Geophys. Res.*, 83, 629–642, doi:10.1029/JA083iA02p00629.
- Cummings, W. D., R. J. O’Sullivan, and P. J. Coleman Jr. (1969), Standing Alfvén waves in the magnetosphere, *J. Geophys. Res.*, 74, 778–793, doi:10.1029/JA074i003p00778.
- Dorelli, J. C., A. Glocer, G. Collinson., and G. Tóth (2015), The role of the Hall effect in the global structure and dynamics of planetary magnetospheres: Ganymede as a case study, *J. Geophys. Res.: Space Physics*, 120, 5377–5392, doi:10.1002/2014JA020951.
- Dupree, T. H. (1963), Kinetic theory of plasma and the electromagnetic field, *Physics of Fluids*, 6, 1714–1729, doi:10.1063/1.1711014.
- Egedal, J., A. Le, and W. Daughton (2013), A review of pressure anisotropy caused by electron trapping in collisionless plasma, and its implications for magnetic reconnection, *Physics of Plasmas*, 20(6), 061201, doi:10.1063/1.4811092.
- Fejer, J. A. (1960), Scattering of radio waves by an ionized gas in thermal equilibrium, *Canadian Journal of Physics*, 38(8), 1114–1133, doi:10.1139/p60-119.
- Gordon, W. E. (1958), Incoherent scattering of radio waves by free electrons with applications to space exploration by radar, *Proceedings of the IRE*, 46(11), 1824–1829, doi:10.1109/JRPROC.1958.286852.
- Gunell, H., L. Andersson, J. De Keyser, and I. Mann (2015), Self-consistent electrostatic simulations of reforming double layers in the downward current region of the aurora, *Annales Geophysicae*, 33(10), 1331–1342, doi:10.5194/angeo-33-1331-2015.
- Gunell, H., J. De Keyser, E. Gamby, and I. Mann (2013), Vlasov simulations of parallel potential drops, *Annales Geophysicae*, 31, 1227–1240, doi:10.5194/angeo-31-1227-2013.
- Gunell, H., M. Holmström, E. Kallio, et al. (2004), X-rays from solar wind charge exchange at Mars: A comparison of simulations and observations, *Geophys. Res. Lett.*, 31, L22801, doi:10.1029/2004GL020953.
- Gunell, H., E. Kallio, R. Jarvinen, et al. (2007), Simulations of solar wind charge exchange X-ray emissions at Venus, *Geophys. Res. Lett.*, 34, L03107, doi:10.1029/2006GL028602.
- Gunell, H., and F. Skiff (2001), Weakly damped acoustic-like ion waves in plasmas with non-Maxwellian ion distributions, *Physics of Plasmas*, 8, 3550–3557, doi:10.1063/1.1386428.
- Gunell, H., and F. Skiff (2002), Electrostatic fluctuations in plasmas with distribution functions described by simple pole expansions, *Physics of Plasmas*, 9, 2585–2592, doi:10.1063/1.1476666.
- Hagfors, T. (1961), Density fluctuations in a plasma in a magnetic field, with applications to the ionosphere, *J. Geophys. Res.*, 66, 1699–1712, doi:10.1029/JZ066i006p01699.
- Henon, M. (1982), Vlasov equation? *Astronomy & Astrophysics*, 114, 211–212.
- Jeans, J. H. (1915), On the theory of star-streaming and the structure of the universe, *Monthly Notices of the Royal Astronomical Society*, 76, 70–84, doi:10.1093/mnras/76.2.70.
- Kallio, E., and P. Janhunen (2001), Atmospheric effects of proton precipitation in the Martian atmosphere and its connection to the Mars-solar wind interaction, *J. Geophys. Res.*, 106, 5617–5634.
- Klimontovich, I. L. (1958), On the method of “second quantization” in phase space, *Soviet Journal of Experimental and Theoretical Physics*, 6, 753–760.
- Krall, N. A., and A. W. Trivelpiece (1973), *Principles of plasma physics*, McGraw-Hill, New York.
- Lehnert, B. (1958), Magneto-hydrodynamic experiments. In B. Lehnert (Ed.), *Electromagnetic Phenomena in cosmic physics, IAU symposium (Vol. 6, p. 50)*. Cambridge University Press.
- Liouville, J. (1838), Note sur la théorie de la variation des constantes arbitraires, *Journal de Mathématiques Pures et Appliquées*, 342–349.
- Löfgren, T., and H. Gunell (1997), Flexible simple-pole expansion of distribution functions, *Physics of Plasmas*, 4, 3469–3476, doi:10.1063/1.872243.
- Markidis, S., G. Lapenta, and Rizwan-uddin (2010), Multi-scale simulations of plasma with iPIC3D, *Mathematics and Computers in Simulation*, 80(7), 1509–1519, doi:https://doi.org/10.1016/Zj.matcom.2009.08.038.
- Müller, J., S. Simon, U. Motschmann, et al. (2011), A.I.K.E.F.: Adaptive hybrid model for space plasma simulations, *Computer Physics Communications*, 182, 946–966, doi:10.1016/j.cpc.2010.12.033.
- Palmroth, M., H. Hietala, F. Plaschke, et al. (2018), Magnetosheath jet properties and evolution as determined by a global hybrid-Vlasov simulation, *Annales Geophysicae*, 36, 1171–1182, doi:10.5194/angeo-36-1171-2018.
- Palmroth, M., S. Hoilijoki, L. Juusola, et al. (2017), Tail reconnection in the global magnetospheric context: Vlasiator first results, *Annales Geophysicae*, 35, 1269–1274, doi:10.5194/angeo-35-1269-2017.
- Pierrard, V., and M. Lazar (2010), Kappa distributions: Theory and applications in space plasmas, *Solar Physics*, 267, 153–174, doi:10.1007/s11207-010-9640-2.
- Poisson, S. D. (1813), Remarques sur une équation qui se présente dans la théorie des attractions des sphéroïdes, *Bulletin de la Société Philomathique de Paris*, 3, 388–392.
- Roederer, J. G. (1967), On the adiabatic motion of energetic particles in a model magnetosphere, *J. Geophys. Res.*, 72, 981–992, doi:10.1029/JZ072i003p00981.
- Rosenbluth, M. N., and N. Rostoker (1962), Scattering of electromagnetic waves by a nonequilibrium plasma, *The Physics of Fluids*, 5(7), 776–788, doi:10.1063/1.1724446.
- Rostoker, N. (1964a), Superposition of dressed test particles, *Physics of Fluids*, 7, 479–490, doi:10.1063/1.1711227.
- Rostoker, N. (1964b), Test particle method in kinetic theory of a plasma, *Physics of Fluids*, 7, 491–498, doi:10.1063/1.1711228.
- Schottky, W. (1924), Wandströme und Theorie der positiven Säule, *Physikalische Zeitschrift*, 25, 342–348.

- Skiff, F., H. Gunell, A. Bhattacharjee, et al. (2002), Electrostatic degrees of freedom in non-Maxwellian plasma, *Physics of Plasmas*, 9, 1931–1937, doi:10.1063/1.1462031.
- Torvén, S., and D. Andersson (1979), Observations of electric double layers in a magnetised plasma column, *Journal of Physics D: Applied Physics*, 12, 717–722, doi:10.1088/0022-3727/12/5/012.
- Van Allen, J. A., G. H. Ludwig, E. C. Ray, and C. E. McIlwain (1958), Observation of high intensity radiation by satellites 1958 alpha and gamma, *Jet Propulsion*, 28(9), 588–592.
- Vlasov, A. A. (1938), On vibration properties of electron gas, *Journal of Experimental and Theoretical Physics*, 8, 291.
- Vlasov, A. A. (1968), The vibrational properties of an electron gas, *Soviet Physics Uspekhi*, 10(6), 721–733, doi:10.1070/PU1968v010n06ABEH003709.
- Yamada, M., R. Kulsrud, and H. Ji (2010), Magnetic reconnection, *Reviews of Modern Physics*, 82, 603–664, doi:10.1103/RevModPhys.82.603.



# **Part II**

## **Fundamental Processes**



# 4

## Magnetic Reconnection in the Near-Earth Magnetotail

Tsugunobu Nagai

### ABSTRACT

Magnetic reconnection is the key process that produces the dynamics of the Earth's magnetosphere, by efficiently converting the magnetic field energy into plasma kinetic energy and thermal energy. The understanding of magnetic reconnection is being revolutionized with in situ spacecraft observations and large-scale computer simulations with particle code. Magnetic reconnection occurs in the microscale region, but has large-scale consequences. The physical processes in magnetic reconnection should be explored on various scales. This chapter summarizes a macroscopic picture of magnetic reconnection and examines the structure of magnetic reconnection on the kinetic level from an observational point of view.

### 4.1. INTRODUCTION

Magnetic reconnection is a physical process that efficiently converts magnetic field energy into plasma kinetic energy and thermal energy. Magnetic reconnection is the main driver in the dynamics of the Earth's magnetosphere. Magnetic reconnection occurs at the dayside magnetopause, in the near-Earth magnetotail, and in the distant magnetotail with radial distances of  $>100 R_E$  ( $1R_E = 6371.2$  km). Magnetic reconnection occurring in the near-Earth magnetotail in association with substorm activity is ideal for exploring the essential nature of magnetic reconnection. Figure 4.1 shows a schematic of magnetic reconnection in the near-Earth magnetotail. In Figure 4.1, the Geocentric Solar Magnetospheric (GSM) coordinate system is used and magnetic reconnection is presented in the two-dimensional ( $x$ - $z$ ) plane, although the  $z$  scale is elongated. In the steady magnetotail, the magnetic field lines are northward ( $B_z > 0$ ) inside the plasma sheet of the magnetotail, and large-scale magnetospheric convection flows are earthward ( $V_x > 0$ ). The

typical convection flow speed is less than  $100 \text{ km s}^{-1}$ . The tail lobe magnetic field lines are transported toward the equatorial plane and the X-line forms in the neutral sheet. As the transport of the magnetic field lines is the magnetohydrodynamic (MHD) process, the tail lobe plasmas are also transported to form inflows. The speed of the inflows is roughly 0.1 of the Alfvén velocity ( $V_A$ ). Tailward outflows with  $B_z < 0$  and earthward outflows with  $B_z > 0$  are produced inside the plasma sheet. As the speed of the outflows can reach the Alfvén velocity, fast tailward plasma flows with  $B_z < 0$  inside the plasma sheet are often used as a signature of magnetic reconnection. This type of magnetic reconnection can be classified as antiparallel reconnection in a symmetrical system with no strong initial guide (out-of-plane) field. The Alfvén velocity is high (usually  $>2000 \text{ km s}^{-1}$ ) so that outflow plasmas generated by magnetic reconnection are easily discriminated from other environmental plasmas. Inflowing plasmas are readily identified. The acceleration and heating of electrons are also evident. The ion inertial length ( $\lambda_i$ ), which probably determines the spatial scale size of magnetic reconnection, can be approximately 1000 km. The speed of a possible motion of the magnetic reconnection site itself is considered to be small, relative to the outflow speed. Therefore, the present and past spacecraft

---

*Institute of Space and Astronautical Science, Japan Aerospace Exploration Agency, Sagami-hara, Japan*

---

*Space Physics and Astronomy Collection Volume 2: Magnetospheres in the Solar System, Geophysical Monograph 259, First Edition.*

Edited by Romain Maggiolo, Nicolas André, Hiroshi Hasegawa, and Daniel T. Welling.

© 2021 American Geophysical Union. Published 2021 by John Wiley & Sons, Inc.

DOI: 10.1002/9781119815624.ch4

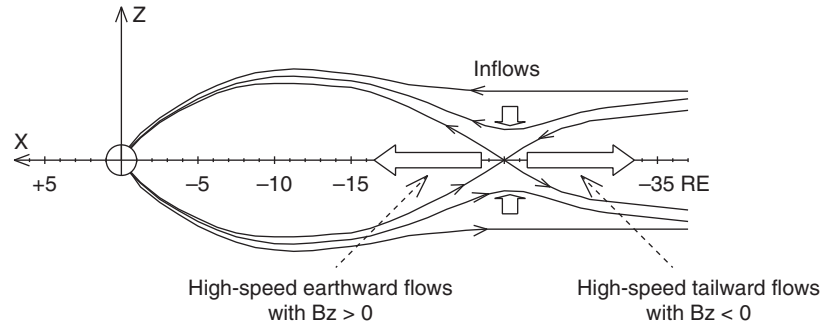


**Figure 4.1** Global picture of magnetic reconnection in the near-Earth magnetotail. Magnetic field lines are represented by solid lines and plasma flows are represented by thick arrows in the tail meridional ( $x$ - $z$ ) plane. Plasmas in the Northern tail lobe and Southern tail lobe are transported with magnetic field lines toward the neutral sheet as inflows. After the merging of field lines at the X-line (the central cross-configuration site), high-speed tailward plasma flows with  $B_z < 0$  and high-speed earthward plasma flows with  $B_z > 0$  are produced as outflows.

observations can easily resolve the structure of magnetic reconnection. This chapter presents the fundamental processes of magnetic reconnection on the basis of in situ observations in the near-Earth magnetotail.

There are many excellent review papers and textbooks on magnetic reconnection. Some classical review papers emphasizing the theoretical aspects of magnetic reconnection are given by Vasyliunas (1975), Sonnerup (1979), and Cowley (1985). Early spacecraft observations are summarized in the monograph by Hones (1984) and review paper by Baker et al. (1996). A comprehensive theoretical textbook on magnetic reconnection at the MHD level is presented by Priest and Forbes (2000). More modern textbooks on theories and observations are provided by Birn and Priest (2007) and Gonzalez and Parker (2016). Recent understandings of magnetic reconnection are summarized by Nishida (2007), Paschmann (2008), Fuselier and Lewis (2011), Paschmann et al. (2013), Treumann and Baumjohann (2013), Keiling et al. (2015), and Hesse et al. (2016). Therefore, this chapter aims to present a modern picture of magnetic reconnection in the magnetotail based on the observational aspects. The kinetic aspects of ion and electron behaviors using velocity distribution function (phase space density) data are discussed. Given that the essential nature of magnetic reconnection is a breakdown of MHD, the fluid treatments of plasmas cannot be applied. Thus, distribution function data must be examined in current and future studies on magnetic reconnection. Magnetic reconnection at the dayside magnetopause is discussed by Fuselier (Chapter 10, this volume) and Burch and Hwang (Chapter 41, this volume), and its relationship to substorm activity is discussed by Nishimura (Chapter 18, this volume). Birn et al. (Chapter 17, this volume) present theory and modeling of magnetotail dynamics. Magnetic reconnection in the magnetospheric boundary layer is discussed by Nakamura (Chapter 12, this volume).

**Table 4.1** Spacecraft names

Spacecraft	Full name	Spacecraft number	Launch year
Vela			1960s
IMP 8	Interplanetary Monitoring Platform		1973
ISEE 1 & 2	International Sun–Earth Explorer		1977
AMPTE/IRM	Active Magnetospheric Particle Tracer Explorer/Ion Release Module		1984
Geotail			1992
Cluster		4	2000
THEMIS	Time History of Events and Macroscale Interactions during Substorms	5	2007
ARTEMIS	Acceleration, Reconnection, Turbulence and Electrodynamics of the Moon’s Interaction with Sun	2	(2010)
MMS	Magnetospheric Multiscale	4	2015

For convenience, Table 4.1 lists the names of various satellites mentioned in this chapter. Vela was the name of 12 satellites used to detect nuclear tests in space during the 1960s. The Vela satellites had high inclination circular orbits with semimajor axes of about  $18 R_E$ . IMP stands for the Interplanetary Monitoring Platform. IMP 8 was launched in 1973. ISEE 1 and 2 stand for the International Sun–Earth Explorer 1 and 2, which were launched in 1977. AMPTE/IRM stands for the Active Magnetospheric Particle Tracer Explorer/Ion Release Module, which was launched in 1984. The spacecraft Geotail

was launched in 1992. Cluster was launched in 2000, and consists of four spacecraft. Launched in 2007, THEMIS stands for the Time History of Events and Macroscale Interactions during Substorms, and consists of five identical spacecraft. Two of the THEMIS spacecraft called ARTEMIS (Acceleration, Reconnection, Turbulence and Electrodynamics of the Moon's Interaction with Sun) are now located near the Moon. The Magnetospheric Multiscale (MMS) mission consists of four identical spacecraft and was launched in 2015.

Section 4.2 presents plasma and magnetic field observations for a clear-cut example of magnetic reconnection in the magnetotail, thus providing a guide for examining plasma and magnetic field data. Section 4.3 discusses the macroscopic view and location of magnetic reconnection in the magnetotail. The dawn–dusk length of the X-line is also examined. Section 4.4 explores the structure of magnetic reconnection from a microscopic point of view and demonstrates ion and electron decoupling. The discussion is limited in ion scales. This section could be a guide for examining velocity distribution function data for magnetic reconnection. Section 4.5 discusses the future prospects.

## 4.2. IN SITU OBSERVATIONS OF MAGNETIC RECONNECTION

A clear-cut example of magnetic reconnection in the near-Earth magnetotail is presented to provide an example of the macroscopic behaviors of magnetic fields and plasmas. Magnetic reconnection was observed by the spacecraft Geotail on 15 September 2017 when the spacecraft was located at  $X_{\text{GSM}} = -22.3 R_E$ ,  $Y_{\text{GSM}} = +9.0 R_E$ , and  $Z_{\text{GSM}} = +1.3 R_E$ . An intense substorm started just after 2300 UT and the minimum AL reached  $-841$  nT at 2322 UT. Figure 4.2 shows the magnetic field data ( $B_x$ ,  $B_y$ ,  $B_z$ , and  $B_t$  in GSM) and plasma moment data (ion flow velocity  $V_{i x}$  and  $V_{i y}$ , electron flow velocity  $V_{e x}$  and  $V_{e y}$ , number density, ion temperature, and electron temperature) for the period of 2240–2340 UT. Figure 4.3 shows ion and electron energy–time spectrograms for four directions (sunward, duskward, tailward, and dawnward). The colors correspond to ion and electron flux values.

The spacecraft was located near the neutral sheet before the substorm onset, as indicated by the  $B_x$  reversal at 2252 UT.  $B_y$  becomes almost zero and the total magnetic field is 1.5 nT at the  $B_x$  zero-crossing, indicating that there is no guide field in this event. Tailward plasma flows with predominantly negative  $B_z$  near the neutral sheet after 2303 UT represent an initial signature of magnetic reconnection. The flow has a significant duskward component ( $V_{i y} > 0$ ) so that plasmas flow tailward and duskward. This is a common signature for tailward outflows in the premidnight sector of the magnetotail. An initial positive

$B_z$  pulse is produced by preexisting tail magnetic fields, which are pushed by reconnection outflows. This bipolar  $B_z$  signature becomes more evident in the distant tail and is recognized as a signature of plasmoids (Hones et al., 1984). The electron and ion flow velocities are almost consistent with one another, indicating that the plasma flows are MHD flows. Ions show almost Maxwellian distributions with temperatures  $>10$  keV (Figure 4.3) and electrons have temperatures of 4 keV (Figure 4.3) before the arrival of the tailward flows. The moment temperature values for ions in Figure 4.2(j) are underestimated, since the values are calculated in the energy range 0–40 keV. The tailward flows consist of ions with energies  $>10$  keV (Figure 4.3). In contrast, electrons appear to be almost isotropic in the energy–time spectrograms, as a bulk velocity of  $100 \text{ km s}^{-1}$  corresponds to  $\sim 3$  eV for electrons. Electron temperature decreases during the MHD tailward flow interval (Figure 4.2(k)). The energy–time spectrograms (Figure 4.3) show that electrons with energies of 1 keV increase while those with energies  $>5$  keV decrease. Lower electron temperature, relative to the temperature of surrounding electron plasmas, is frequently observed inside MHD outflows for magnetic reconnection in the near-Earth plasma sheet.

Observations of ongoing magnetic reconnection are made during the 2317–2332 UT period. The prominent feature during this period is the heating of electrons, as indicated in Figure 4.3. Electron distributions in the plasma sheet can usually be fitted well with Maxwellians, so that 2–10 keV electrons are dominant, and electrons with energies  $<1$  keV coexist. During this period, electrons with energies  $>5$  keV are dominant and electrons with energies less than 1 keV disappear. Electrons are highly heated and the electron temperature becomes  $>10$  keV (Figure 4.2(k)). It is evident that plasma density becomes extremely low, even when the spacecraft is located in the neutral sheet (the  $B_x$  zero crossing). The plasma density here is almost comparable to that in the tail lobes. Furthermore, the electron flow velocity significantly exceeds the ion flow velocity (Figure 4.2). For the x-direction, the electron flow direction is consistent with the ion flow direction. However, even when the ion flow direction is duskward, electrons flow downward. These electrons consequently become carriers of the duskward cross-tail currents. In general, an intense cross-tail current sheet is detected in magnetic reconnection. Tailward flows are reversed to earthward flows near 2324 UT, and  $B_z$  becomes predominantly positive. Earthward flowing ions and tailward flowing ions appear intermittently with corresponding  $B_z > 0$  and  $B_z < 0$  fields. This behavior is common in magnetic reconnection. The X-line (i.e., site of magnetic reconnection) can move tailward and earthward, as reported by the Cluster multi-point observations (Alexandrova et al., 2015).

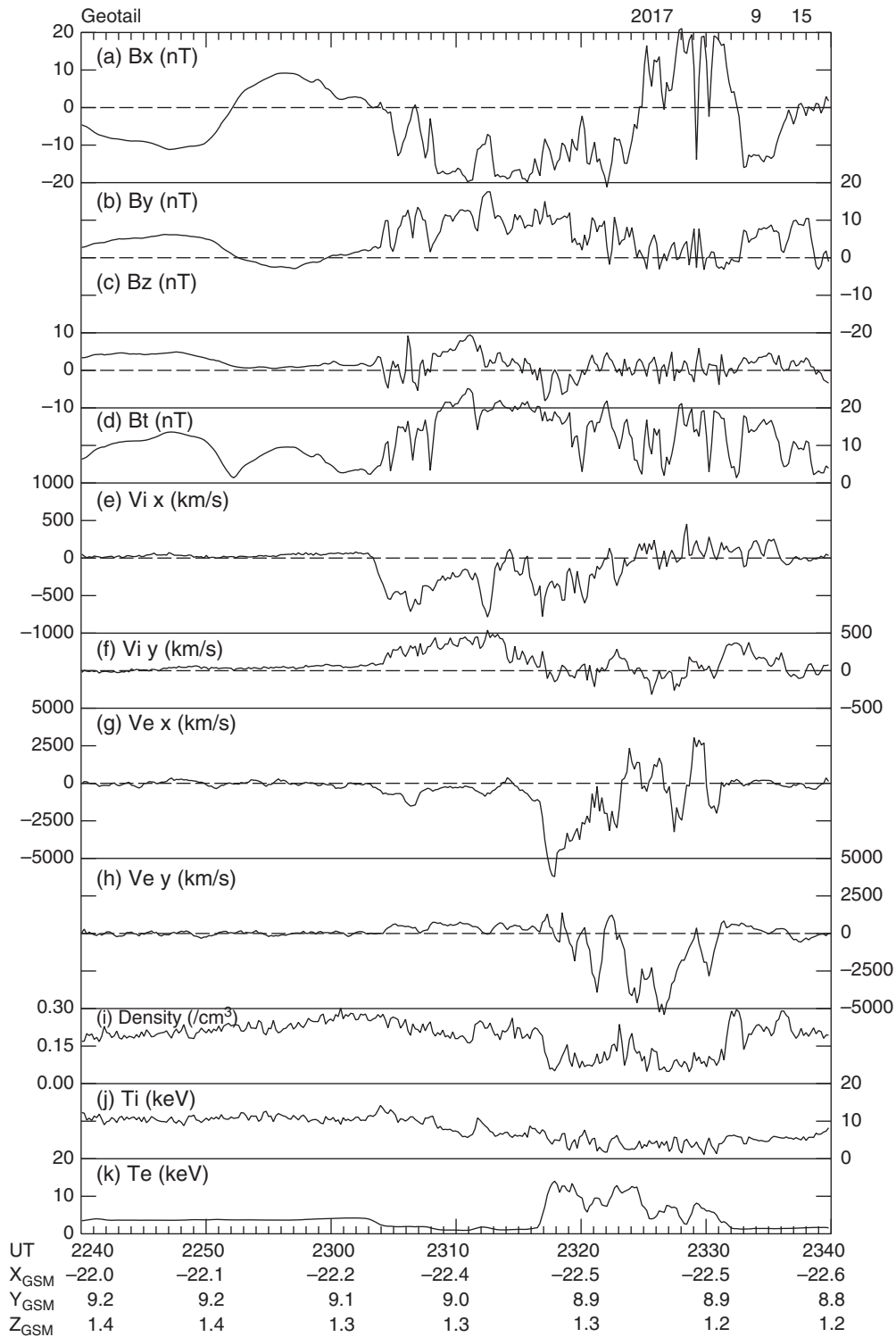


**Figure 4.2** Overview of magnetic reconnection observations by the spacecraft Geotail for the period from 2240 to 2340 UT on 15 September 2017. (a–d) The magnetic field  $B_x$ ,  $B_y$ ,  $B_z$ , and  $B_t$  in the GSM coordinate system. (e–f) Ion flow velocity  $V_{i x}$  and  $V_{i y}$  and (g–h) electron flow velocity  $V_{e x}$  and  $V_{e y}$ . (i) Number density. (j) Ion temperature and (k) electron temperature.

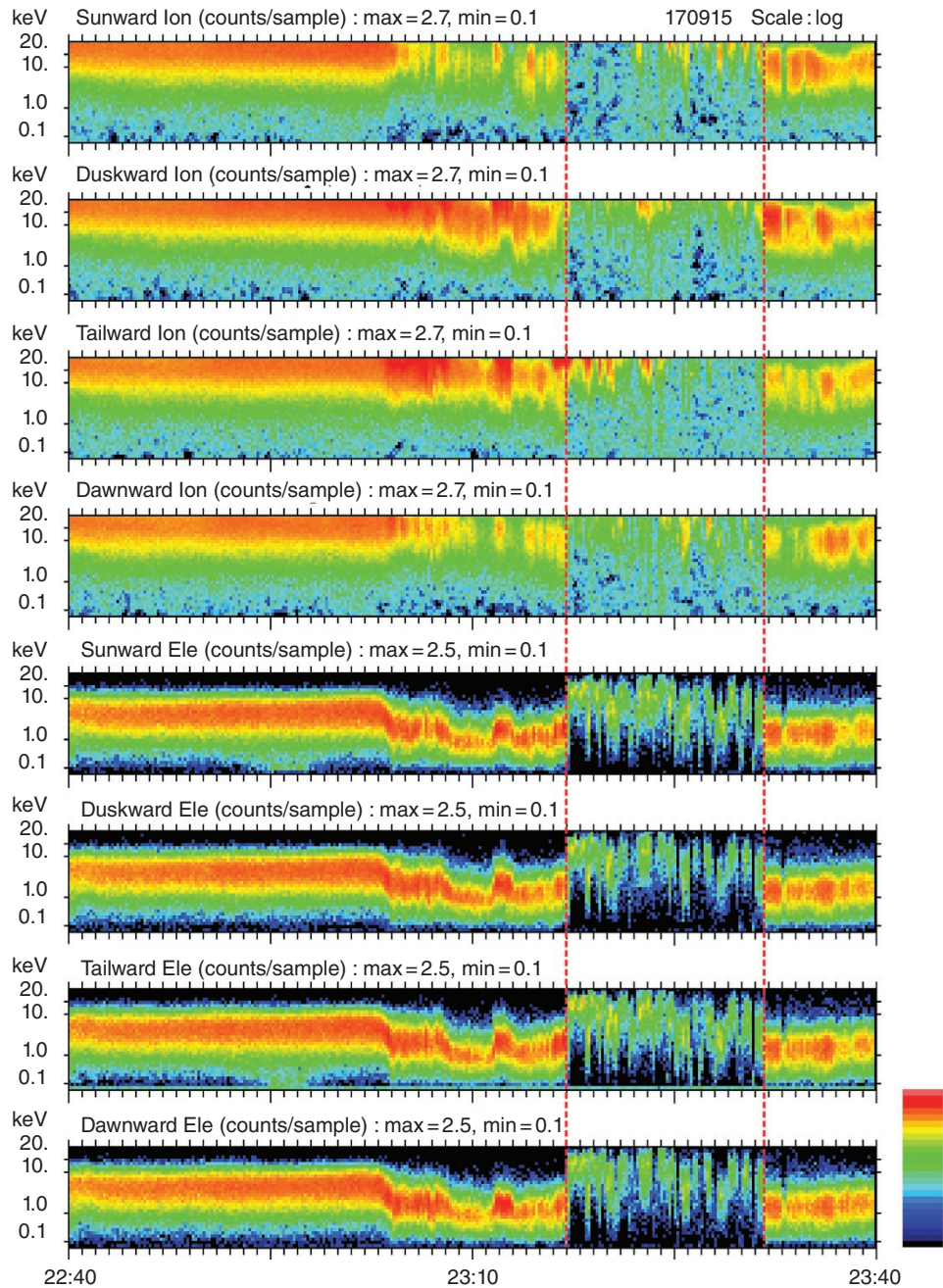


**Figure 4.3** Ion and electron energy–time spectrograms for the period of 2240–2340 UT on 15 September 2017. Sunward (earthward), duskward, tailward, and dawnward ions and electrons (counts/sample) are color coded according to the logarithmic color bar on the right side. Ion counts/sample are from 0.1 to  $10^{2.7}$  and electron counts/sample are from 0.1 to  $10^{2.5}$ . The electron heating period is indicated by vertical red dashed lines.

These in situ magnetic reconnection observation signatures are terminated by an exit into the tail lobe or a rather rapid appearance of the MHD plasmas. In this event, MHD plasmas appear after 2332 UT and ions show bulk duskward flows. It is not known in the present stage whether these duskward MHD flows are related to magnetic reconnection occurring at different sites. Although

flow activities subside at Geotail in the magnetotail, substorm activity progresses on the ground and AL continues to be less than  $-500$  nT.

The coexistence of high-energy (a few to tens of keV) ions and electrons and strong electron heating can be good indicators of in situ observations of magnetic reconnection in the magnetotail. These signatures can be seen in

observations by various spacecraft, such as Geotail (Nagai et al., 1998), Cluster (Nakamura et al., 2006), and THEMIS (Oka et al., 2016). In past observations, IMP 8 observed the events, probably near the ongoing magnetic reconnection site (Bieber et al., 1984).

### 4.3. SUBSTORM-ASSOCIATED MAGNETIC RECONNECTION

#### 4.3.1. Location of Magnetic Reconnection

It was postulated that magnetic reconnection forms in the plasma sheet some 15 or 20  $R_E$  tailward of Earth in association with substorm onsets (Russell and McPherson, 1973; Hones, 1977). High-speed tailward flows with negative  $B_z$  in the plasma sheet indicate that magnetic reconnection occurs earthward of the observation point. However, the spacecraft ISEE 1 and 2 (with apogee of 22  $R_E$ ) and IRM (with apogee of 19  $R_E$ ) seldom observe tailward flows inside the plasma sheet. The IMP 6, 7, and 8 spacecraft, which made observations of the plasma sheet beyond 30  $R_E$ , provided many tailward flows with negative  $B_z$  (Hones, 1979; Hones and Schindler, 1979). The spacecraft Geotail has surveyed the plasma sheet at radial distances of 10–30  $R_E$  since 1996 (in an orbit having an apogee of 31  $R_E$  and a perigee of 10  $R_E$ ) and provided almost continuous plasma and magnetic field measurements in the magnetotail over two solar cycles.

A simple way of determining the location of magnetic reconnection is to make statistics of fast tailward plasma flows with negative  $B_z$  and fast earthward plasma flows with positive  $B_z$ . For example, a flow survey was conducted at radial distances of 10–50  $R_E$  from 1994 to 1996 by Nagai et al. (1998). An examination of plasma flows associated with substorm onsets can more definitely indicate the location of magnetic reconnection in the magnetotail (Nagai and Machida, 1998). Both studies reveal that tailward (earthward) flows with negative (positive)  $B_z$  are observed predominantly at  $X_{GSM} < -20 R_E$  ( $X_{GSM} > -30 R_E$ ). Moreover, flows are observed predominantly in the premidnight sector. It is thus concluded that magnetic reconnection often forms in the premidnight sector of the plasma sheet at radial distances of 20–30  $R_E$ . It is important to take into account the spacecraft residence times in the plasma sheet. Therefore, the occurrence frequencies of tailward and earthward flows should be examined. The occurrence frequency of tailward flows increases at  $X_{GSM} < -20 R_E$ , as the radial distance increases. The occurrence frequency of earthward flows increases at  $X_{GSM} > -30 R_E$ , as the radial distance decreases. This has been verified by an independent study using the spacecraft THEMIS (Imber et al., 2011).

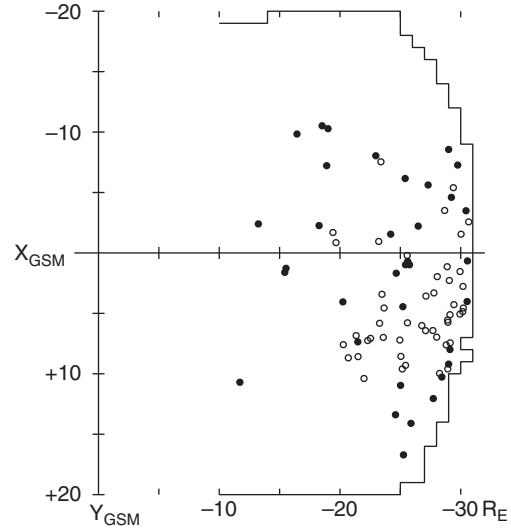


**Figure 4.4** The location of the magnetic reconnection event in the GSM  $x$ - $y$  plane ( $X_{GSM} = -10$  to  $-31 R_E$ ) observed by Geotail in 1994–2014. The open circle indicates the event for  $K_p \leq 3$ , and the dot indicates the event for  $K_p \geq 3+$ . The outer boundary indicates the survey area (with Geotail staying in the plasma sheet for  $\geq 1$  hour in  $1 \times 1 R_E$  box).

Figure 4.4 shows the locations of 82 magnetic reconnection events determined based on the electron heating signatures described in Section 4.2 (Nagai et al., 2015b). The survey was conducted by Geotail in the plasma sheet of  $X_{GSM} < -10 R_E$  during the period of 1994–2014. Although the  $Y_{GSM}$  range of the survey was extended to the spacecraft apogee of 31  $R_E$ , plasma sheet observations are extremely rare for  $Y_{GSM} < -20 R_E$  and  $Y_{GSM} > +20 R_E$ . It is evident that magnetic reconnection is mainly observed at  $X_{GSM} < -20 R_E$ . This is true even when the occurrence frequency of magnetic reconnection is calculated. The preference of magnetic reconnection in the premidnight sector is clear in the occurrence frequency diagram (Nagai et al., 2015b).

#### 4.3.2. Controlling Factor of the Magnetic Reconnection Location

The spacecraft Cluster has observed many magnetic reconnection events within 19  $R_E$  (Eastwood et al., 2010). This appears to contradict the conclusion given in section 4.3.1. Geotail observed tailward convection flows with negative  $B_z$  at  $X_{GSM} = -8.6 R_E$  during an intense magnetic storm on 30 October 2003 (Nagai, 2006). Hence, there may be a control factor that determines the location of magnetic reconnection in the magnetotail. Several solar wind parameters prior to magnetic reconnection were examined (Nagai et al.,

2005). The most probable factor is the solar wind electric field ( $E_y = -V_x \times B_z$ ). For strong solar wind electric field conditions, magnetic reconnection tends to form closer to the Earth. This can resolve the puzzle of the location of magnetic reconnection in the magnetotail. The first report on magnetic reconnection in the magnetotail was provided by the Vela observations in 1967–1968 (Hones et al., 1971). The Vela spacecraft stayed in the plasma sheet only around a radial distance of  $18 R_E$ . Although solar wind data were not available, and the period of 1967–1968 was not in the solar maximum, the Vela events were associated with intense substorms. The ISEE 1 and 2 spacecraft had apogees of  $22 R_E$ , and made observations in 1978–1980 during the solar maximum phase. Although tailward flows with negative  $B_z$  were indeed observed (Hones et al., 1986), occurrence frequency of tailward flows is low and fast flows are predominantly earthward inside  $21 R_E$  (Cattell and Mozer, 1994; Angelopoulos et al., 1994). This might be due to the high inclination ( $23^\circ$ ) of the spacecraft. The AMPTE/IRM spacecraft had an apogee of  $19 R_E$  and made the tail survey in 1985 and 1986 for the solar minimum phase. Occurrence of tailward flows were very low in the IRM observations. Cluster had an apogee of  $19.6 R_E$  near the equatorial plane of the tail and made several in situ observations of magnetic reconnection in 2001–2002, especially for substorms during high geomagnetic conditions (Eastwood et al., 2010). Thus, the past observations of magnetic reconnection inside  $20 R_E$  were likely made under intense solar wind electric field conditions.

#### 4.3.3. The Dawn–dusk Length of the X-line

The X-line of magnetic reconnection apparently develops across the full width of the middle tail. Fast tailward flows with negative  $B_z$  were observed in the full dawn–dusk extent of the tail at radial distances  $>30 R_E$  in early spacecraft observations (Hones, 1979), and plasmoids and travelling compression regions (TCRs) were observed everywhere in the distant tail beyond  $100 R_E$  (Hones et al., 1984, Slavin et al., 1985, Moldwin and Hughes, 1992, Ieda et al., 1998, Eastwood and Kiehas, 2015). However, reconnection-related-phenomena are observed preferentially in the premidnight sector of the near-Earth magnetotail, as evident in various studies (Nagai et al., 1998; Raj et al., 2002; Genestreti et al., 2014). Furthermore, fast earthward flows in the near-Earth magnetotail appear to have a finite dawn–dusk width (Nakamura et al., 2004). Unfortunately, there were no observations in which two or more spacecraft could determine the dawn–dusk length of the X-line. Some statistical studies were thus conducted to obtain information on the dawn–dusk length of the X-line. It should be noted that the database may be a strong

function of the spacecraft orbit. When one spacecraft has an apogee of  $20 R_E$  in the equatorial plane, it can survey the region of  $X_{GSM} = -20 R_E$  near the midnight meridian. Resident times of the spacecraft in the plasma sheet become smaller for the large  $Y_{GSM}$  for  $X_{GSM} < -15 R_E$ . Moreover, full spacecraft operations are often reduced near the midnight meridian due to eclipses (the spacecraft enters the shadow of the Earth). Observations near the midnight meridian are also reduced. It is known that the dawn–dusk length of the X-line can develop both dawnward and duskward in three-dimensional simulations (Huba and Rudakov, 2002, Shay et al., 2003, Nakamura et al., 2012). Therefore, deducing any conclusive results requires some caution.

Cluster observations provided 18 clear-cut encounters of magnetic reconnection in the 2001–2005 period (Eastwood et al., 2010). Magnetic reconnection is observed between 15 and  $20 R_E$  from the Earth (with the apogee being  $19.6 R_E$ ) and all events are in the region of  $Y_{GSM} = -5$  to  $+11 R_E$ . This data set probably provides the upper limit of the dawn–dusk length of the X-line in the near-Earth magnetotail inside  $20 R_E$ . Note that the full tail width is more than  $40 R_E$  at  $X_{GSM} = -20 R_E$ . In the region of  $X_{GSM} = -20$  to  $-30 R_E$ , Geotail observations in 1994–2014 provided 44 clear-cut encounters of magnetic reconnection (Nagai et al., 2013a, 2015b). The dawn–dusk length of the X-line is most likely  $6 R_E$  with its center in the premidnight sector for moderate substorms and is mainly extended dawnward for larger substorms. The duskside edge of the X-line is clearly identified and the dawnward edge is somewhat obscured. This is consistent with simulation results showing that the X-line is mostly extended dawnward when electrons are the major carriers of the cross-tail current (Nakamura et al., 2012). Bieber et al. (1984) reported five events close to the magnetic reconnection site observed by IMP 8 at  $X_{GSM} = -32$  to  $-34 R_E$ . These events were distributed at  $Y_{GSM} = -1$  to  $+8 R_E$ . Kiehas et al. (2013, 2018) examined tailward outflows in the lunar distance (around  $60 R_E$ ) and found that tailward flows are confined in the dusk sector, using the ARTEMIS spacecraft in 2010–2015. Runov et al. (2018) examined plasma properties of tailward flows in the lunar distance and found that these plasma flows originated from magnetic reconnection inside  $30 R_E$ . It is likely that the dawn–dusk length of the X-line is not elongated significantly inside  $X_{GSM} = -60 R_E$ . The wide spatial occurrence of plasmoids and TCRs are probably caused by the dawnward and duskward components of tailward outflows originating from magnetic reconnection inside  $30 R_E$ . Thus, it is likely that the full length of the X-line at the site of near-Earth magnetic reconnection is less than half of the tail width.

#### 4.4. MICROSCOPIC VIEW OF MAGNETIC RECONNECTION IN THE MAGNETOTAIL

Geotail made an in situ observation of magnetic reconnection for a moderate substorm (with the AL index reaching  $-347$  nT) on 15 May 2003. This marked the best event in the 26-year Geotail observations for revealing various important physical processes in magnetic reconnection. There is an intense current layer, in which dawnward moving electrons are a major carrier of the currents. Electrons show “flat-top” distributions, indicating acceleration and heating in the current layer. Both inflowing and outflowing ions are clearly separated. Inflow ions make counterstreaming features in the north–south direction in the center of the current layer and ions are accelerated in the inflow process. Ions that approach to the field reversal region make “meandering” motions near the central current layer. The Hall current system (Sonnerup, 1979) forms in the ion–electron decoupling region.

##### 4.4.1. Overview of a Magnetic Reconnection Event

Figure 4.5 shows the magnetic field ( $B_x$ ,  $B_y$ ,  $B_z$ , and  $B_t$ ), ion and electron flow velocities ( $V_x$  and  $V_y$ ), and ion density for the 10-minute period from 1051 UT on 15 May 2003. The spacecraft was located at  $X_{GSM} = -27.77 R_E$ ,  $Y_{GSM} = +3.35 R_E$ , and  $Z_{GSM} = +3.53 R_E$  at 1050 UT. The magnetic field data have a time resolution of 0.0625 s. The magnetic field component  $B_x$  shows several zero crossings and the total magnetic field  $B_t$  is mostly less than 10 nT, indicating that the observations are made near the equatorial plane of the magnetotail. Ion and electron flow velocities are calculated from ion and electron velocity distribution functions in the energy range of 0–40 keV. As one full velocity distribution function is needed for a plasma sampling time of 12 s, plasma data are shown at 12-s time resolution. Because ions and electrons have multiple populations at the site of magnetic reconnection, plasma moment values only give a global view of the structure of magnetic reconnection, thus requiring an examination of the velocity distribution functions, as described later. Plasma flow starts near 1053 UT. Tailward ion flows are observed until 1055:44 UT, and then flows become earthward. There is a clear flow reversal in this event, and the  $V_x$  velocity change from  $-1000$  km s $^{-1}$  to  $+900$  km s $^{-1}$  occurs within one minute. Electron flows are almost the same as the ion flows initially, and deviated significantly from the ion flows after 1054:43 UT. The ion and electron flows show more evident differences for the period 1054:43–1056:57 UT. Electron  $V_x$  reaches  $-3000$  km s $^{-1}$  and  $+2000$  km s $^{-1}$ , while ion  $V_x$  is in the range of  $-1000$  to  $+1000$  km s $^{-1}$ . Because electrons and ions behave quite differently in this time period, this region can be called the ion–electron

decoupling region. The magnetic field  $B_z$  also shows a clear reversal from southward to northward at 1055:44.157 UT. This timing unintentionally coincides with that of the 12-s plasma data sampling for the first earthward flows. In this event, the flow reversal coincides with the  $B_z$  reversal, indicating that the X-line passes close to the spacecraft. After the flow reversal, the negative values of  $V_x$  appear for the period of 1055:56–1058:121 UT in Figure 4.5(e). It is important to examine the electron distribution functions. There are low-energy ( $<5$  keV) inflowing (tailward) electrons as well as high-energy ( $>10$  keV) outflowing (earthward) electrons near the separatrix layer, as discussed in section 4.4.5. Consequently, moment  $V_x$  values can become negative even in the earthward outflow region. It is also noted that small fluctuations appear in all the magnetic field components, indicating the existence of intense wave activities in the ion–electron decoupling region (Shinohara et al., 2016).

Magnetic reconnection should occur in the so-called electron diffusion region where the magnetic connectivity is broken. Violation of the frozen-in condition occurs in the diffusion region, although it does not uniquely define the diffusion region. Since enhanced dissipation near the X-line indicates the diffusion region, a dissipation measure,  $De$ , is proposed (Zenitani et al., 2011). Zenitani et al. (2012) detected an enhanced dissipation rate of  $45$  pW m $^{-3}$  in the region of  $1-2 \lambda_i$  including the magnetic field and flow reversal around 1056 UT during this event.

Figure 4.6 shows ion and electron velocity distribution function data with plasma flow velocity values in the period 1053–1059 UT (Nagai et al., 2013b). Here the distribution function values, often called phase space densities (PSDs), are summed in all directions and presented by a function of energy. Ion and electron distribution functions can be classified as Classes M, F, A, and C (Nagai et al., 2013b). The flow velocity perpendicular to the local magnetic field ( $V_{\perp}$ ), which corresponds to the convection flow in the MHD regime, is presented using  $V_{\perp x}$ , and  $V_{\perp y}$ . For the convection flow, the 12-s averaged magnetic field values are used. Electron  $V_{\perp y}$  reaches  $-3000$  km s $^{-1}$  while ion  $V_{\perp y}$  is generally positive. This indicates that there are significant duskward cross-tail currents with a typical current density of  $10$  nA m $^{-2}$  in the center of the current layer and that a major current carrier is dawnward moving electrons. The current layer corresponds to the region for fast tailward and earthward electron outflows, which are often called electron jets.

##### 4.4.2. Electron Dynamics in the Current Layer

Electrons in the current layer for the period 1054:43–1056:57 UT can be characterized as flat-top distributions, as seen in Classes F and A in Figure 4.6(c). The phase space density is almost constant below 3 keV. This

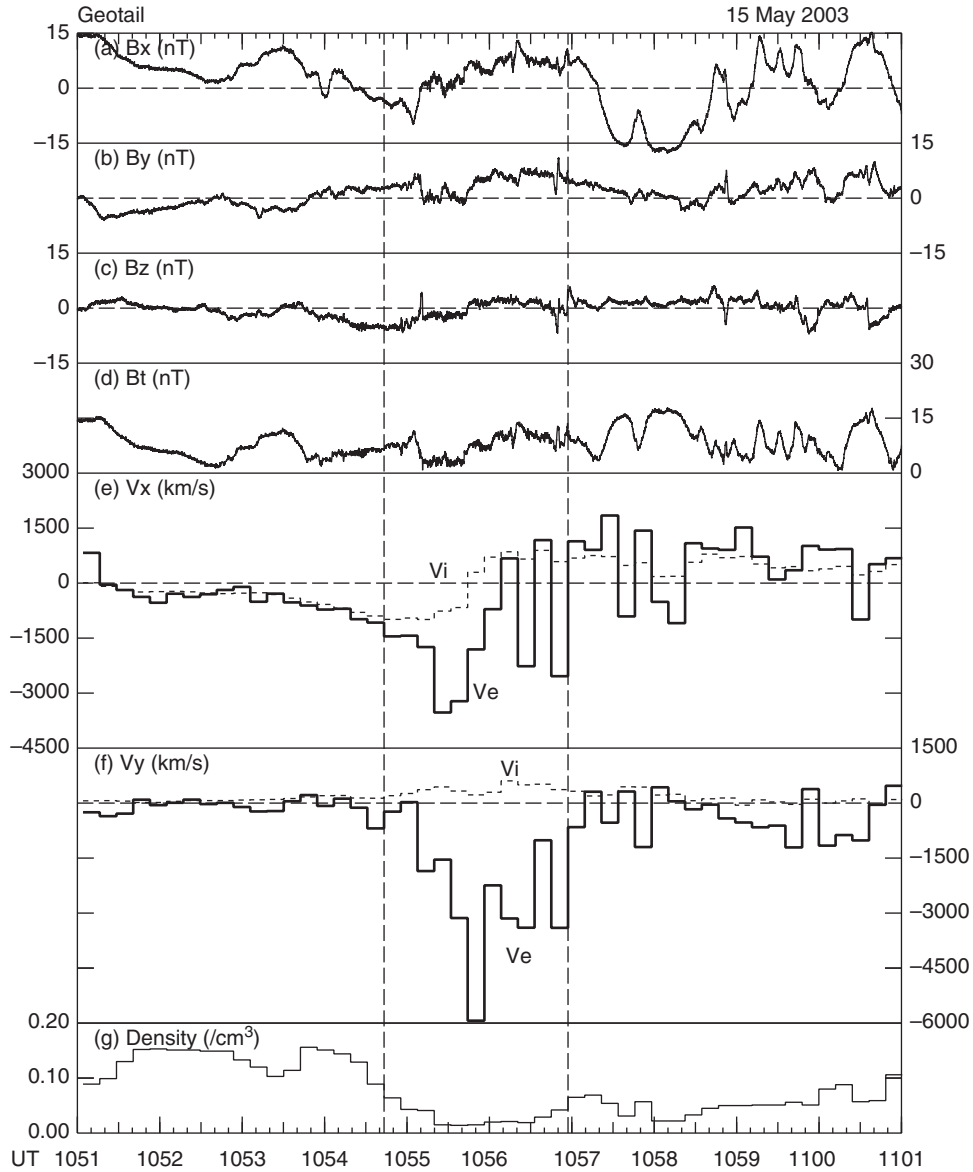


**Figure 4.5** Magnetic field and plasma data from Geotail for the period from 1051 to 1101 UT on 15 May 2003. (a–d) The magnetic field  $B_x$ ,  $B_y$ ,  $B_z$ , and  $B_t$  with time resolution of  $1/16$  s in the GSM coordinate system. (e–f) Ion flow velocity  $V_{ix}$  and  $V_{iy}$  and electron flow velocity  $V_{ex}$  and  $V_{ey}$  with time resolution of 12 s. (g) Number density. The time interval of strong electron heating from 1054:43 to 1056:57 UT is indicated by vertical dashed lines.

contrasts with the Maxwellian (thermal) distribution outside the current layer, as indicated by Class M in Figure 4.6(c). Electrons with energies  $<3$  keV are significantly reduced, so that the phase space density becomes constant due to the small velocity space volume. At the center of the current layer, the flat-top feature is less clear, as seen in Class C (Figure 4.6(c)). Figure 4.7 presents the representative electron velocity distribution functions in the  $V_{\parallel}$ - $V_{\perp}$  plane.  $V_{\parallel}$  is the velocity parallel to the local magnetic field. In order to easily understand the flow direction, the positive  $V_{\parallel}$  direction is taken to be

earthward (i.e., the upward direction) and the positive  $V_{\perp}$  direction is taken to be approximately duskward. In the center of the current layer (at 1055:44 UT, Figure 4.7(c)), a downward shift of the electron population (i.e., negative  $V_{\perp}$  direction) is evident and produces  $V_{\perp}$  of  $-3000$  km s $^{-1}$ . In the center of the current layer where the current density has a maximum, the flat-top distribution becomes less clear, although electrons are largely accelerated compared with electrons in the tail lobe (i.e., inflow region). This is reasonable as electrons still lack acceleration experience. Electrons just off the

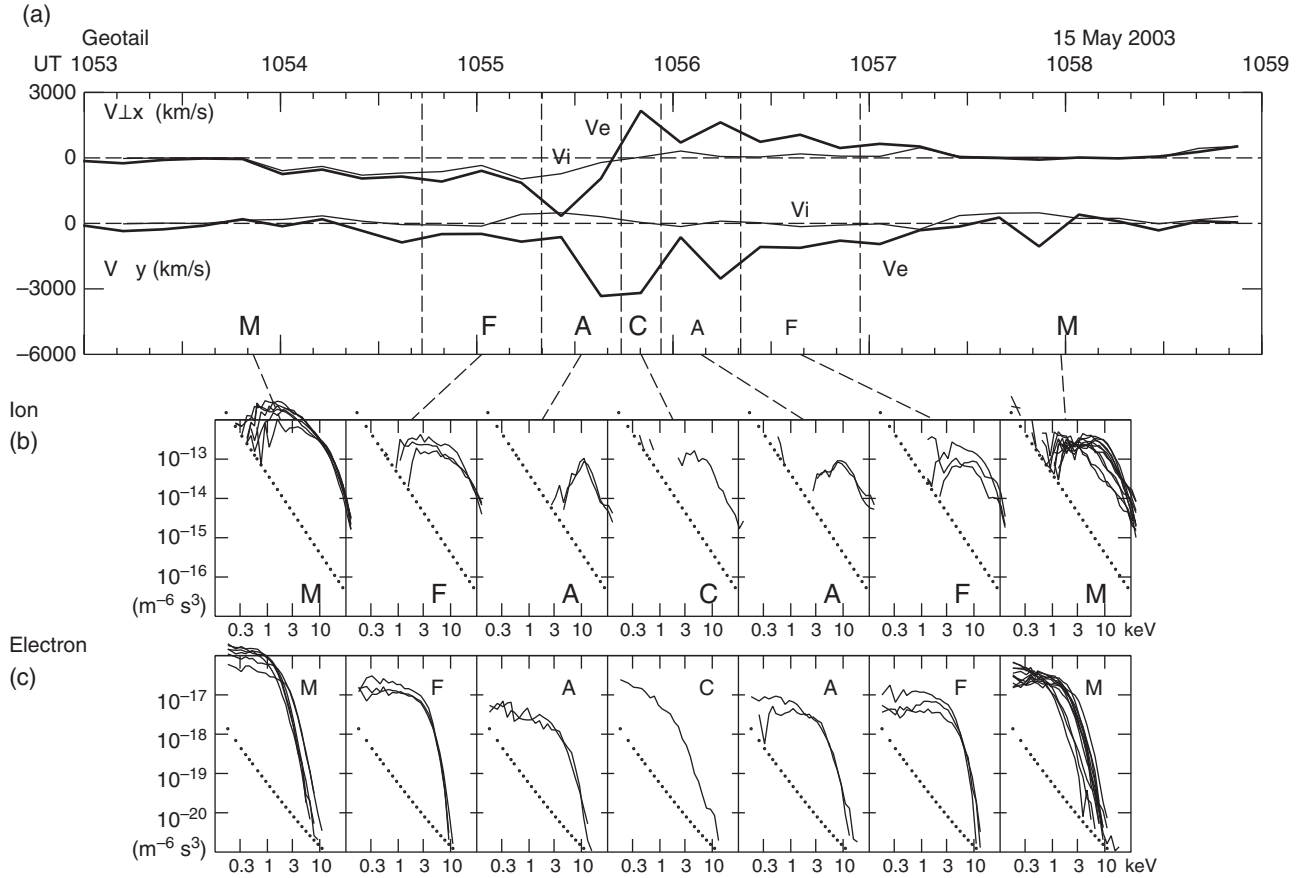


**Figure 4.6** (a) Ion and electron flow velocities perpendicular to the local magnetic field ( $V_{\perp x}$ ,  $V_{\perp y}$ ,  $V_{e\perp x}$ , and  $V_{e\perp y}$ ) for the period from 1053 to 1059 UT on 15 May 2003. (b) Ion distribution functions are presented as a function of energy. (c) Electron distribution functions are presented as a function of energy. Phase space densities (PSDs) are summed for all directions. Distribution functions are classified as Classes M, F, A, and C.

center of the current layer are accelerated inside the current layer, probably in the Speiser orbit (Zenitani and Nagai, 2016). Electrons can enter the current layer as field-aligned beams, make a half gyration, and then exit from the current layer as field-aligned beams (Speiser, 1965). Figure 9.16 in the textbook by Kivelson and Russell (1995) gives a good illustration for the Speiser orbit. Electrons are accelerated much more in the outer part of the current layer as seen in Class F. Although the Class F (at 1054:55 UT in Figure 4.7(b)) and Class A (at 1055:56 UT in Figure 4.7(d)) electron distributions appear to be isotropic, the small asymmetry of PSDs produces significant  $V_{e\perp x}$  and  $V_{e\perp y}$  moment values. Class M (at 1054:31 UT in Figure 4.7(a)) shows typical Maxwellian in the electron distribution.

#### 4.4.3. Ion Dynamics in the Current Layer

Figure 4.8 shows representative ion velocity distribution functions in the current layer. Here, the x axis and y axis are in the equatorial plane, and the positive x

direction is toward the Earth and the positive y direction is duskward. The positive z direction is northward. The most intriguing distribution can be seen at the center of the current layer as Class C at 1055:44 UT. Ions with energies  $>20$  keV are confined into the duskward sector of the equatorial 2-D cut (see the  $V_x$ - $V_y$  diagram in Figure 4.8 (d)). These ions show a semicircular feature in the cross-sectional 2-D cut (pointed to by the red arrow in the  $V_y$ - $V_z$  diagram in Figure 4.8(h)). These ions are those making meandering motions in the antiparallel magnetic field structure, as illustrated in Figure 4.9 (Nagai et al., 2015a). The  $y$ - $z$  plane shown in Figure 4.9 (right) corresponds to the cross-section of the magnetotail, viewing toward the Earth. The magnetic field is inward (outward) in the plane as the Northern (Southern) Hemisphere of the magnetotail. Energetic ions make Larmor motion under the magnetic field. These ions complete only a half circle in the upper plane and the lower plane, respectively, near the field-reversal region. Velocity vectors 1–3 in the upper part and velocity vectors 4–5 in the lower part are mapped into the same left half plane and form a half circle in the

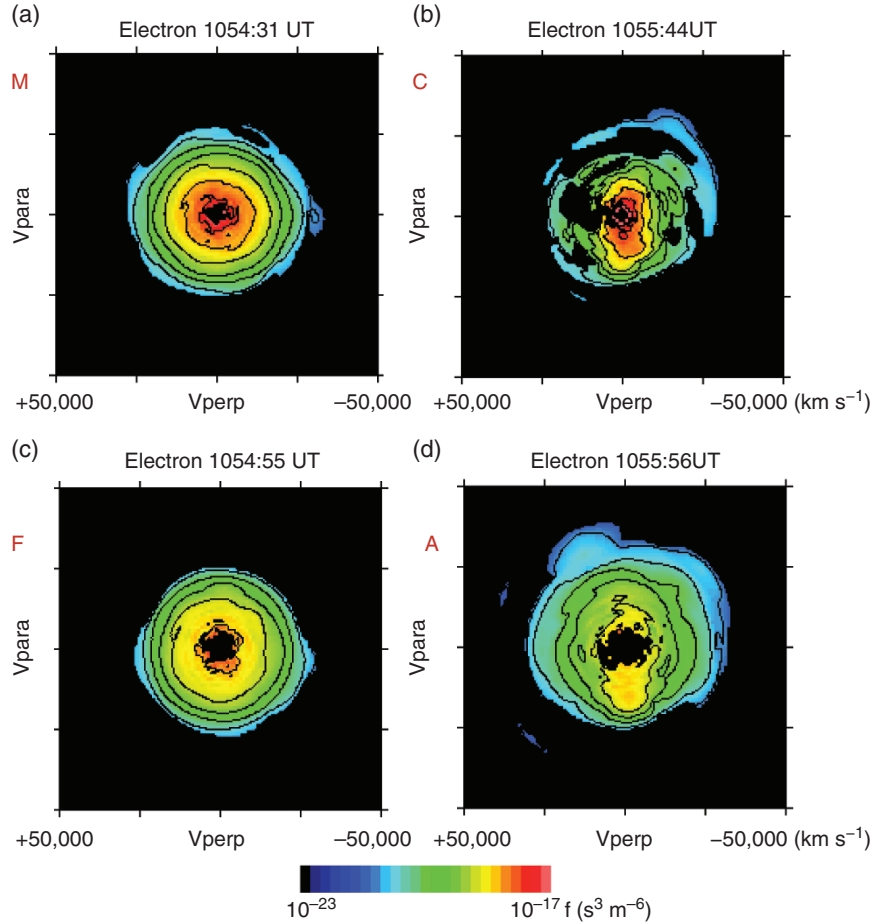


**Figure 4.7** (a–d) Electron velocity distribution functions in the  $V_{\parallel}$ – $V_{\perp}$  plane at 1054:31 UT (Class M), at 1054:55 UT (Class F), at 1055:44 UT (Class C), and at 1055:56 UT (Class A, Hall electrons). In all presentations, the upper direction is almost toward the Earth and the left direction is almost duskward.

$V_y$ – $V_z$  plane (Figure 4.9 left). Hence, the “half-circle” feature represents the meandering motion. In general, the reconnection electric field is duskward (i.e., positive  $y$  direction), so that ions can be accelerated during the meandering motion. There are other ion populations near the  $V_z$  axis in the  $V_y$ – $V_z$  diagram (pointed to by the blue arrows in Figure 4.8(h)). Ions with energies of 1 keV form counterstreaming feature with one population moving northward and another moving southward. These are inflowing ions. The inflow speed reaches approximately  $>400 \text{ km s}^{-1}$ .

Just off the center of the current layer, the counterstreaming features of ions are much more evident at 1055:31 UT (Figure 4.8(g)). Inflowing ions have energies of 10 keV (at inflow speed  $>1000 \text{ km s}^{-1}$ ) and show a local peak in the distribution function as Class A in Figure 4.6. The meandering motion of ions is also seen in Class A.

Farther off the center of the current layer, ions show outflow features in Class F and the flow direction is tailward at 1055:07 UT (Figure 4.8(b)). The inflow ions make

a downward motion (Figure 4.8(f)) due to the Hall electric field described later, and energies of inflowing ions become lower (3–5 keV). In the current layer, both inflowing and outflowing ions are clearly identified.

Outside the current layer, plasmas become MHD and ions show the Maxwellian (thermal) distribution as Class M (Figures 4.8(a) and 4.8(e)). Any inflowing ions are not evident here. Note that the density becomes significantly high in this region. This is caused by a pile-up of plasmas with significant deceleration processes. Ion distribution functions observed by THEMIS far from the reconnection site are discussed by Zhou et al. (2009).

#### 4.4.4. Structure of the Ion–Electron Decoupling Region

Figure 4.10 illustrates a summary of ion and electron dynamics from the observations (Nagai et al., 2013b). The full length (in the  $x$  direction) of the current layer is approximately  $11 \lambda_i$  and the central intense currents are confined in the region of  $0.5$ – $1 \lambda_i$ . These lengths

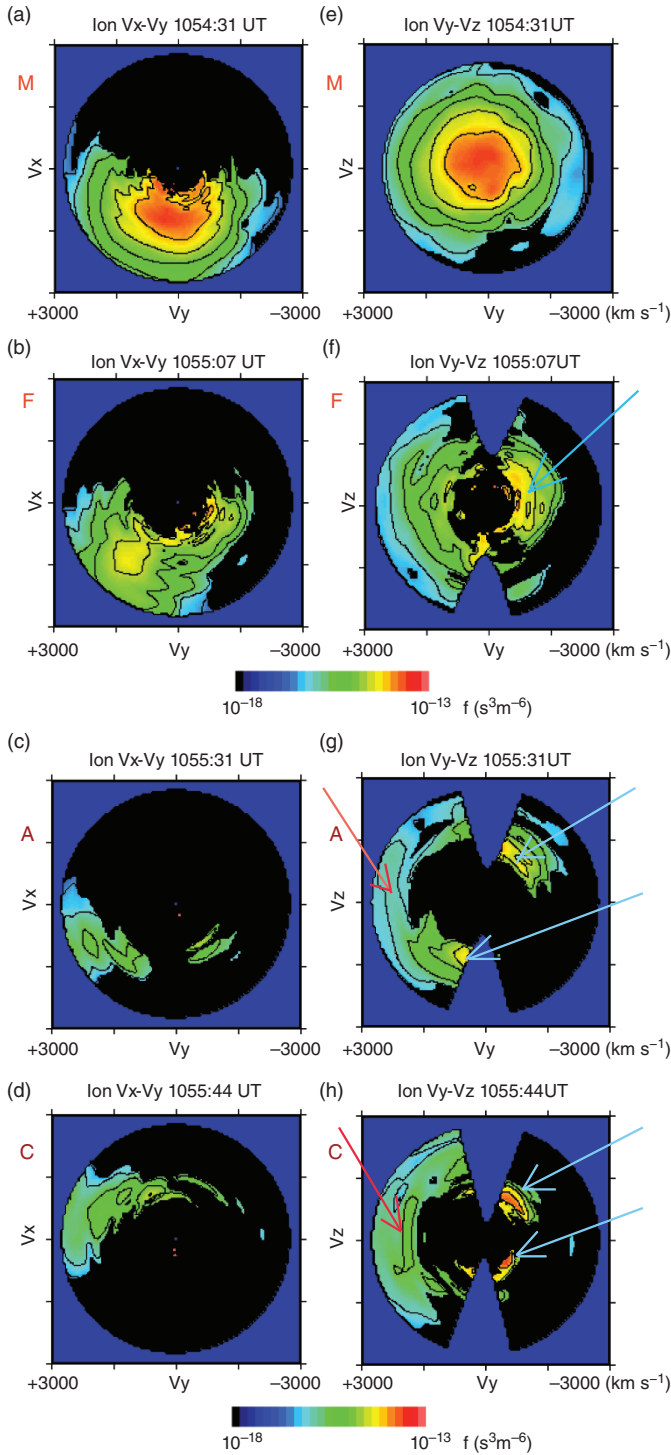


**Figure 4.8** (a–d) Ion velocity distribution functions in the  $V_x$ - $V_y$  plane at 1054:31 UT (Class M), at 1055:07 UT (Class F), at 1055:31 UT (Class A), and at 1055:44 UT (Class C). (e–h) Ion velocity distribution functions in the  $V_y$ - $V_z$  plane at  $V_x = 0$  (except at  $V_x = -1050 \text{ km s}^{-1}$  at 1054:31 UT). Red arrows indicate ions making the meandering motion described in the text, while blue arrows indicate inflowing ion components.

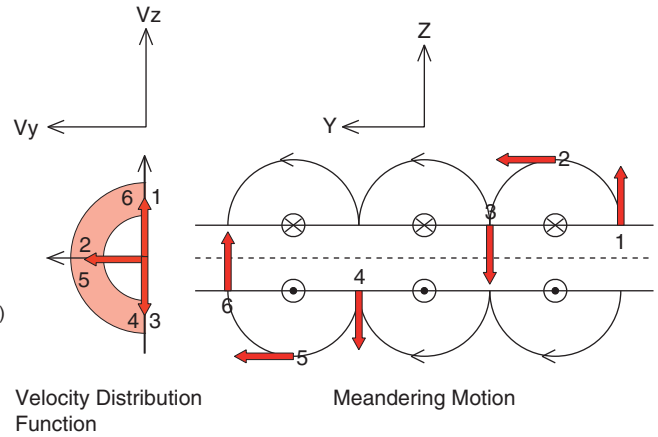


**Figure 4.9** Schematic of ion meandering motion in the  $y$ - $z$  plane (tail cross-section view from the distant tail) and its corresponding pattern of ion velocity distribution function in the  $V_y$ - $V_z$  plane. (right) Ions move toward  $+y$  direction (duskward) with a half-circle Larmor motion in the Northern Hemisphere ( $B_x > 0$ ). (left) Velocity vectors 1, 2, and 3 of the Larmor motion in the Northern Hemisphere are presented in the  $V_y$ - $V_z$  cut of the velocity distribution function, and velocity vectors 4, 5, and 6 in the Southern Hemisphere are also presented in the  $V_y$ - $V_z$  cut. The semicircular features in the  $V_y$ - $V_z$  plane (on the left) are constructed by velocity vectors from the meandering motion (on the right).

are estimated from the velocity of the detected X-line motion. Electron jets extend over half of the current layer and electrons show “flat-top” distributions in the entire current layer. Ions have a lot of 10 keV ions in the electron jet regions as inflows. Ions with energies  $>20$  keV become abundant near the outer boundary of the current layer. Just outside of the current layer, ions and electrons are decelerated and become MHD, and the flux-pile results in a bump (or dip) in the magnetic field  $B_z$ .

Figure 4.11 presents representative two-dimensional simulation results of magnetic reconnection in particle code (from Nagai et al., 2011). Figure 4.11(a) shows the magnetic field structure, with the X-line forming in the center. The unit is ion inertial length ( $\lambda_i$ ) used in the simulations. Note that the full-scale length is  $16 \lambda_i$  in the  $x$  direction and  $4 \lambda_i$  in the  $z$  direction. The central current layer is very thin (the central blue region with thickness of  $<0.2 \lambda_i$  in the simulation). As presented in Figure 4.11(b), electrons make fast-speed flows (electron jets) on both sides of the X-line at a speed reaching  $2 V_A$  within  $1 \lambda_i$  from the X-line. The electron flow speed gradually decreases. Ions make rather low-speed outflows near the X-line and the flow speed gradually increases. First, the electron flow speed slows down to the  $E \times$

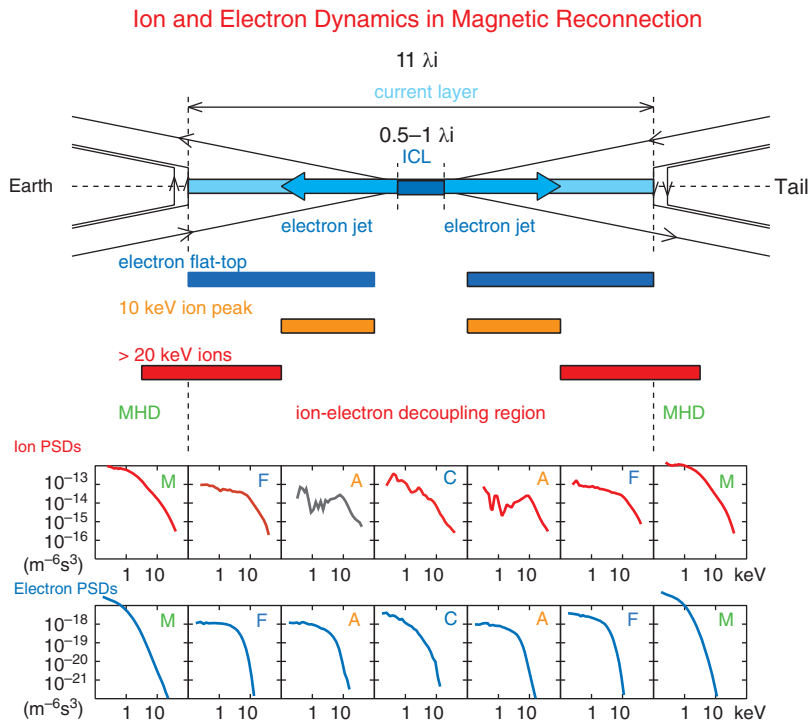


**Figure 4.10** Structure of the ion–electron decoupling region of magnetic reconnection. The X-line is located in the central intense current layer and flux piles up at each edge. Electron outflow jets pervade the central parts of this region. Electrons show a flat-top shape in distribution functions here (Class F and Class A), except near the central intense electron current layer (Class C). Ion PSDs have a peak at 10 keV in Class A, while high-energy ( $>20$  keV) ions appear near and beyond the edge. Both ions and electrons show thermal distributions for Class M in the MHD regions.

B drift speed, which is still higher than the ion flow speed. The electron flow speed continues to decrease, while the ion flow speed continues to increase. Finally, the electron flow speed, the ion flow speed, and the  $E \times B$  drift speed become the same, resulting in the MHD flow (Zenitani et al., 2013). In this simulation (Figure 4.11), the width of the intense central current layer is confined into  $2 \lambda_i$  in the x direction. The electron flow speed  $V_{ey}$  exceeds  $4V_A$  (Figure 4.11(c)), a value nearly twice the electron jet speed. These features are commonly seen in spacecraft observations (the corresponding observation values are presented in Figures 4.11(d)–4.11(f)).

#### 4.4.5. The Hall Current System

The observations indicate the existence of an ion–electron decoupling region in the center of the magnetic reconnection site. The pioneer study by Sonnerup (1979) is useful for understanding physical processes in the ion–electron decoupling region. In the inflow regions for magnetic reconnection, electrons are tightly magnetized and carried into the diffusion region with magnetic field lines. Here, the diffusion region is the so-called

electron diffusion region where electrons are demagnetized in the vicinity of the X-line. Observationally, it coincides with the central intense current layer. Since an ion inertial length is approximately 40 times larger than an electron inertial length, ions can easily become demagnetized and escape from magnetic field lines. Electrons can enter the diffusion region but ions cannot catch up with the electrons. The difference in ion and electron motions produces currents flowing out of the diffusion region in the inflow regions. In the outflow regions, electrons are transported with reconnected magnetic field lines at a high speed, while ions move more slowly near the diffusion region. The difference in ion and electron motions produces currents flowing into the diffusion region in the outflow regions. In the symmetric system, a four-loop current system forms in the vicinity of the magnetic reconnection site, as illustrated in Figure 4.12 (based on observations, unlike the concept of the original work described here). The current system is usually called the Hall current system and the magnetic field produced by the Hall current system is called the Hall magnetic field.

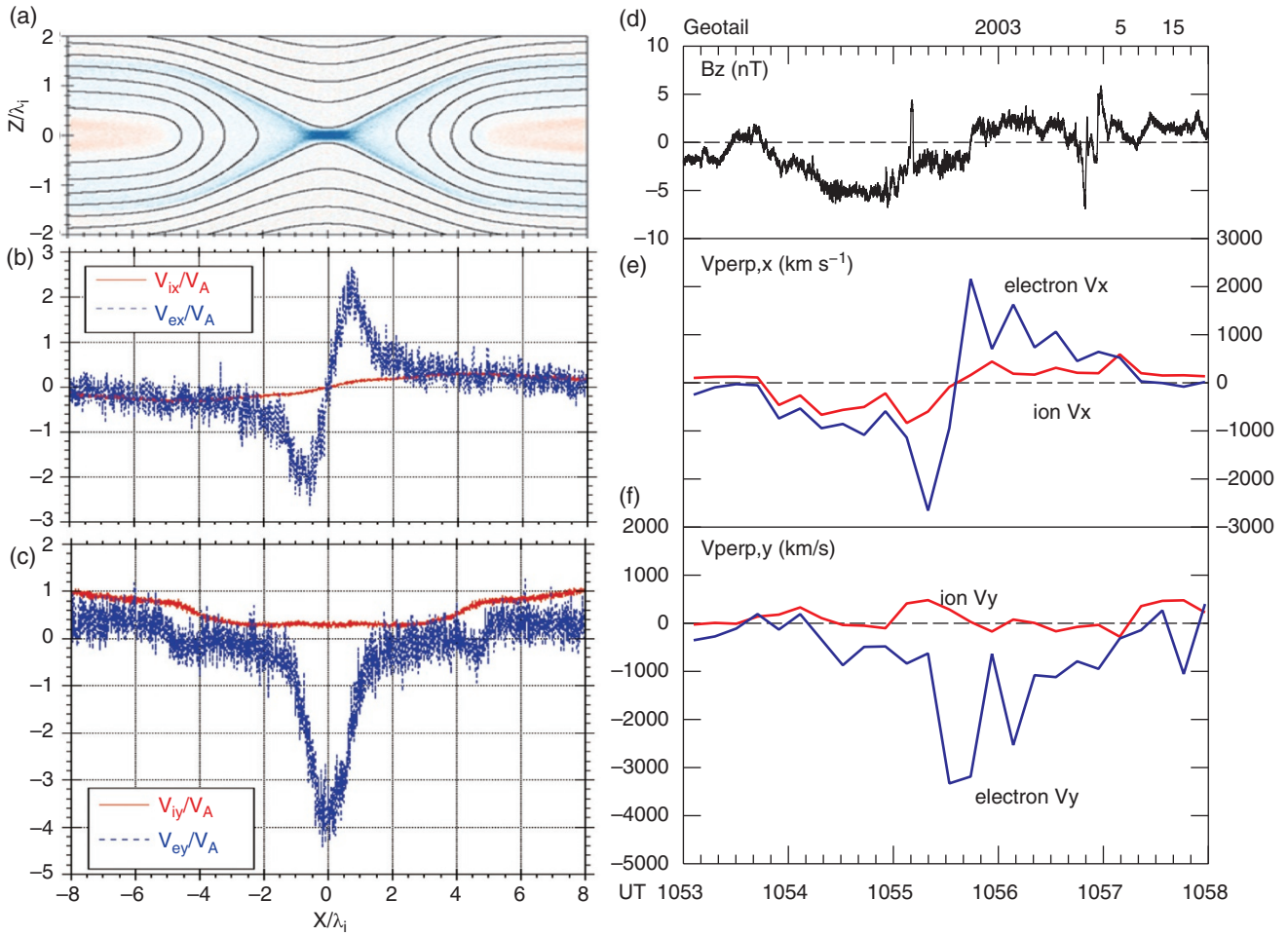


**Figure 4.11** (a–c) The magnetic field structure,  $V_{ex}$  and  $V_{ix}$ , and  $V_{ey}$  and  $V_{iy}$  from a simulation for magnetic reconnection. (d–f)  $B_z$ ,  $V_{e\perp x}$ ,  $V_{i\perp x}$ , and  $V_{e\perp y}$ , and  $V_{i\perp y}$  from the Geotail observations on 15 May 2003.

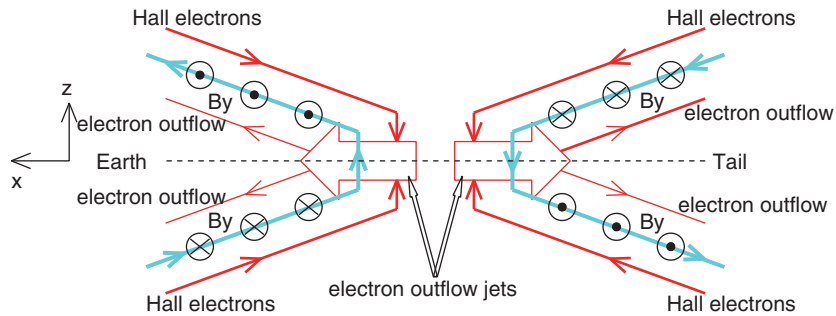


**Figure 4.12** Schematic of electron motion in the vicinity of the X-line for the Hall current system illustrated in the 2-D  $x-z$  plane. Inflowing Hall electrons produce almost field-aligned currents flowing out of the diffusion region, while outflowing high-speed electrons produce currents flowing into the diffusion region. These electron motions make the four-loop Hall current system, which results in a quadrupole magnetic field structure. The magnetic field configuration inevitably becomes 3-D, and the central region should be located inside the plane.